Computational Exploration of Two-Dimensional Materials for Photocatalytic Water Splitting

Abdulrahman Haidar Abdulrahman Alhaidar

MEng (Mech)

Submitted in fulfilment of the requirements for the degree of Doctor of Philosophy

School of Chemistry and Physics

Faculty of Science

Queensland University of Technology

2024

Keywords

Clearage energy, band gap, bilayer density functional theory (DFT), electronic, first-principles calculation, structure, light absorption, photocatalytic, strain engineering, stress, two-dimensional, phonon spectrum and water splitting.

Abstract

The environmental pollution and the energy crisis brought by the fast-growing economy have become serious challenges of the twenty-first century. Over the past decade, hydrogen production has received increasing attention due to the rapid increase in energy demand and environmental concerns. Photocatalytic water splitting provides a promising approach to tackling energy and environmental problems using sunlight to generate hydrogen. Water-splitting photocatalysts have received tremendous attention in recent years.

Two-dimensional (2D) materials have outstanding electronic and physical properties, both in theory and practice, which make them suitable for hydrogen production using water splitting. The exploration of new 2D materials that have excellent visible-light absorption and suitable band alignment is essential for efficient photostatic water splitting. In this work, we computationally studied **structural properties, edge positions** of the conduction band minimum (CBM) and the valence band maximum (VBM), and electronic, and optical properties for unexplored 2D materials using density functional theory (DFT). This thesis is divided into three main studies.

First, exploring novel 2D water-splitting photocatalysts and finding strategies to boost their efficiency are two important tasks in the current energy climate. Here, employing first-principal calculations, we proposed a novel 2D material, $MgAl_2S_4$ monolayer, and studied its potential applications in photocatalytic water splitting. This monolayer is noble metal-free and possesses great thermal and dynamical stability.

The cleavage energy is around 16 meV/Å^2, which is even lower than graphene, indicating the high feasibility for experimental fabrications. The band edge positions, and the optical absorption spectra indicate the pristine $MgAl_2S_4$ monolayer can work as a photocatalyst upon ultraviolet irradiation. Its high electron mobility, around 745 $cm^2v^{-1}s^{-1}$, and high CBM position suggest a high reduction ability. Furthermore, we illustrated that the oxidation and light absorption abilities of this monolayer can be significantly enhanced by applying tensile strain. The complementary marriage of $MgAl_2S_4$ and $SnSe_2$ monolayers can form a direct z-scheme heterostructure, which can fully utilise the photocatalytic potential of both components.

Second, we studied the potential applications of the newly developed 2D photocatalytic material, $AgGaP_2Se_6$ monolayer, based on first-principals calculations. In addition, this monolayer possesses high thermal and dynamical stability. This material also has lower cleavage energy than graphene, so fabrication in an experiment is expected to be very feasible. A photocatalyst can be generated from the pristine $AgGaP_2Se_6$ monolayer by irradiating it with visible-region light. $AgGaP_2Se_6$ monolayer has a high position of its CBM, suggesting a high reduction ability.

Third, the purpose of this study is to provide a comprehensive overview of selected materials from the Computational 2D Materials Database (C2DB). This database was carried out to screen some possible 2D photocatalysts for water splitting. We aimed to investigate several 2D materials that have not yet been synthesised or studied before. We investigated structure, electronic and optical properties of many materials by considering some criteria for candidate selection such as ABC materials from groups 6 and 7, band gap from 1.6 to 2.8 eV via HSE calculation, and these monolayers should not be magnetic. We found AlSI, AlSeBr, AlSeI, ScSI, ScSeBr,

ScSeCl, ScSeI and InSI (the space groups of these materials are Pmmn (no. 59)) can be used as photocatalytic water splitting. These materials were dynamically stable and possessed excellent visible light absorption. The calculation band gaps were between 2.2 and 2.8 eV and their edge positions of the CBM and VBM perfectly fit the water oxidation and reduction potentials.

List of Figures

List of Tables

Type of thesis

Thesis by monograph.

List of Research Publications

This thesis is based on scientific articles that have been published or submitted. In accordance with conventional scientific publication format, each chapter includes an introduction, computation details, results and discussion, and a conclusion.

PUBLISHED JOURNAL ARTICLES

First-authored papers

1. **Alhaidar, A**., Du, A. & Zhang, L. Two-dimensional $MgAl_2S_4$ as potential photocatalyst for water splitting and strategies to boost its performance. *Appl. Surf. Sci.* **605**, 154826 (2022). **Incorporated in chapter 4.**
2. **Alhaidar, A** Two-dimensional Materials AlSI, AlSeBr, AlSeI, ScSI, ScSeBr, ScSeCl, ScSeI and InSI for Photocatalytic Water Splitting under Visible Light. **Incorporated in chapter 6.** This paper is submitted to the Journal of Natural and Applied Sciences 2023.

Submitted papers:

a) **Alhaidar, A**., Du, A. & Zhang, L. Strategies to Enhance the Performance of $AgGaP_2Se_6$ as a Two-dimensional Photocatalyst for Water Splitting. **Incorporated in chapter 5.** This paper is submitted to the Arabian Journal of Chemistry 2023.

CONFERENCE POSTER PRESENTATIONS

1) Poster presentation 2022 international symposium on Advanced Materials and Sustainable Technologies (AM&ST22) from 30th NOV- 2dn Dec 2022 at Cairns, Australia.

2) Poster presentation 2022 the 4th International Conference on Emerging Advanced Nanomaterials (ICEAN) from 17th -21st Oct 2022 at Newcastle, Australia.

3) Poster presentation 2021 Molecular Modelling 2021 (MM2021) from 6th-8th December 2021 Brisbane, Australia.

List of Abbreviations

2D	Two Dimensional
3D	Three Dimensional
AIMD	Ab-initio molecular dynamics
BP	Black Phosphorus
BSE	Bethe-Salpeter equation
C2DB	Computational 2D Materials Database
CBM	Conduction Band Minimum
CB	Conduction Band
DFT	Density Functional Theory
e-h	electron hole
eV	electron Volt
GGA	Generalized Gradient Approximation
HER	Hydrogen Evolution Reaction
HF	Hybrid Functional
HPC	High-Performance Computing
HSE	Heyd−Scuseria−Ernzerhof
LDA	Local Density Approximation
NCI	National Computational Infrastructure
OECs	Oxygen evolution catalysts (OECs)
OER	Oxygen Evolution Reaction
PAW	Projector augmented wave

PBE	Perdew−Burke−Ernzerhof
PEC	Photoelectrochemical
PDOS	Projected Density of State
Pt	Platinum
PV	Photovoltaic
SOC	Spin-orbital Coupling
TMD	Transition-metal dichalcogenides
VASP	Viena *ab intio* Simulation Package
VB	Valence Band
VBM	Valence Band Maximum
VESTA	Visualization for Electronic and Structural Analysis
vdW	the van der Waals

Acknowledgements

It's hard to believe that my PhD study at QUT is coming to an end. The moment I am writing this, I am full of gratitude.

Firstly, I would wish to express my sincere gratitude to my principal supervisor Prof. Aijun Du for his thorough guidance and thoughtful support in my research. His vision and discipline in science will continue to guide me in my future research as an independent researcher. The wisdom that Professor Aijun Du shares is also very beneficial to me, as he shares it without reservations. Being one of his students and spending over three years under his supervision has been one of the greatest honours of my life.

Additionally, I wish to extend my sincere appreciation for all the help and support I received from Dr. Lei Zhang during my study process. I am grateful for all the constructive comments and encouragement that enhanced my research. It was a pleasure to hear about his perspective, and I am thankful for it.

I also want to thank Prof Ting Liao and associate supervisor Dr Liangzhi Kou for his contribution to my research. The authors would also like to express their gratitude to my group members: Dr. Cheng Tang, Dr. Xin Mao, Dr. Gupreet Kour, Dr. Dimuthu Wijethunge, Fahhad Abdullah M Alsubaie, Muhammad Ahmed, Munirah Muraykhan F Alsubaie, Hanqing Yin, Yun Han, Qingchao Fang, and Chee Kian Yap whom they would like to thank for their valuable contributions. This team of wonderful people has made it a pleasure to study with them; we are not just colleagues; we are good friends as well.

In addition, I would like to express my sincere appreciation to all the members of staff at QUT who have supported our study and research activities throughout our

time at the university. Also, it is very much appreciated that Dr. Bronwin Dargaville proofread and edited my thesis.

Furthermore, I would like to thank the Saudi Ministry of Education as well as the Saudi Arabian Cultural Mission (SACM) for providing financial support to my Scholarship.

The last and most important thanks I would like to extend my appreciation to my very loving parents my father Dr. Haidar Alhaidar and my mother Hissah Abu Theeb, my beautiful wife Dr. Sarah Alhammad, my windfall daughters Hissah, Norah and Fajer, as well as all my sisters, brothers, and friends in Saudi Arabia. My sincere appreciation goes out to them during this trying time for me and I appreciate their patience and endurance. No matter how challenging the circumstances in my life may be, as long as you support and encourage me, I will be able to overcome any challenge.

Greetings to all of you and best wishes for the future.

Table of Contents

Chapter 1: Introduction

This chapter outlines the main purpose of the research. In Section 1.1, we explore the motivation for the selected research topic is explored, along with the basis of the central problem. Section 1.2 outlines the research context, describing the choice of focal point, given the many options available. The research problem is briefly described in Section 1.3. The purpose of this thesis is mentioned in Section 1.4, which describes the aims and objectives of the research along with selected questions to be answered by the completion of the project. Then, a description of the scope of the research is presented in Section 1.5. Finally, the thesis chapter outlines are given in Section 1.6.

1.1 Background

Fossil fuels have been used for thousands of years, but their impact on the environment and human health has become increasingly concerning[1,2]. The burning of fossil fuels releases greenhouse gases into the atmosphere, leading to global warming and climate change, air and water pollution, land degradation, and environmental disasters[2–7]. Although there has been a growing recognition of the need to transition to cleaner and more sustainable sources of energy, fossil fuels remain the dominant source of energy worldwide, and the transition to renewable energy will take time and require significant investment and policy changes[4,8].

Global warming is a phenomenon that results from the increased concentration of greenhouse gases in the Earth's atmosphere, particularly carbon dioxide, which is primarily emitted by human activities such as burning fossil fuels, deforestation, and

industrial processes[3,6,7]. This phenomenon has negative effects on the environment, including rising sea levels, more frequent and severe weather events, changes in ecosystems, and negative impacts on human health and well-being[5,9,10]. To mitigate the impacts of global warming, renewable energy sources such as sunlight, wind, water, and geothermal heat are considered to be important solutions since they produce little or no greenhouse gas emissions[11,12]. The Figure 1 below, illustrate the energy consumption worldwide from 2000 to 2019, with a forecast until 2050[13].

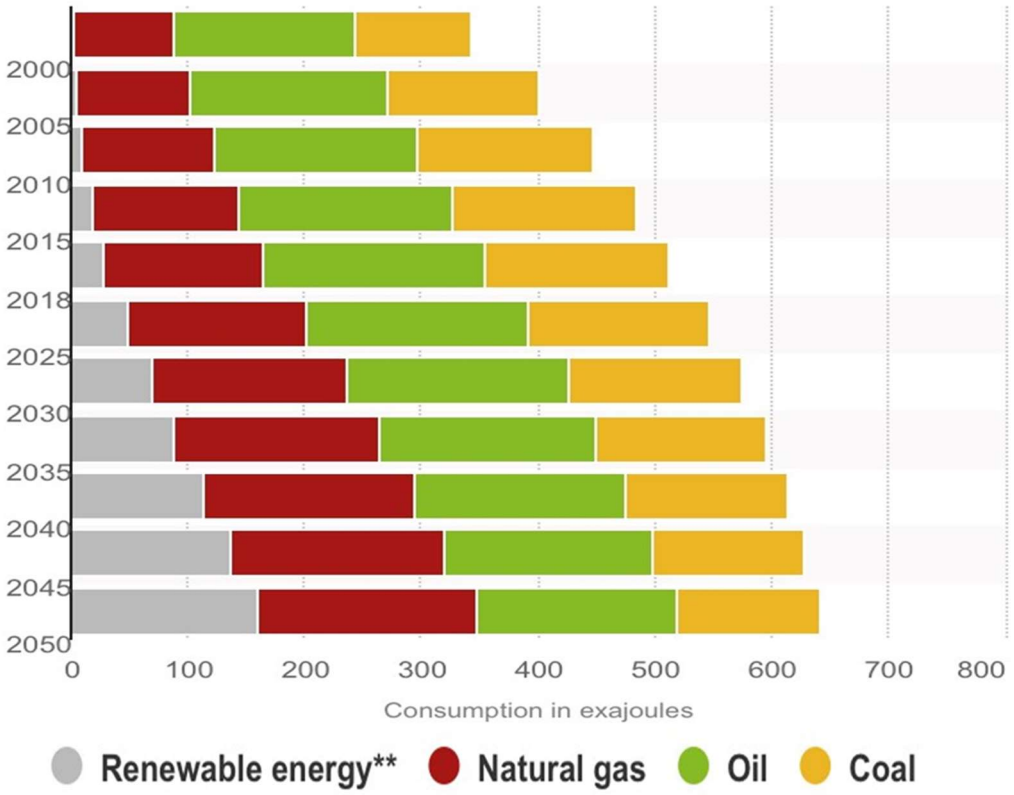

Figure 1 Energy consumption worldwide from 2000 to 2018, with a forecast until 2050[13].

There is a direct relationship between global warming and renewable energy since the shift towards renewable energy sources can help to reduce greenhouse gas emissions, which can mitigate global warming[2]. This reduction in the amount of

carbon dioxide (CO_2) and other greenhouse gases released into the atmosphere can slow down the rate of global warming[8,14,15]. As a result, many countries have set targets to increase their use of renewable energy in order to reduce their carbon footprint and contribute to global efforts to mitigate climate change[11,16]. This has led to significant growth in the renewable energy sector, with new technologies and innovations being developed to harness the power of renewable resources in increasingly efficient ways[17]. Increasing the use of renewable energy is crucial in ensuring a sustainable future for generations to come and is a crucial step towards diminishing global warming[11,15,18].

With the aim of narrowing the gap between energy production and consumption, while avoiding fossil fuel depletion and ecological contamination, hydrogen production using water splitting has emerged as a highly productive, efficient and environmentally friendly process. Water splitting using photocatalysts is one of the key research areas to produce and store hydrogen. With this technology, solar energy can be converted into hydrogen fuel without the use of fossil fuels or CO_2 emissions.

For a photocatalyst to be operationally feasible, it must meet certain requirements. These requirements include effective harvesting of visible light photons to generate electron-hole pairs, lower band gaps, unhindered mobility of charge carriers, a low electron-hole pair recombination rate, and a larger surface area, which results in more active sites exposed.

There are several limitations to conventional photocatalysts such as zinc oxide (ZnO) and titanium dioxide (TiO_2), for example, the wider band gap energy that allows the material to absorb UV light instead of visible light. Another limitation is the inaccessibility of active sites in bulk material. Research in this field has concluded that

nanomaterials are better photocatalysts due to their high surface area in comparison to 3D bulk materials. Two-dimensional (2D) materials are promising photocatalyst alternatives due to their favourable electrical, thermal, and mechanical properties. This research is a continuation of previous efforts to discover new 2D materials for photocatalysis for water splitting.

1.2 Context

As we mentioned in the background, the impact of fossil fuel and global warming and some limitations for some materials that is already used as photocatalytic. In this research we are concentrating to find new 2D materials ether synthesized or not synthesized yet to work as an excellent photocatalytic water splitting.

Renewable energy resources are sources of energy that are replenished naturally and can be sustained in the long term. These resources include[19]:

1. **Solar energy:** Energy from the Sun is captured using solar panels and converted into electricity.
2. **Wind energy:** Energy from the wind is harnessed using wind turbines and converted into electricity.
3. **Hydropower**: Energy from moving water is captured using turbines and generators to produce electricity.
4. **Geothermal energy:** Heat from the Earth's core is harnessed using geothermal power plants to generate electricity.
5. **Biomass energy:** Energy from organic matter, such as wood, crops, agricultural and food waste, is converted into electricity or fuel.

6. **Tidal energy:** Energy from the movement of tides is captured using tidal turbines to generate electricity.

Each of these renewable energy sources has its advantages and disadvantages. For example, solar and wind energy are abundant and widely available, but their output can be variable depending on weather conditions. Hydropower is a reliable source of energy, but it can have significant environmental impacts, such as altering river ecosystems. Geothermal energy is a relatively stable source of energy, but it is only available in certain regions. The use of renewable energy is essential to reduce greenhouse gas emissions and mitigate the impacts of climate change[18]. In recent years, there has been significant growth in renewable energy installations around the world, driven by falling costs and policy incentives. As renewable energy becomes increasingly competitive with fossil fuels, it is expected to play a more significant role in the global energy mix in the coming decades[12]. Solar energy efficiency by photocatalytic conversion to chemical or solar fuels is one of the most likely long-term solutions for global energy and environmental problems[20–22]. In the following paragraphs, the alternative of photocatalysis will be reviewed in detail.

The notion of developing a hydrogen-based energy system has emerged as a viable solution to tackle the prevailing energy crisis and its associated environmental predicaments[23]. This approach is seen as a promising solution, with the potential to provide fuel in various contexts, such as automotive, fuel cells, and other similar scenarios. Furthermore, hydrogen can be produced, stored, transported, and used on a massive scale ranging from several grams to millions of tonnes[24,25]. These attributes render hydrogen energy a realistic and practical option for the wider community.

Photocatalysis is a chemical process that uses light energy to speed up chemical reactions[20,26–29]. It is a type of energy conversion process that involves a catalyst, usually a semiconductor material, that absorbs light and promotes chemical reactions at the surface of the material[30]. The most widely studied photocatalyst is TiO_2[31,32], which is a versatile and highly stable material that can be used for a range of applications, including air and water purification, self-cleaning surfaces, and energy conversion[33].In photocatalysis, light energy is absorbed by the photocatalyst, which excites electrons from the valence band (VB) to the conduction band (CB), creating electron-hole (e-h) pairs[34]. These electron-hole pairs can then react with adsorbed molecules on the surface of the catalyst, promoting chemical reactions that would not occur in the absence of light[35]; see Figure 2. One of the most significant applications of photocatalysis is in the degradation of organic pollutants in water and air[36]. When a photocatalyst is added to polluted water or air and exposed to light, the photocatalyst reacts with the pollutants, breaking them down into harmless substances, such as water and carbon dioxide[37]. This process is known as photocatalytic degradation and is

highly effective for removing a range of organic pollutants, including pesticides, dyes, and pharmaceuticals[38].

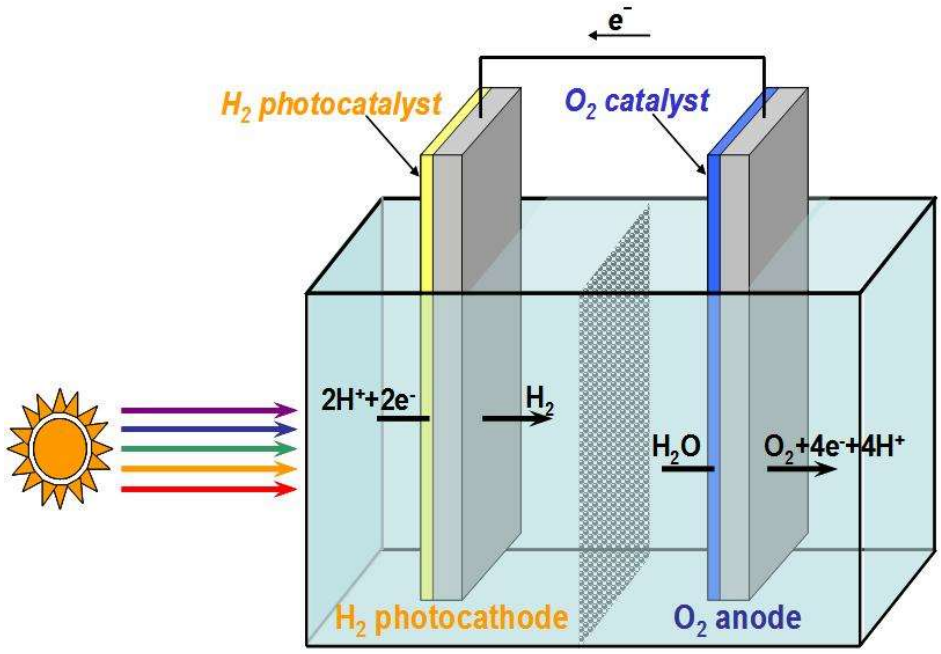

Figure 2 Excitation generation concept using water splitting

Photocatalysis also has potential applications in energy conversion, such as the production of hydrogen fuel by splitting water using sunlight[20,27–29]. Hydrogen is a high energy carrier that can be used in engines and fuel cells[39–41]. While photocatalysis has great potential for a range of applications, it is still a developing technology with ongoing research to improve its efficiency and practical applications.

1.3 Research problem

As a result of utilising fossil fuel, the world faces many environmental issues, such as global warming and climate change. There is a need for a clean source of energy for electricity production to reduce the negative impacts on the environment, that is, a process in which no carbon is used. Photoelectrochemical (PEC) cells use light energy to split water into its chemical components, hydrogen and oxygen. It is an efficient system for solar water splitting[28,39,42,43]. In PEC, the anode or the cathode

should be a light-absorbing semiconductor. It is important to highlight that if both anode and cathode are light absorbing semiconductors, this is known as a tandem PEC cell. A single semiconductor with suitable conduction band minimum (CBM) and valence band maximum (VBM) band structure positions is enough to achieve oxygen evolution reaction (HER) and hydrogen evolution reaction (OER) in the same cell, and one aim of this research is to identify such materials.

As mentioned in the previous sections, two-dimensional materials have outstanding electronic and physical properties[44–50], both in theory and practice, which make them suitable for hydrogen production using water splitting. However, many of the studied 2D materials have limitations, such as stability, carrier mobility, and the use of solar energy. This can restrict the use of such materials in physical applications, especially those that use visible light. Moreover, although extensive research has been done on 2D materials in water splitting, some 2D materials are largely unexplored. The focus of this research covers two aspects: (1) designing and discovering 2D materials for water splitting applications due to their remarkable mechanical and electronic properties, compared to their bulk (3D) counterparts; and (2) conducting further experiments on previously studied materials. The 2D materials that this research is investigating are shown in Table 1 The materials that we uesd in this research and we listed only the exellent materials for water splitting. The reasons for selecting these materials are as follows: (1) they are new materials that to our knowledge have not been researched before; and (2) they are suitable for water splitting because of their band gap.

Table 1 The materials that we uesd in this research and we listed only the exellent materials for water splitting

n	Materials	Space Group	n	Materials	Space Group
1	**$MgAl_2S_4$**	R-3m	**9**	**InSI**	Pmmn59
2	**$AgGAP_2Se_6$**	P$\bar{3}$1c	**10**	**AlSI**	Pmmn59
3	**AlSeI**	Pmmn59	**11**	**ScSI**	Pmmn59
4	**AlSeBr**	Pmmn59	**12**	**ScSeI**	Pmmn59
5	**ScSeBr**	Pmmn59	**13**	**ScSeCl**	Pmmn59

1.4 Purposes

This research focused on finding a semiconductor that is two-dimensional and composed of a single layer of atoms or unit cells, also known as single-layer materials. In addition to high-performance gas sensors[51] and electronics, 2D materials have been used in photovoltaics, spintronics and catalysis[52,53]. Special properties of these materials include the ability to absorb more incident light than bulk materials. Furthermore, they can be easily integrated into waveguides for high performance light modulation in optoelectronics and are suited to heterostructures. Therefore, one of the core research areas of this work was to investigate the potential to produce hydrogen fuel from water splitting.

Research aim

The main aim of this study was to identify 2D materials as catalysts for improving hydrogen production through water splitting. The process of producing electricity by this method is not simple to execute. This thesis aims to identify an ideal method to reduce the dependency on fossil fuel using an alternative way to produce energy, with minimal impact on the environment. To reach this aim, water splitting could be used with some 2D materials that have not been tested before. Such materials

include $MgAl_2S_4$, $AgGAP_2Se_6$, AlSI, AlSeBr, AlSeI, ScSI, ScSeBr, ScSeCl, ScSeI and InSI. In the research, high carrier mobility, good light absorption, mechanical flexibility and thermal conductivity materials need to be considered. Density functional theory (DFT) and the software VESTA and Material Studio will be used to assess these materials. Origen, photoshop and Diagram applications will be used to render results as images.

Objectives

1. Testing photocatalysis characterisation parameters such as optical, electronic, phonon spectra and band gap of unexplored two-dimensional materials.
2. Design two-dimensional materials (transition and post-transition metal chalcogenides) and analyse their suitability and select the most appropriate structures for use as electron or hole-transporting materials for water splitting.

1.5 Significance, scope, and definitions

The research study selected for this project is significant for various reasons. **Firstly,** the primary goal of this fundamental research is to theoretically predict the properties of new or extensively researched materials. **Secondly,** the study contributes to addressing the global issue of climate change. **Thirdly,** the research aims to pre-empt experimental studies, thus save time and expenses, and eliminate futile efforts in doing unproductive experiments. **Fourthly,** the study emphasises the theoretical characterisation of less-researched 2D materials, such as oxides or chalcogenides of elements from Group IV-V, for alternative perovskite solar cells materials, which would provide opportunities for further studies. Additionally, the research aims to identify low-cost processing and production of simply structured materials. It also explores the design of new organic structures for carbon quantum dots to enhance charge transport in solar cells. Moreover, the study is engaged in producing solar fuels,

that is, hydrogen and oxygen, from solar water-splitting, and it provides opportunities for further studies on emerging photovoltaic technology, such as perovskite solar cells.

1.6 Thesis outline

The thesis is organised into seven chapters. In Chapter 2, the literature review and research problem are discussed. Chapter 3 provides information on the research design, including theoretical physics models, computational methods and resources used. Chapters 4 to 6 cover the completed work and any published and submitted manuscripts. Chapter 7 presents the conclusion of the thesis and the future scope of research. Error! Reference source not found. provides a snapshot of the thesis structure, summarising the different sections and their organisation.

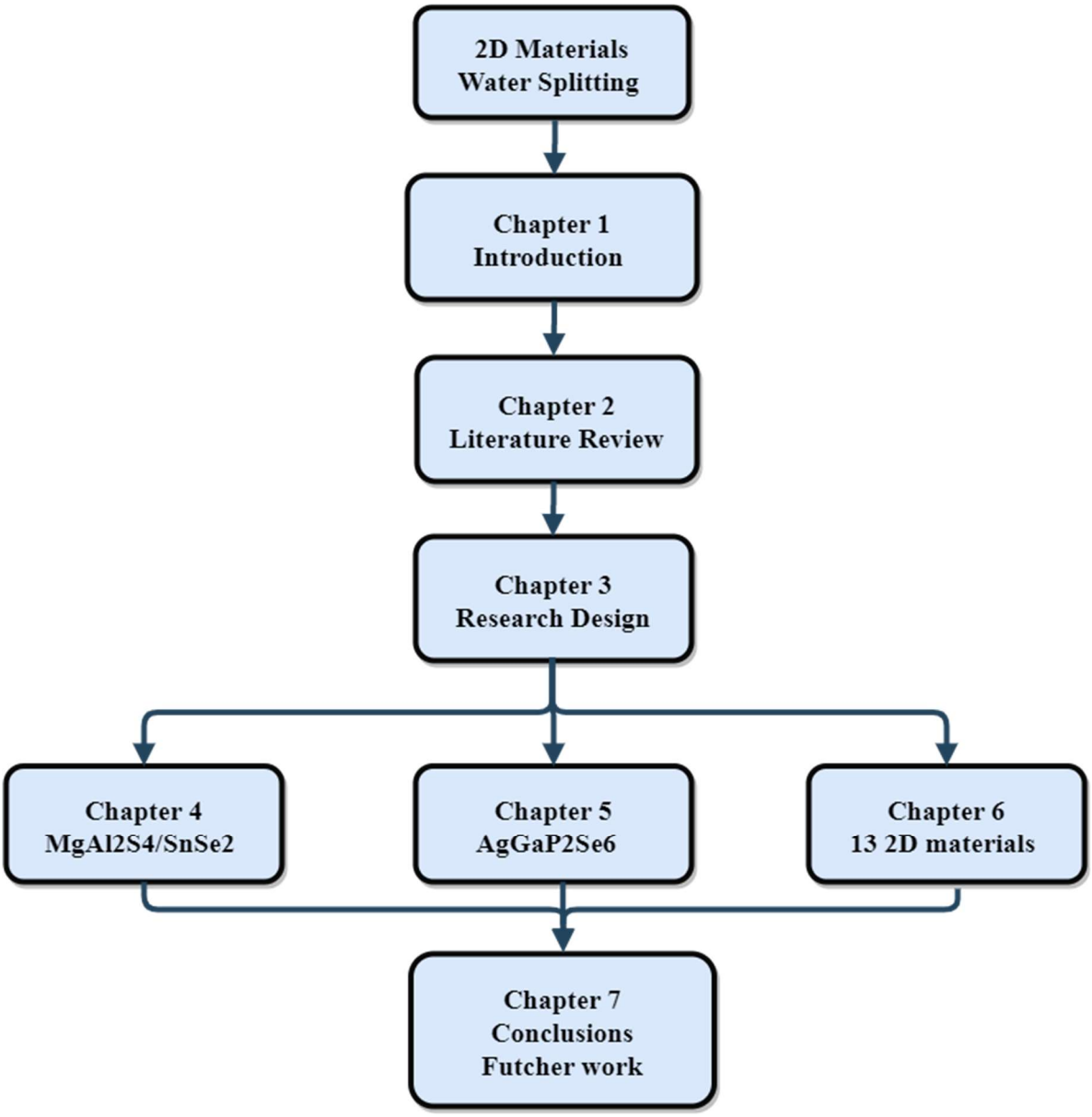

Figure 3 The thesis structure, summarising the different sections and their organisation.

Chapter 2: Literature Review

As a part of this chapter, a review of the literature on photocatalytic water splitting has been presented. The purpose of section 2.1 is to provide background information on the process of photocatalytic water splitting. Section 2.2 provides a list of two-dimensional photocatalyst materials that can be used in two-dimensional photocatalysis. A detailed description of the methods for splitting water is presented in section 2.3. As a conclusion, section 2.4 summarizes the main points that have been discussed in this chapter.

2.1 Background of photocatalytic water splitting

Since Honda and Fujishima successfully decomposed water into H_2 and O_2 using solar energy in the 1970s using TiO_2[54,55], there have been many studies to find effective photocatalysts for water splitting. The following sections will discuss some of the related works in the literature.

Due to an energy shortage and the negative implications of fossil fuels on the environment, such as global warming, climate change and pollution, there is an increasing interest in using clean energy sources to meet the global demand. There are several renewable energy resources that can be used to produce clean energy. Hydrogen is one type of clean energy recourse that could replace fossil fuel[40,41,56,57]. According to Acar et al.[58], there are several methods that can be used for hydrogen production using fossil fuel, water or biomass. The techniques that can use water for hydrogen production are: photocatalysis, PV electrolysis, photoelectrochemical, electrolysis, thermolysis, thermochemical processes water splitting and photo-electrolysis[58]. Hydrogen can be produced by solar energy from the water splitting

process, and this can be an effective alternative for generating energy to reduce the dependency on using fossil fuels[56]. Hydrogen fuel can be utilised in many applications, such as powering electric engines with no toxic emissions. The process of hydrogen production using photocatalytic water splitting has been termed artificial photosynthesis[59,60]. In the process of water splitting, a semiconductor is used as a photocatalyst that absorbs photonic energy. Then, electron-hole (e-h) pairs are formed as photons hit the photocatalyst and the generated electrical charge is used for water separation. That is, the energy generates excited electrons that can split water into hydrogen and oxygen[56,59]; see Figure 4. To dissociate the water into hydrogen and oxygen the conduction band minimum (CBM) of the photocatalyst should be above the reduction potential of water, -4.44 eV, and the valence band maximum (VBM) should be less than the oxidation potential, -5.67 eV[60–64]. Therefore, the band gap for water splitting photocatalysis should not be lower than 1.23 eV[65,66] and not larger than 3.00 eV [60]. If the band gap is higher than 3.00 eV, there will be very low light absorption[60].

The photocatalytic water splitting process can be expressed by the following reaction equations[58,60] :

Photo-reduction: $2H_2O + 2e^- \overset{hv}{\rightarrow} H_2 + 2OH^-$

Photo-oxidation: $2H_2O \overset{hv}{\rightarrow} O_2 + 4H^+ + 4e^-$

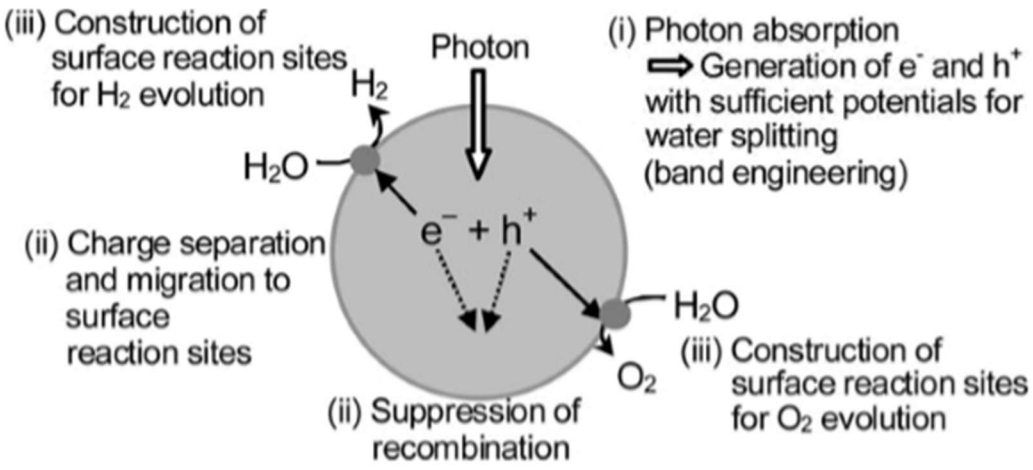

Figure 4 Steps of water splitting using photocatalysis[27]

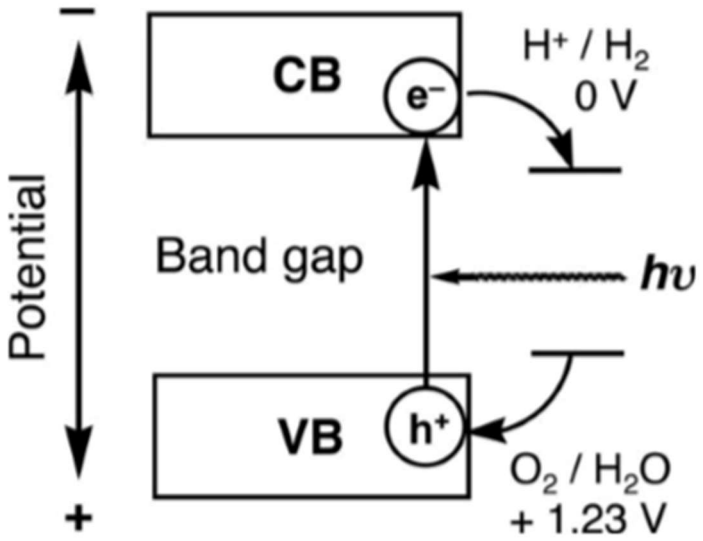

Figure 5 Band gap of semiconductor photocatalysis[27]

Criteria for selecting an appropriate semiconductor for water splitting.

There are four basic requirements that need to be satisfied when selecting a semiconductor for water splitting [67]:

- Suitable band gap and band alignment with the redox potential of water (Figure 5)
- Effective charge separation
- Fast charge transport

- Long-term durability in aqueous environments.

In addition to the main criteria, efficient photocatalyst should also meet the Goldilocks principle as follows [55]:

- High photon harvesting
- Good charge carrier mobility
- Low recombination rate (e-h) pairs
- Active sites for fast energy and charge exchange with other species (as mentioned above).

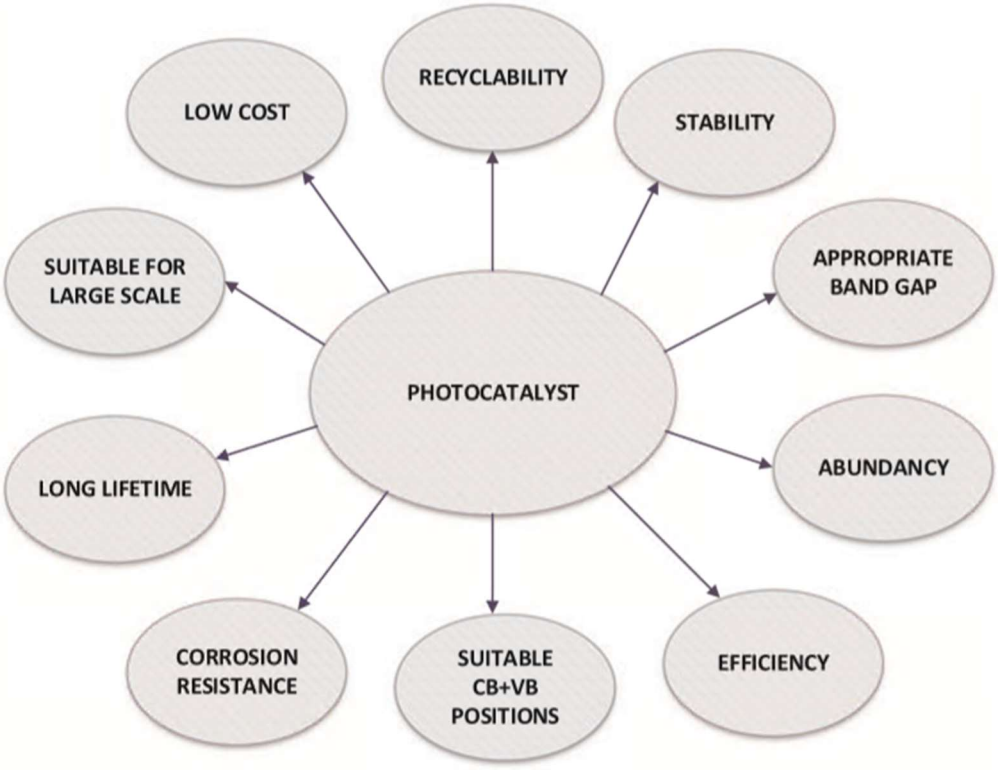

Figure 6 Photocatalyst properties for hydrogen production adapted form[58]

After Honda and Fujishima successfully decomposed water into H_2 and O_2 using solar energy in the 1970s using TiO_2 [54,55], there have been many studies searching for effective photocatalysts for water splitting in the UV region[68–76]; see Figure 7. The following sections will discuss some of the related works in the literature.

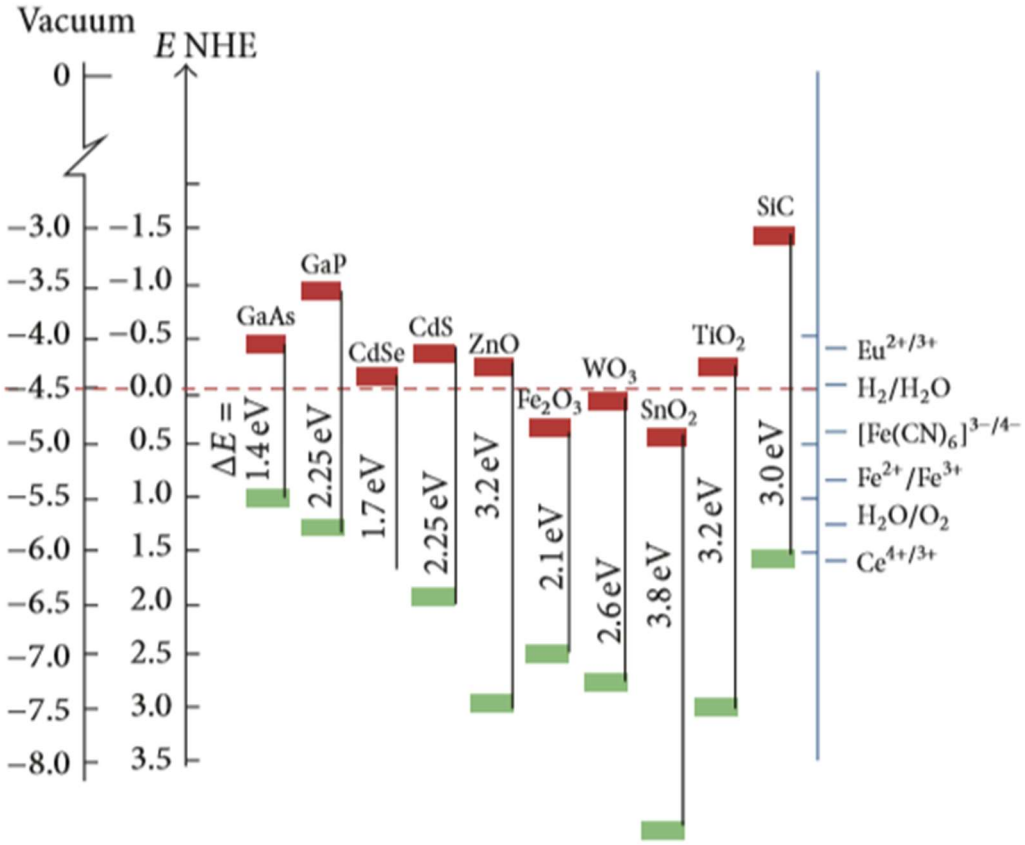

Figure 7 Comparison between different semiconductors and water redox potential[77]

2.2 Two-dimensional photocatalysts materials

The development of highly efficient photocatalysis can help to achieve practical water splitting. In the literature, there has been much study of photocatalysis for water splitting. Two-dimensional materials and three-dimensional materials can be used as photocatalysts in both the UV and visible regions of the electromagnetic spectrum. According to Tang et al., the optical and electronic properties of 2D materials are usually better than those of 3D materials [56,78]. Two-dimensional materials generally have a small charge transport distance and high surface-to-volume ratio, which make them more suitable to be used as photocatalysts[59]. Particle size and crystal structure

have a high impact on the performance of photocatalysts. In the overall photocatalytic water splitting literature, many nanomaterials have been found to be more efficient than those with large particle size[79]. However, that is not always the case as the performance depends on the nanomaterial features.

Following graphene discovery[47], many 2D materials have been discovered for applications in water splitting[55]. There has been large interest in finding effective 2D materials for water splitting in regards to optical properties[80–82], thermal[83,84], electronic[85–88] and distinctive mechanical properties[89]. Interestingly, defects[90,91], solvents[92,93], adsorption[94,95], stress[96,97], and external electric fields[98,99] can effectively modulate the physical and chemical properties of 2D materials, greatly expanding the potential for their application. Two-dimensional materials are also very interesting in photocatalytic water splitting because of their intrinsic advantages: high specific surface, adequate adsorption and catalyst sites, high mobility of transporters, short migration distances of transporters and excellent mechanical properties[100–103]. Nevertheless, there are some challenges encountered with 2D materials when it comes to implementing them in water splitting. Because 2D materials are thin, the carriers that are excited by light tend to remain in the same area and rapidly combine with each other. Photocatalytic water splitting is negatively affected by the rapid recombination of photoinduced carriers[104,105]. The photocatalytic performance of certain 2D materials is restricted by their surface catalytic activity and their limited capacity for light absorption[106].

The following sections will discuss several promising 2D materials for hydrogen production.

2.2.1 Metal oxides

Many metal oxides, such as TiO_2, ZnO, WO_2, and $BiVO_4$ [107,108], have been studied both theoretically and experimentally to demonstrate their performance as materials for 2D photocatalytic water splitting [109–114]. TiO_2 nanosheets have a large band gap (3.2 eV to 3.8 eV) compared to their bulk form but similar semiconducting traits. The e-h photogenerated pairs in nanosheets have better redox ability as these pairs have higher CB and lower VB than the bulk[115]. Su et al. reported that compared to planar, heterojunction is an effective technique that helps to enhance efficiency by combining features from each element [107]. They concluded that $WO_3/BiVO_4$ heterojunction films improved the PEC performance, as a result of high surface area and charge separation of the $WO_3/BiVO_4$ interface[107,108]. Tungsten trioxide, WO_3, and bismuth vanadate, $BiVO_4$, showed promising properties as a photocatalyst.[116–120] Wang and Liu reported that 2D WO_3 nanomaterial increased charge transport and reduced the recombination rate, which can increase surface area when using it as supporting material.

A variety of techniques have been used to improve the photocatalytic and PEC activity of $BiVO_4$. These methods involve: forming nanocomposite structures[107], controlling morphologies[121,122], doping[123] and coupling with oxygen evolution catalysts (OECs)[124]. In their study, Zhang et al. found that TiO_2 surface and bulk defects can help split electron-hole pairs, improve light absorption and improve donor capacity.[125]

It's worth noticing that very recently, researchers have successfully exfoliated 2D Fe_2O_3 monolayer within a few of angstroms (hematene) from natural iron ore hematite (α-Fe_2O_3)[126]. The amazing part of this work is that different from graphene or MoS_2, hematene is a non-van der Waals 2D material derived from bulk hematite of

which layers are tightly bonded by chemical bonds (as shown in Figure 8 (a)). This discovery could open a new gate for the exploration of 2D materials with exotic properties. Heterostructure composed of hematene and titania nanotubes has shown enhanced visible light photocatalytic activity. The band alignment of this heterostructure is shown in Figure 8 (b): photoelectrons in the CB of hematene transferred to the CB of TiO_2 and then reduce water into H_2 while the holes in the VB of hematene turned water into O_2. The drawback of 2D metal oxide is obvious: due to the strong chemical bonds between its atomic layers, more energy is needed to obtain ultrathin monolayers from its bulk phase.

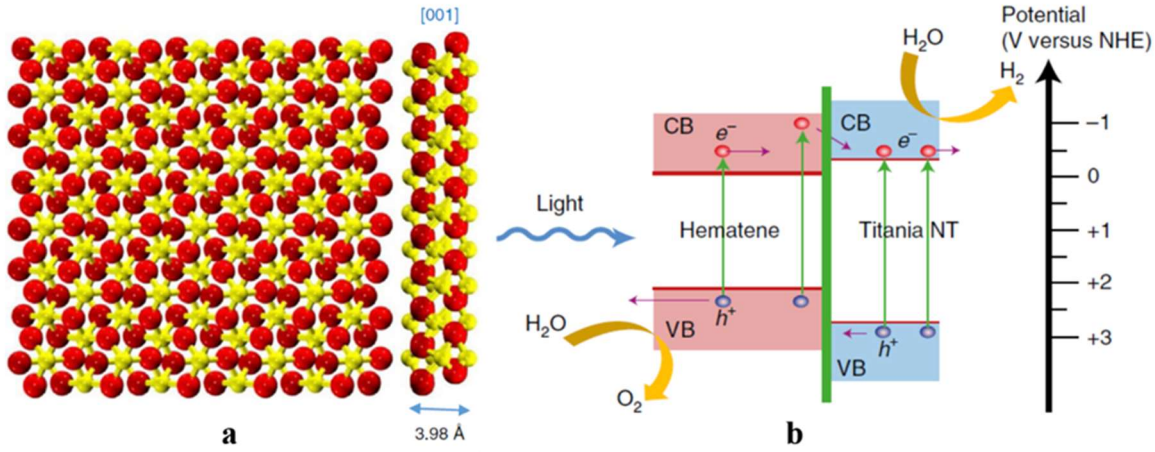

Figure 8 (a) Atomic structure of 2D hematene. (b) schematic representation of e-h transfer between hematene and TiO_2[126]

.

2.2.2 Transition metal Dichalcogenides

Many transitions metal dichalcogenides (TMD) have attracted attention as promising candidates for photocatalysis. Hai et al. stated that a single layer MoS_2 nanosheet has a band gap of 1.8 eV[127] and that this can make it suitable for water splitting. They produced MoS_2 and WSe_2 nanosheets by mechanical exfoliating and their study demonstrated that MoS_2 and WSe_2 can be used in hydrogen production

applications[127]. Monodisperse tin disulfide, SnS_2, has been claimed by Jing et al. to have properties for photocatalysis application[128]. The obtained SnS_2 nanosheets showed high photocatalytic hydrogen production, and the results demonstrated that SnS_2 nanosheets have outstanding response in the visible light region in comparison with other SnS_2 morphologies[128]

When exfoliated from its bulk phase, 2D MoS_2 nanosheet has a direct band gap of 1.8 to 1.9 eV[129] which makes it a perfect photocatalyst with proper band edges and good visible-light absorption ability. As shown in Figure 9 (a), with the decrease of thickness, the band gap of MoS_2 increases and shows an indirect to direct conversion.[32] The black arrow in Figure 9 (a) shows the thickness dependent band gap. It can be seen clearly from Figure 9 (b) that the CBM (vs. NHE) of bulk MoS_2 is too high to trigger the reduction of water while the CBM of monolayer MoS_2 is lowered to an appropriate position so that it can have high enough potential to split water into H_2.

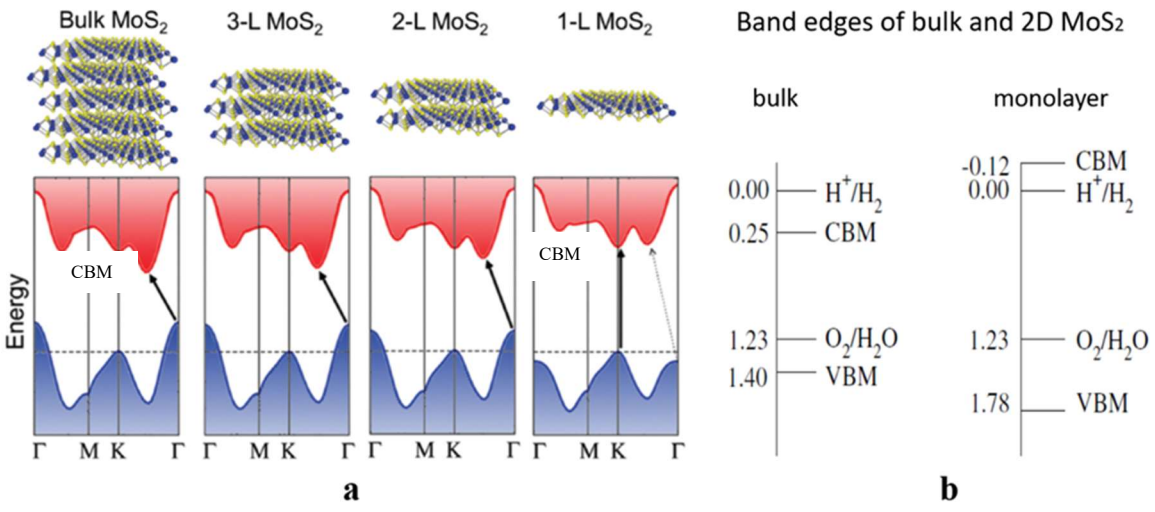

Figure 9 (a) Thickness dependent band structures of bulk, 3-layered, 2-layered and monolayer MoS_2.[130] (b) Band edges of bulk and monolayer MoS_2, (vs. NHE)[131].

Besides 2D MoS_2, there are also many other 2D metal chalcogenides which can be used as suitable photocatalysts, such as XS_2 (X = Sn, Ti, W, and Zr)[127,128,132–

[134], XSe_2 (X = Mo and W)[127,135]. They are attracting not only because of their excellent catalytic and absorption properties but also due to their low cost compared to noble metals. The mainly limitation for 2D metal chalcogenides is their low carrier mobility. For example, the carrier mobility of MoS_2 only ranges from 0.5 $cm^2V^{-1}s^{-1}$ to 180 $cm^2V^{-1}s^{-1}$ [136], depending on the different contacting substrates. Such low carrier mobility will greatly hinder the transport of e-h pairs and decrease the photocatalytic efficiency.

2.2.3 Metal free photocatalysts

There are many metal-free 2D materials, such as graphene[137], phosphorus[138], binary carbon nitride[139], graphitic carbon nitride and hexagonal boron nitride (h-BN)[140] and so on. Graphene is the first kind of 2D material people ever found, by mechanically exfoliating from its bulk phase. It has a hexagonal structure due to the sp^2-hybrid carbon atoms, shown in Figure 10 (a). The carrier mobility of graphene is very high, and it has excellent stability and large surface area. However graphene has no bandgap[46] (shown in Figure 10 (b)) thus it cannot be used as photocatalyst because it has no band gap, although it has high stability and surface area[141]. The band position of GO is shown in Figure 10 (c) and the CB of GO has high overpotential to generate H_2 from water and excited electrons could interact with the water molecules directly, whereas the holes in VB of GO interact with hole accepter (methanol) instead of water molecule.

Graphitic carbon nitride (g-C_3N_4) has some features that can make it a suitable catalyst, including large surface area and good stability[142]. Zheng et al. improved the conductivity of g-C_3N_4 by combining it with carbon, and they showed it to be a promising oxygen reduction reaction (ORR) electrocatalyst[142]. Ping et al. proposed a thermal oxidation method to prepare g-C_3N_4 nanosheets from the bulk. Their nanosheet experiment results showed larger surface area, increased band gap and

better electron transport compared with bulk g-C_3N_4 under UV–visible and visible light[139]. Black phosphorus (BP) showed potential as a good alternative 2D material for several electronic applications[138].

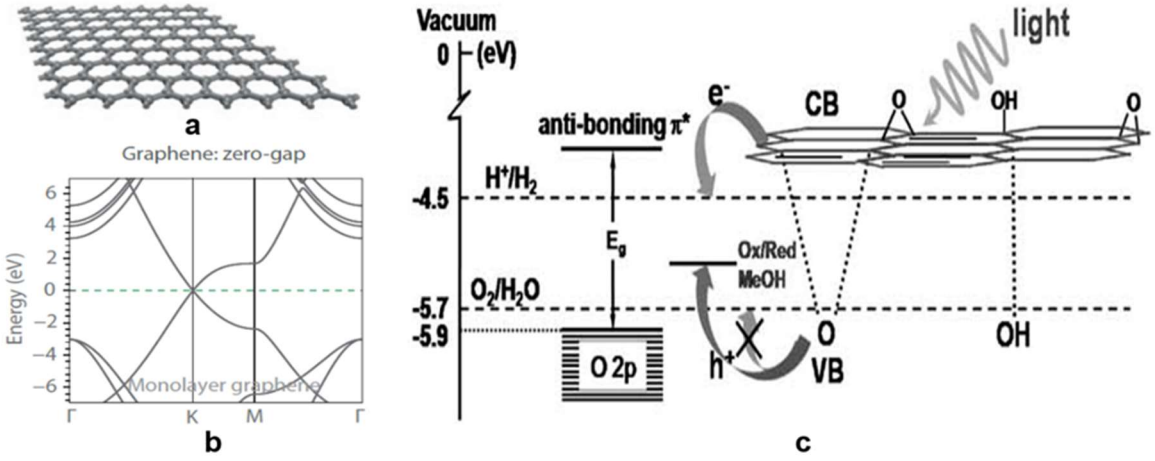

Figure 10 (a) Structure of graphene[141]. (b) Band structure of graphene[141]. (c) Schematic energy-level diagram of GO[143].

g-C_3N_4 has become increasingly popular because of its eco-friendly composition, easy manufacturing and appropriate band alignments[144–149]. Different shapes, such as nanosheets and hollow spheres, have been proposed[139,150]. Introducing sulfur to g-C_3N_4 through doping can alter its band structure and lead to increased reactivity[151–153]. The band structure of 2D g-C_3N_4 are shown in Figure 11 (a). The band gap calculated by Perdew-Burke-Ernzerhof (PBE) functional is only 1.2 eV (Figure 11 (b)) which is far smaller than the experimental value of 2.7 eV. However, the HSE06 functional gives us a more accurate description of the band gap 2.7 eV for g-C_3N_4, as shown in Figure 11 (c). This difference is understandable since PBE always underestimates the band gap. If we want to get the accurate band gap by DFT calculations, applying HSE functional in the calculation will be a good choice. The

main problems of the above-mentioned metal free 2D materials are the poor light absorption due to the large band gaps and the unstable structures.

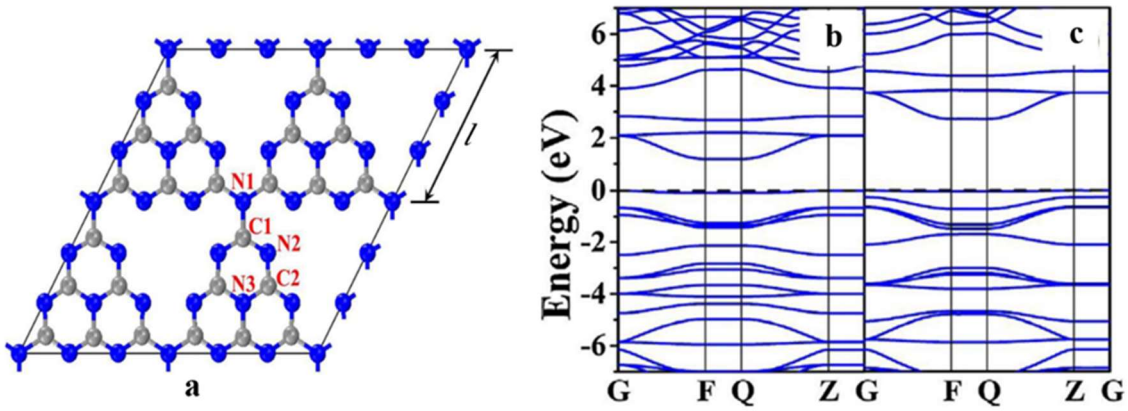

Figure 11 (a) structure of g-C3N4. (b) Band structure calculated by PBE functional. (c) Band structure calculated by HSE06 functional[154].

2.2.4 Improving Photocatalytic Performance of 2D Material

This section will briefly summarise the most popular and practical ways to improve the photocatalytic activity of 2D materials. The first method is band engineering-the band structure of 2D material could be modified by elemental doping, straining and defect engineering. Doping means introducing impurities to the host material, which can effectively increase the number of charge carriers and result in positive visible light response. Some successful examples are nitrogen doped graphene[155], phosphorous doped g-C_3N_4[156], Rh doped $Ca_2Nb_3O_{10}$[157], Tb doped $Ca_2Ta_3O_{10}$ nanosheets[158], etc.. Defects would influence the structure of material thus have remarkable effects on the photocatalytic properties. For example vacancy in MoS_2 accelerates the capture of free water molecules[159]. Defects in g-C_3N_4 would lead to a narrower band gap, enhancing the solar absorption property of g-C_3N_4[160]. Monolayer material can also sustain high mechanical strain which give us freedom to manipulate the band structure of 2D materials by strain. For example the band gap and band edges of phosphorene can be modified by applying strain[161]. Another method is

to construct heterojunctions or co-catalysts. The main idea is combining light harvesting semiconductors and appropriate co-catalyst together which usually promotes the process of photocatalytic water splitting.

2.3 Methods for water splitting

2.3.1 Photoelectrochemical (PEC) Water Splitting

Water splitting using photoelectrochemical technology holds great promise for capturing and storing Earth's abundant solar energy[43,54,147,162]. Water oxidation is the most challenging reaction in this technology, involving four electrons and four protons. A large energy input is typically required to drive this electrochemical reaction because of the kinetic barriers.

In PEC, usually one or two photoelectrodes are used to absorb photonic energy and one of the photoelectrodes is coated with semiconductor materials[58]. In 1972, Fujishima and Honda used a titanium dioxide, photoanode and a platinum (Pt) cathode as the first PEC device for water splitting[54]. Since then, many semiconductors have been studied for use in PEC, such as ZnO, $BiVO_4$, WO_3 and n-type and p-type silicon [58].

PEC Principle:

When solar light reaches the semiconductor electrode, part of the sunlight is absorbed by electrons in the VB. Gaining more energy, the electrons jump to the CB, which creates a hole (positive charge) in the VB, and these electron-hole pairs are excitons. When achieving separation of these excitons into an electron and a hole, these will cross the system and the electron creates electricity. The pH of the cell influences the reaction to assist with water splitting. In an acidic cell (low pH) the

charge transfer occurs by holes (h^+) and generates H^+ ions and produces an oxygen evolution reaction (OER).

$$2H_2O\ (l) + 4h^+ \rightarrow O_2\ (g) + 4H^+ \text{ (at low pH) at anode}$$

The hydrogen ions, H^+, diffuse through the water while the electrons in the anode travel through an external circuit to the cathode. Then these electrons combine with H^+ to produce hydrogen gas, and this known as a hydrogen evolution reaction (HER).

$$4H^+ + 4e^- \rightarrow 2H_2\ (g) \text{ (at low pH) at cathode}$$

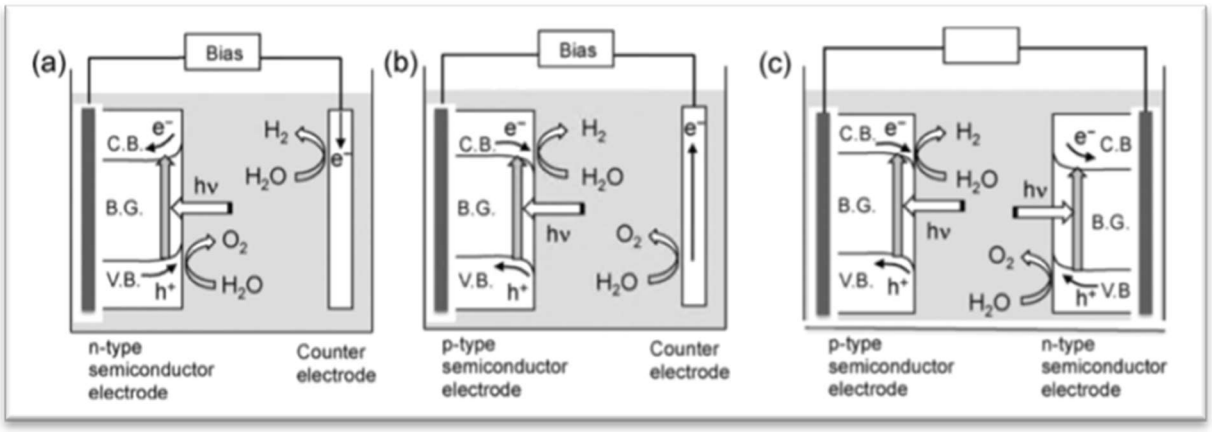

Figure 12 Photoelectrochemical water splitting systems using n-type semiconductor photoanode (a), p-type semiconductor photocathode (b), and tandem system (c)[163]

2.3.2 Photocatalysis / Photovoltaic (PV) Electrolysis Water Splitting

In the photocatalysis process, water is split into H_2 and O_2 with the use of the electron holes pairs that are produced by a photocatalyst [58,164–166]. In PV electrolysis, PV panels are utilised as an electricity source[58]. According to Joshi et al., hydrogen production through PV methods has low efficiency compared to other methods, and this might be due to low PV efficiency[167].

2.4 Summary and Implications

This research project focused on hydrogen production using photocatalysis water splitting, and discovering effective semiconductors, with particular emphasis on

2D materials, also known as single-layer materials. Such materials are claimed to have unique properties, such as absorbing much higher incident light compared to their 3D counterparts. Dimensionality reduction could be beneficial in increasing surface area and decreasing migration distance; therefore, these properties can improve photocatalytic performance to a certain degree. This research focused on identifying materials that may be candidates for improving performance in the field of water splitting technology.

Chapter 3: Research Design

The Methodology and research design are described in Section 3.1, which illustrates the density functional theory used in this research. A description of the instrument can be found in Section 3.2. More information about the analysis used in this research is outlined in Section 3.3.

3.1 Methodology and Research Design

3.1.1 Methodology

The methodology used in this research involved the application of theoretical principles from quantum physics to determine and forecast the properties of nanoscale materials. This was accomplished by conducting a computational study using computer software for all the topics presented in the research. In this research, the calculations were based on density functional theory that is implemented in the Vienna Ab initio Simulation Package (VASP)[168,169]. The use of simulation is efficient and more cost and time effective than performing experiments when testing conditions for obtaining the best performance of 2D materials. The properties that are important for a crystal to be used as a photocatalyst involve suitable band gap, stability, electronic properties, band-edge alignment, charge transfer, optical absorption and strain response; these can be calculated using the DFT method, and the approximation equations are mentioned below.

3.1.2 Schödinger Equation

The Schrödinger equation is a differentiation equation that can be used for multi-particle systems to describe the way particles behave through space and time. It can be expressed as the following:

$$\widehat{H}\psi(r,R) = E\psi(r,R) \quad (1)$$

Where $\widehat{H}$ *is* Hamiltonian operation, $\psi(r,R)$ is the wave function of a quantum system, E is total energy at $\psi(r,R)$, r is a set of all electronic coordinates and R is a set of nuclear coordinates.

The **Born-Oppenheimer approximation** is a simplified interpretation of the Schrödinger equation. It can be expressed as:

$$H\varphi(r,R) = (H_e + H_{e-N})\varphi(r,R) = E\psi(r,R) \quad (2)$$

Because nuclei are heavier and slower than electrons, it is more reasonable to treat each one separately (variable separation) and that is the purpose of the Born-Oppenheimer approximation.

The Hamiltonian operator in the above equation for N-electron systems can be represented as

$$H(r,R) = H_e + H_N + H_{e-N} = T_e(r) + V_e(r) + T_N(R) + V_N(R) + V_{e-N}(r,R) =$$

$$\sum_i^N \left(-\frac{\hbar^2}{2m_i}\nabla_i^2 - \sum_I^M \frac{Z_I e^2}{|r_i - R_I|}\right) + \frac{1}{2}\sum_{i,j}^N \left(\frac{e^2}{|r_i - r_j|}\right) + \sum_I^M \left(-\frac{\hbar^2}{2M_I}\nabla_I^2\right) + \frac{1}{2}\sum_{i,j}^M \left(\frac{Z_I Z_J e^2}{|R_i - R_j|}\right)$$

(3)

where, $T_e(r)$, $V_e(r)$, $T_N(R)$, $V_N(R)$ and $V_{e-N}(r,R)$ represent kinetic energy of electrons, Coulomb interaction between electrons, kinetic energy of nuclei, Coulomb interaction between nuclei and Coulomb interaction between electrons and nuclei,

respectively. Since there are too many electrons and nuclei, it is impossible to solve the equation exactly. A reasonable approximation is necessary to simplify the complicated equation.

Because the mass of a nucleus is 10^3–10^5 times larger than that of an electron, the velocity of a nucleus is far less than that of an electron. It is reasonable to treat the movements of electrons and nuclei separately. That is the main idea of the Born-Oppenheimer approximation. In this approximation, it is assumed that nuclei are stationary when considering the motion of electrons and nuclei are moving in a negative electric field made by electrons. Thus, the Schrödinger equation will be simplified as follows:

$$H\varphi(r,R) = (H_e + H_{e-N})\varphi(r,R) = E\psi(r,R) \qquad (4)$$

3.1.3 Hartree-Fock Approximation

Even after the Born-Oppenheimer approximation simplified the Schrödinger equation, it is still a difficult process to precisely calculate the interactions between electrons. Hartree's hypothesis was that electrons are moving in an average potential field, and therefore the motion of a single electron depends only on the average density distribution of the whole electron cloud. The multiplication of all electrons can substitute the wave function of the system by:

$$\varphi(r) = \varphi_1(r_1)\varphi_2(r_2) \dots \varphi_n(r_n) \quad (5)$$

and this is called the Hartree wave function. Then, the Hartree equation can be derived:

$$\left[-\nabla^2 + V(r) + \sum_{i'(\neq i)} \int dr' \frac{|\varphi_{i'}(r')|^2}{|r'-r|}\right]\varphi_i(r) = E_i\varphi_i(r) \quad (6)$$

The Hartree-Fock equation can be obtained by taking the anti-symmetry of electronic exchange into account; the equation involves the interaction between electrons but does not consider the anti-parallel spin electrons:

$$[-\nabla^2 + V(r)]\varphi_i(r) + \sum_{i'(\neq i)} \int dr' \frac{\left|\varphi_{i'}(r')\right|^2}{|r-r'|}\varphi_i(r) - \sum_{i'(\neq i),\|} \int dr' \frac{\varphi_{i'}^*(r')\varphi_i(r')}{|r-r'|}\varphi_{i'}(r) = E_i\varphi_i(r) \quad (7)$$

3.1.4 Kohn-Sham Equation

The function of electron density can express the ground state properties of a system. Kohn and Sham introduced the idea that kinetic energy can be obtained by non-interacting particles that produce the same density as the system of interacting particles. Using the Kohn-Sham equation, the properties of a material in the ground state and also the wave function of the ground state can be obtained. Knowing that the electron density of N particles is $\rho(r) = \sum_{i=1}^{N}|\varphi_i(r)|^2$, the Kohn-Sham equation is:

$$[-\frac{1}{2}\nabla^2 + v_{eff}(r)]\psi_i(\mathrm{r})=\varepsilon_i\psi_i(\mathrm{r}) \ (8)$$

where $v_{eff}(r)$ is the Kohn-Sham potential and can be written as:

$$v_{eff}(r) = v(r) + \int dr' \frac{\rho(r\prime)}{|r-r\prime|} + \frac{\delta E_{xc}(\rho)}{\delta\rho(r)} \ (9)$$

3.1.5 Exchange-Correlation Functional

There are some methods that have been introduced to estimate the exchange correlation functional of certain physical quantities, and they are:

a) Local Density Approximation (LDA)

LDA is a class of density functional theory where functional values can be estimated from the value of ρ at a point. LDA can be expressed as follows:

$$E_{xc}^{LDA}[\rho(r)] = \int \rho(r)\, \varepsilon_{xc}[\rho(r)]dr \ (10)$$

where ε_{xc} is the exchange correlation energy at position r, and it can be computed exclusively from the local value of ρ. LDA is derived from uniform electron gas, that is, uniform density at every position in the space. There are a number of forms for LDAs, for example, Perdew-Zunger (PZ81), Cole-Perdew (CP) and Perdew-Wang (PW92) All these forms are based on E_{xc}^{LDA}[170–172].

b) General gradient approximation (GGA)

GGA is a more sophisticated and accurate estimation of exchange correlation functional than LDA, which usually fails to describe systems with rapid electron density change. GGA considers the gradient of the electron density, and it can be expressed as:

$$E_{xc}^{GGA}[\rho(r)] = E_{xc}[\rho(r), |\nabla\rho(r)|] \quad (11)$$

GGA shows improvements in accuracy over LDA. GGA is a useful method for obtaining accurate outcomes for molecular geometries, electronic structures, ground-state energies, and other relevant properties. There are various forms of GGA available, including PW91, PBE, and Becke88[172–174]. Each form has its unique characteristics and is appropriate for different types of computations. Utilising GGA in computational research provides a reliable way to evaluate complex systems and helps researchers better understand the fundamental principles underlying a range of physical phenomena.

c) Hybrid Functional (HF)

For more accurate band structures, HF can be used in some of the calculations. HF involves a portion of exact Hartree-Fock approximation, and the rest of the terms are from semi-local or local density or PBE functional. There are many kinds of HF

functionals, for instance, HSE03 and HSE06 [175,176]. The exchange-correlation of HSE06 functional can be expressed as:

$$E_{xc}^{HSE} = \frac{1}{4}E_x^{SR}(\mu) + \frac{3}{4}E_x^{PBE,SR}(\mu) + E_x^{PBE,LR}(\mu) + E_c^{PBE} \quad (12)$$

3.2 Research Design

The main aim of this research was to identify novel two-dimensional materials as catalysts for improving hydrogen production through water splitting. The process of producing electricity by this method is not simple to execute. This thesis aims to identify an ideal method to reduce the dependency on fossil fuel using an alternative way to produce energy with minimal impact on the environment. To reach this aim, Water Splitting could be used with some 2D materials that have not been tested before. Such materials include $MgAl_2S_4$, $AgGAP_2Se_6$, AlSI, AlSeBr, AlSeI, ScSI, ScSeBr, ScSeCl, ScSeI and InSI. More information on these materials can be found in Chapters 4 to 6. This research investigates materials properties by looking for high carrier mobility, good light absorption, mechanical flexibility, thermal conductivity. DFT and the software VESTA and Material Studio were used to test these materials. Origen, Photoshop, and Diagram applications were used to render results as images.

3.3 Instruments

A. Software:

- Vienna Ab initio Simulation Package (VASP)
- Xshell
- phonopy
- QuantumEspresso
- CALYPSO

- Excel
- Zotero
- Visualization for Electronic and Structural Analysis (VESTA)
- Materials Studio
- Origin

B. Hardware:

- Desktop computer
- Printing facilities
- High Performance Computing (HPC) & Research Support
- National Computational Infrastructure (NCI)
- Magnus
- Material projects

Most of these facilities are currently provided by QUT.

- The library database, as well as the printing facilities are two of the other resources available.

3.4 Analysis

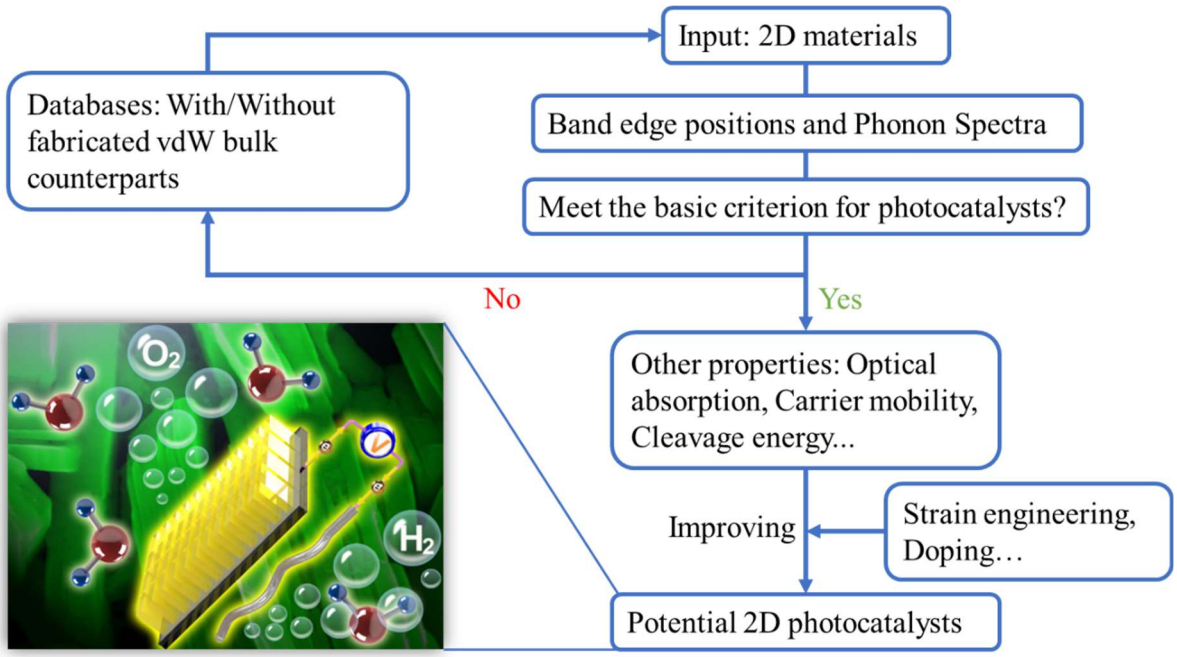

Figure 13 The method used to investigate the materials of interest in this research.

This research focuses on discovering 2D materials with exceptional properties using first-principles calculations, specifically through DFT calculations using the Vienna Ab initio Simulation Package (VASP) to analyse atomic geometry, electronic structure, atomic forces, magnetic properties, electric polarisation and optical absorption. To further process the outputs of the DFT calculations, we employed Phonopy, CALYPSO, and Monte Carlo codes for phonon spectra, structural prediction and critical temperature. Figure 13 shows how the method used to investigate the materials of interest in this research.

For all calculations, five different files were required: INCAR, POSCAR, POTCAR, KPOINTS and a Linux OS-dependent job-script file, each with a different purpose. The INCAR file is specific to the software and includes 'key-tags' and a numerical value assigned to the desired characteristic related to the calculation. The

POSCAR file includes the sequence of elements and the atomic Cartesian coordinates of each atom in the material's defined crystal structure. The POTCAR file contains the 'pseudopotential' of each atomic species used in the calculations, and the VASP software supplier provides the POTCAR files of all elements in a periodic table for user simulations/calculations. The KPOINTS file includes the coordinates of the symmetry points in the first Brillouin zone of the material according to its crystal lattice. The first four input files (INCAR, POSCAR, POTCAR, KPOINTS) should not be changed for any material system, while the job-script file can be named according to conventional computer file naming.

All calculations related to our research were conducted using supercomputing facilities from the National Computational Infrastructure (NCI), supported by the Australian Government through QUT, and the High-Performance Computing (HPC) at QUT. We have published three peer-reviewed journal articles, and a fourth article has been submitted for review and publication.

The study focuses on 2D structures of selected compounds, including $MgAl_2S_4$, $AgGaP_2Se_6$, AlSI, AlSeBr, AlSeI, ScSI, ScSeBr, ScSeCl, ScSeI and InSI. The research methods included are:

- Geometrical optimisation through ground state energy relaxation.
- Phonon structure analysis.
- Ab-initio molecular dynamics (AIMD) calculation.
- PBE and HSE06/Wannier90 band structure analysis.
- Band gap estimation.
- Optical properties for estimating light harvesting properties.

- Band gap variation with respect to tensile strain and compressive stress.
- Schematic representation of calculated properties to assess potential photocatalytic applications.
- Band edge calculations.
- Alignment correction with vacuum potential after HSE06 band structure predictions.
- Interface charge density difference calculations for perovskite surfaces and potential HTM materials (organic and inorganic).

Chapter 4: Two-dimensional $MgAl_2S_4$ as Potential Photocatalyst for Water Splitting and Strategies to Boost its Performance

4.1 2D materials, $MgAl_2S_4$

Exploring novel 2D water-splitting photocatalysts and finding strategies to boost their efficiency are two important tasks in nowadays energy regime. Here, employing first-principal calculations, we predicated a novel 2D material, $MgAl_2S_4$ monolayer, and studied its potential applications in photocatalytic water splitting. This monolayer is noble metal-free and possesses great thermal and dynamical stability. The cleavage energy is around 16 meV/Å^2 which is even lower than graphene, indicating the high feasibility for experimental fabrications. The band edge positions, and the optical absorption spectra indicate the pristine $MgAl_2S_4$ monolayer can work as a photocatalyst upon ultraviolet irradiation. Its high electron mobility around 745 $cm^2v^{-1}s^{-1}$ and high conduction band minimum (CBM) position suggest a high reduction ability. Furthermore, we illustrate the oxidation and light absorption abilities of this monolayer can be significantly enhanced by tensile strain. The complementary marriage of $MgAl_2S_4$ and $SnSe_2$ monolayers can form a direct z-scheme heterostructure, which can fully utilize the photocatalytic potential of both components.

Statement of Contribution of Co-Authors for Thesis by Published Paper

The authors listed below have certified that:

1. they meet the criteria for authorship in that they have participated in the conception, execution, or interpretation, of at least that part of the publication in their field of expertise;
2. they take public responsibility for their part of the publication, except for the responsible author who accepts overall responsibility for the publication;
3. there are no other authors of the publication according to these criteria;
4. potential conflicts of interest have been disclosed to (a) granting bodies, (b) the editor or publisher of journals or other publications, and (c) the head of the responsible academic unit, and
5. they agree to the use of the publication in the student's thesis and its publication on the QUT's ePrints site consistent with any limitations set by publisher requirements.

Title and Date: Two-dimensional $MgAl_2S_4$ as Potential Photocatalyst for Water Splitting and Strategies to Boost its Performance 2022.

Contributor	Statement of contribution*
Abdulrahman Alhaidar	Investigation, Data curation, Writing – original draft.
Aijun Du	Supervision, Funding acquisition.
Lei Zhang	Conceptualization, Investigation, Formal analysis, Writing – review & editing, Supervision.

Two-dimensional $MgAl_2S_4$ as Potential Photocatalyst for Water Splitting and Strategies to Boost its Performance

Abdulrahman Alhaidar[1,2], Lei Zhang[1,2] and Aijun Du[1,2] *

1 Centre for Materials Science, Queensland University of Technology, Brisbane, QLD
4000, Australia

2 School of Chemistry and Physics, Science and Engineering Faculty, Queensland University of Technology, Gardens Point Campus, Brisbane, QLD 4000, Australia

4.2 Introduction

Hydrogen production by photocatalytic water splitting has drawn intensive research interest nowadays due to the increasing demand for clean and renewable energy[43,54]. The key in to sunlight-driven water splitting is the semi-conductive photocatalysts which can generate photoexcited electron-hole pairs with redox abilities upon light irradiation[20,28,177]. Nevertheless, the conventional three dimensional (3D) photocatalysts have a low specific surface area, leading to limited reactive sites participating in the water redox reaction. The interior photoexcited carriers also need to migrate to the surface which would increase the possibility of their recombination. Such intrinsic flaw can limit the photocatalytic efficiency of the 3D photocatalysts[27,178]. As a result, the 2D photocatalysts have been paid continuous attention in the past decade due to their intrinsic high specific surface area and minimum carrier migration distance compared with their 3D counterparts[55,179–182].

To date, a wide variety of 2D materials have been discovered but only a few of them show photocatalytic capacity because some basic criteria have to be met. A potential candidate must possess band edge positions straddling the water redox potential, the ability to absorb solar irradiation, and stable a freestanding structure[20,55]. The wide light absorption range, low e-h recombination rate, spatially separated catalytic sites, and strong redox ability under various pH conditions are also highly desired to improve the photocatalytic efficiency[178]. Unfortunately, it is extremely hard to find a perfect photocatalyst possessing all these advantages simultaneously. Most of the discovered 2D photocatalysts have their flaws such as high cost (PtSSe[183] and $PdSeO_3$[179] containing noble elements), low carrier mobility (MoS_2),[184] low light absorbance (g-C_3N_4),[185] unstable structures (2D metal oxides like Fe_2O_3),[126] and so forth. Hence, the hunt for novel 2D photocatalysts with as many merits as possible

remains imperative. Moreover, searching for effective strategies to fulfill the potential of a proposed photocatalyst is also a challenging but crucial task. 2D materials have flexible structures and intrinsic reduced dimensions, which make it possible to tune their photocatalytic performance via strain modulation[186–188] and heterostructures design[189,190]. However, the inappropriate strain and unfitting components for a heterostructure can even lead to declined photocatalytic ability. It would be instructive to shed light on how to improve the photocatalytic capacity by these two methods when proposing a new 2D photocatalyst.

In this work, using density functional theory (DFT) calculations, we theoretically predict a new kind of 2D material, $MgAl_2S_4$ monolayer, and studied its potential applications in photocatalytic water splitting. 2D $MgAl_2S_4$ is noble elements free and does not contain toxic compositions which will benefit commercial use. They possess great thermal and dynamical stability and can be easily exfoliated from their bulk phases. Hybrid functional calculations revealed the indirect band structure of 2D $MgAl_2S_4$ and it shows high electron mobility around 1500 $cm^2v^{-1}s^{-1}$. The band edge positions of pristine $MgAl_2S_4$ straddle the water redox potential in all pH conditions. A moderate tensile strain can be applied to further enhance its oxidation and light absorption abilities. Moreover, a direct z-scheme $MgAl_2S_4/SnSe_2$ heterostructure can be constructed which possesses high redox ability, spatially separated e-h pairs, and pronounced light absorbance.

4.3 Computational details

The DFT calculations were carried out by the Vienna Ab Initio Simulation Package (VASP).The exchange-correlation and electron-ion interactions were described by generalized gradient approximation (GGA) of the Perdew-Burke-Ernzerhof (PBE) type[191] and the projector augmented-wave (PAW) method,[192]

respectively. The kinetic energy cut-off was set to 400 eV, and the Gamma-Centred k-point mesh of 11×11×1 was applied to sample the first Brillouin zone. The structures were fully optimized until the maximum residual force acting on each atom and the energy of the whole system were converged to 0.005 eV/Å and 10-6 eV, respectively. The electronic structures were calculated by Heyd-Scuseria-Ernzerhof (HSE06) hybrid functional[193] and the optical absorption spectra including excitonic effects were predicted by solving the Bethe-Salpeter equation (BSE)[194] on top of single-shot GW (G0W0)[195] calculations. The phonon spectra were computed using the density functional perturbation theory (DFPT) as implemented in the Quantum ESPRESSO code[196,197]. The thermal stability of the $MgAl_2S_4$ monolayer was studied by an Ab initio molecular dynamics (AIMD) simulation lasting for 10 ps. The time step of 1 fs and NVT ensemble controlled by Nose-Hoover thermostat[198] were applied in the simulation.

For 2D materials, the carrier mobility is given by the following expression[199–202]:

$$\mu_{2D} = \frac{e\hbar^3 C_{2D}}{k_B T m_e^* m_d (E_l)^2} \qquad (2)$$

where e is the electron charge, $\hbar$ is the reduced Plank constant, k_B is the Boltzmann constant and T is the temperature. C_{2D} is the elastic constant in the transport direction derived from $(E - E_0)/S_0 = C(\Delta l/{l_0}^2)/2$, where E and S_0 are the total energy and surface area of the 2D material respectively, l_0 is the lattice constant along the transport direction and Δl is the corresponding deformation. m_e^* is the effective mass of the charge carriers and m_d is the average effective mass calculated by $m_d = \sqrt{m_a^* m_b^*}$. For hole mobility, m_a^* and m_b^* denote the carrier effective mass along with GM and KG respectively. While for electron mobility, m_a^* and m_b^* represent the carrier effective mass along with GM and MK respectively. E_l is the deformation potential of the VBM

or the CBM along the transport direction, defined as $E_l = \Delta V/(\Delta l/l_0)$ where ΔV is the change of VBM or CBM upon deformation Δl.

4.4 Results and discussion

4.4.1 Properties of pristine $MgAl_2S_4$ monolayer

The bulk phase of the $MgAl_2S_4$ exhibits stratified structures with the space group of R-3m[203,204]. Each unit cell contains three monolayers stacking to each other with van der Waals interaction, indicating the feasibility to prepare the $MgAl_2S_4$ monolayer by mechanical exfoliation method. The calculated lattice constants of the bulk crystal are a=3.69 Å and c=36.60 Å, which are in good agreement with the experiment data, as listed in Table S (1). The $MgAl_2S_4$ monolayer possesses sandwich-like structures consisting of AlS-MgS_2-AlS atomic layers as shown in Figure 14 (a-b). It's clearly shown in Table S (1) that the calculated lattice constants of the monolayer are quite close to that of the bulk phase, demonstrating the interlayer interactions in the bulk $MgAl_2S_4$ are considerably weak, which is desired for the mechanical exfoliation at a low energy cost.

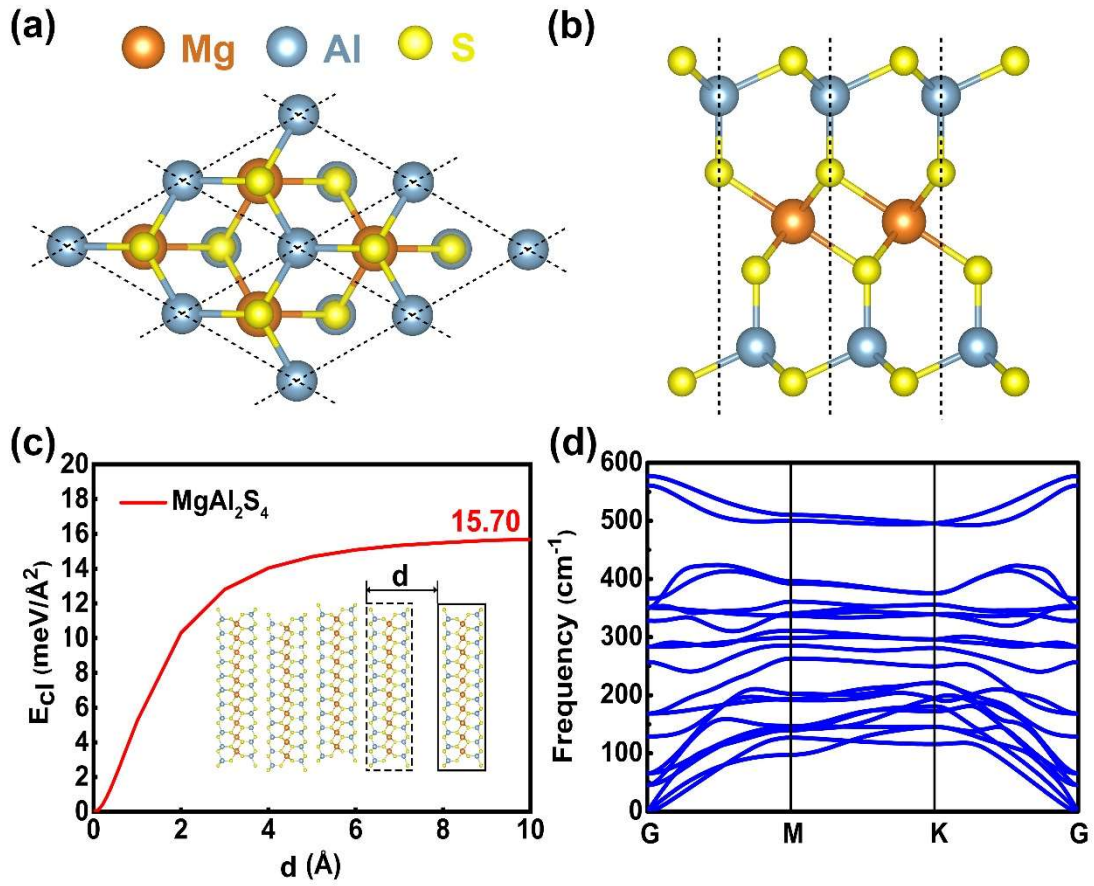

Figure 14 (a) and (b) Top view and side view of the $MgAl_2S_4$ monolayer respectively. The dashed line represents the border of the unit cell. (c) Cleavage energy E_{cl} as a function of separation distance d. Inset is the model used to calculate E_{cl}. (d) Phonon spectrum of the $MgAl_2S_4$ monolayer.

To verify the feasibility of obtaining a $MgAl_2S_4$ monolayer, two computational methods were applied. The first one is calculating the formation energy, E_f, which determines the strength of the interlayer van der Waals interactions. The lower the E_f is, the less energy is needed to exfoliate the monolayer from its bulk phase. The E_f is defined as[59,187]

$$E_f = \frac{E_{2d}}{n_{2d}} - \frac{E_{3d}}{n_{3d}} \quad (1)$$

where E_{2d} and E_{3d} are the total energy of the 2D and 3D unit cells respectively, and n_{2d} and n_{3d} are the numbers of atoms in the 2D and 3D unit cells respectively. The

calculated E_f for $MgAl_2S_4$ is 27.31 meV/atom, which is far smaller than that of MoS_2 (77 meV/atom)[205]. To give a more intuitionistic description of the energy cost when exfoliating a $MgAl_2S_4$ monolayer, the cleavage energy (E_{cl}) is calculated by evaluating the energy consumption to extract the top layer from the surface of the bulk phase. As shown in Figure 14 (c), the $MgAl_2S_4$ has a small E_{cl} of (15.70 meV/Å^2) and it is noticeable that this value is even smaller than that of graphene (~21 meV/Å^2) and phosphorene (~22.7 meV/Å^2)[206] which have already been fabricated by experimental methods. Considering the small E_f and E_{cl}, it's expected the $MgAl_2S_4$ monolayer can be extracted from its bulk forms at a low energy cost. The stability of $MgAl_2S_4$ monolayer is then checked by the phonon spectrum and AIMD calculations. Its phonon spectrum is shown in Figure 14 (d). It can be seen that there are no imaginary frequency phonons in the whole Brillouin zone which demonstrates the dynamical stability of $MgAl_2S_4$ monolayer. Its thermal stability is proved by AIMD simulations, as shown in Figure S1. It's clear that, even under a high temperature of 900 K, its structure only oscillates around the equilibrium positions and the energy fluctuates within a narrow window, indicating the great thermal stability of 2D $MgAl_2S_4$.

After examining the stability of $MgAl_2S_4$ monolayer, we now focus on its electronic properties. The orbital projected band structure calculated by the HSE06 functional is presented in Figure 15 (a). It's clear that the $MgAl_2S_4$ monolayer exhibits an indirect band gap of 3.14 eV. The VBM is located at the G point and dominated by the *p*-orbitals of chalcogen elements, whereas the CBM lies at the M point and originates from the *p*-orbitals of Al atoms. It's worth noting that the different compositions of CBM and VBM imply the electrons and holes upon photoexcitation will have different spatial locations. This is further illustrated in the partial charge densities of CBM and VBM, as shown in Figure 15 (c). The charge density of CBM is

located on the surface of the monolayer while the charge density of VBM is around the inner S atoms, which can reduce the probability of electron-hole recombination. The carrier effective mass and carrier mobility of $MgAl_2S_4$ monolayer were then investigated based on the electronic structures. As listed in Table 2, the electron mobility of the $MgAl_2S_4$ monolayer reaches about 745 $cm^2v^{-1}s^{-1}$ which is significantly larger than many 2D photocatalyst such as MoS_2 (<200 $cm^2v^{-1}s^{-1}$),[136] hydrogenated graphene (105 $cm^2v^{-1}s^{-1}$)[200] and $MnPSe_3$ (625 $cm^2v^{-1}s^{-1}$)[180]. It can be seen that the electron mobility shows a strongly directional dependence. The electron mobility along the M-K line is almost twice times larger than that along the G-M line, which originates from the anisotropic effective electron mass along the two directions. Moreover, the huge difference between the electron and hole mobility will also benefit the separation of electron-hole pairs.

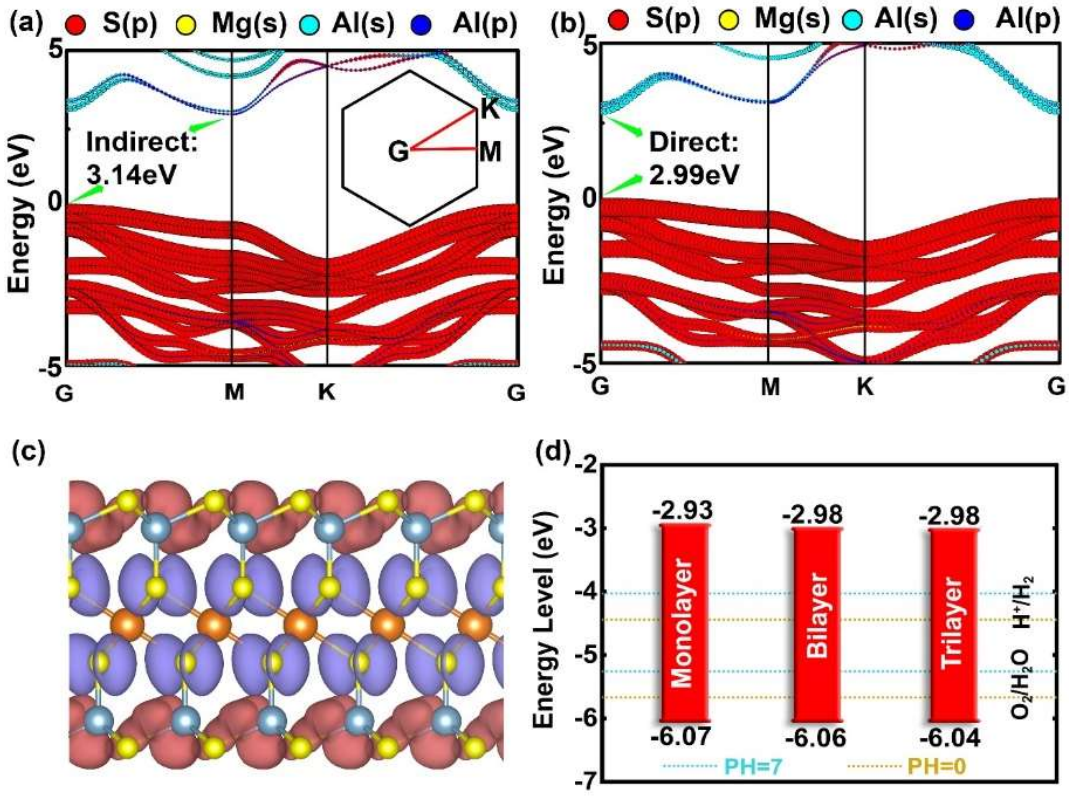

Figure 15 (a) and (b) Orbital projected band structures of pristine and 3% stretched $MgAl_2S_4$ monolayer. The insets represent the first Brillouin zones, and the size of dots illustrates the projected weight of the orbitals. Fermi levels are set to zero. (c) Partial density of charge of band edge. Pink and purple colour represents the charge density of CBM and VBM respectively. (d) Band edge positions of monolayer, bilayer, and trilayer $MgAl_2S_4$.

Table 2 Carrier mobility of $MgAl_2S_4$ monolayer calculated by HSE06 at the temperature of 300K. m* represents the carrier effective mass (in electron mass) for a given direction; E_{def} and C_{2D} are the deformation potential and 2D elastic modulus, respectively.

Carrier type	Direction	m*	E_{def} (eV)	C_{2D} (Jm^{-2})	μ ($cm^2v^{-1}s^{-1}$)
Electron	GM	0.85	4.32	122.57	393.34
	MK	0.21	6.80	142.27	745.71
Hole	KG	1.56	6.50	142.27	20.17
	GM	3.31	5.84	122.57	10.17

A potential photocatalyst shall possess appropriate band edge positions so that the excited electron and holes would have enough driven forces to actuate the splitting of water. The CBM has to be higher than the reduction potential of H^+/H_2 (E_{H^+/H_2}) meanwhile the VBM shall be lower than the oxidation potential of O_2/H_2O (E_{O_2/H_2O}). The redox potentials with respect to the vacuum level depend on the pH value and we take this into consideration by the following equations[207]:

$$E_{H^+/H_2} = -4.44\ \text{eV} + \text{pH} \times 0.059\ \text{eV} \quad (3)$$

$$E_{O_2/H_2O} = -5.67\ \text{eV} + \text{pH} \times 0.059\ \text{eV} \quad (4)$$

As shown in Figure 15 (d), the $MgAl_2S_4$ monolayer has adequate band edge positions straddling the redox potentials at all pH values from 0 to 7, implying its robust photocatalytic capacity under various pH conditions. It's worth noting that its CBM level is 1.51 eV above the water reduction potential at pH = 0 condition. With such a high CBM level and electron mobility, an ideal reduction efficiency can be expected for 2D $MgAl_2S_4$. Furthermore, the band edge positions of 2D $MgAl_2S_4$ are less dependent on the thickness due to the weak interlayer interactions (the band structures of the bilayer, trilayer, and bulk $MgAl_2S_4$ are shown in Figure S (2), which will benefit the practical fabrications because the requirement for the thickness of photocatalysts can be loosened. In the following part, we will mainly focus on the monolayer as the monolayer has the highest specific surface area.

Another important property of a photocatalyst is its ability to absorb light. To explore the optical response, the light absorbance spectrum was calculated by the G0W0-BSE method, as shown in Figure 16 (b) It's clear that 2D $MgAl_2S_4$ shows pronounced optical absorption in the ultraviolet (UV) region. However, the light

absorption onset is only about 385 nm, suggesting the unmodified $MgAl_2S_4$ monolayer may behave poorly in the visible region of sunlight. 2D $MgAl_2S_4$ is expected to have promising photocatalytic efficiency upon UV light, just like the most famous photocatalyst, TiO_2 (light absorption onset of 390 nm)[208]. It should be noted the light-harvesting ability could be further enhanced by applying external strain or constructing heterostructure, as discussed below.

4.4.2 Strategies to improve the photocatalytic ability

So far, we have illustrated the potential applications of the $MgAl_2S_4$ monolayer in photocatalytic water splitting and some drawbacks were also unveiled. $MgAl_2S_4$ monolayer can efficiently catalyze the redox reaction of water splitting in various pH conditions, but its visible light absorption is poor. Is there any way that we could eliminate the disadvantage and fulfill the potential of 2D $MgAl_2S_4$? Strain modulations are widely applied to modify the electronic or optical properties of 2D materials,[209] raising a potential route to enhance the photocatalytic ability of 2D $MgAl_2S_4$. We first checked the maximum strain the monolayer can withhold as shown in Figure S (3a). 2D $MgAl_2S_4$ possesses flexible structures that can even sustain a biaxial strain as large as 26%, giving a large space for strain engineering. The band edge positions and band gaps as functions of biaxial strain on the PBE level are shown in Figure S (3b). As the increase of strain, the VBM shows a continuous decreasing trend while the CBM and band gaps exhibit a volcano-like change. A small amount of tensile strain can lower the band gap of $MgAl_2S_4$ (thus increasing its optical absorption onset) and decrease the VBM (thus enhancing the oxidation ability). It should be noted that the CBM drops more significantly than the VBM when tensile strain is applied, thus the magnitude of tensile strain should be carefully controlled to avoid the total loss of reduction capacity.

The tensile strain of 3% and 6% was then applied to $MgAl_2S_4$ monolayer and their properties were studied by HSE06 and BSE calculations to prove our PBE results. As shown in Figure 16 (a), the strain diminishes the band gaps significantly (from 3.14 eV to 2.99 eV and 2.68 eV for the strain of 3% and 6%, respectively) and the band edge levels are downshifted by the tensile strain which is the same as our PBE prediction. It's remarkable that even if a large tensile strain of 6% is applied, the CBM of $MgAl_2S_4$ is still 0.21 eV higher than the reduction potential of H_2/H_2O at pH=7 (0.62 eV higher at pH=0). This gives large freedom to control the electronic properties of 2D $MgAl_2S_4$ by tensile strain. Due to the decreased band gap, a prominent redshift (shown in Figure 16 (b)) is observed for stretched $MgAl_2S_4$ monolayer. The optical absorption onset is lifted to the visible light region: ~430 nm for 3% strain and ~480 nm for 6% strain, indicating the optical absorption ability is efficiently strengthened by tensile strain. Besides, an interesting indirect to direct band gap transition is observed for - $MgAl_2S_4$ monolayer when tensile strain is applied. The band structure of 3% stretched $MgAl_2S_4$ monolayer is shown in Figure 16 (b) as an example. The CBM moves from M point to G point while the VBM remains at G point, resulting in a direct band gap. It's known the direct excitation is easier to take place because such excitation requires no assistance of phonon, thus stretched 2D $MgAl_2S_4$ can have a higher exciton generation rate which is important to improve the photocatalytic efficiency.

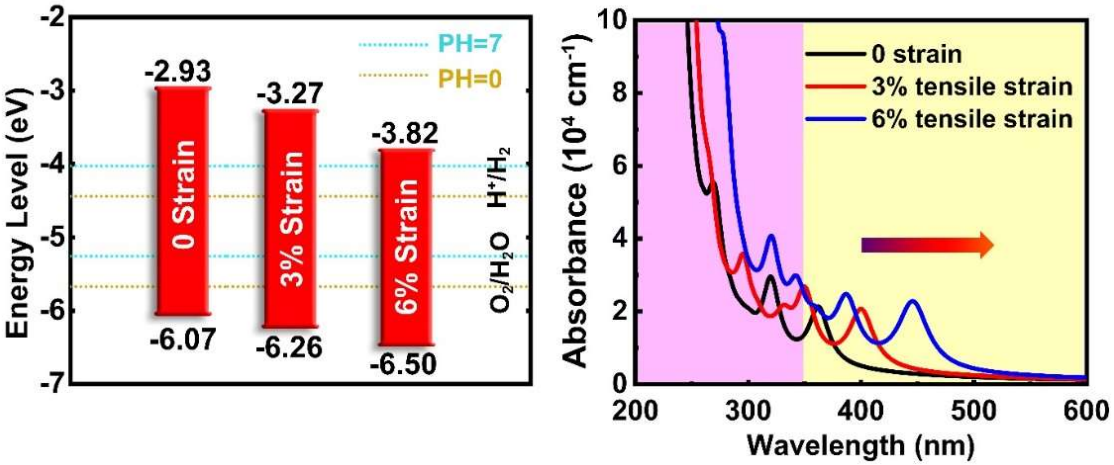

Figure 16 (a) Band edge positions of $MgAl_2S_4$ monolayer with and without tensile strain with respect to the vacuum level. The redox potentials at pH=0 and pH=7 is represented by brown and blue dotted lines respectively. (b) Light absorption spectra of $MgAl_2S_4$ monolayer with and without tensile strain. The purple and yellow area represents the ultraviolet and visible region of sunlight respectively.

Another promising strategy to boost the photocatalytic potential of a material is to construct heterostructures. Among various types of heterojunction structures, the direct Z-scheme photocatalysts have drawn intensive research interests due to their merits in separating photoexcited electron-hole pairs and maintaining the respective advantages of each component[210]. The designing principle of direct Z-scheme heterostructures is discussed in detail in Mukhokosi et al work[211]. Guided by this principle, we theoretically designed a $MgAl_2S_4/SnSe_2$ direct Z-scheme heterostructure as shown in Figure 17 (b). The $SnSe_2$ monolayer has been experimentally fabricated[211] and it has a small band gap of 1.39 eV and quite negative VBM level as shown in Figure S (4), indicating its great light absorption and oxidation abilities. However, its CBM level is too low to trigger the water reduction reaction, thus cannot be directly used as an overall water-splitting photocatalyst. The lattice constant of 2D $SnSe_2$ (3.84 Å) is quite similar to that of $MgAl_2S_4$ (3.69 Å), making it a perfect partner to construct

heterostructure with $MgAl_2S_4$ monolayer. As shown in Figure 17 (a), the work function of $SnSe_2$ is 6.46 eV (on the HSE06 level) which is much larger than that of $MgAl_2S_4$ (5.90 eV). Thus, when $SnSe_2$ and $MgAl_2S_4$ monolayers are in contact, the electrons of $MgAl_2S_4$ would flow to $SnSe_2$ until their Fermi levels are aligned. This is also validated by the charge density difference of $MgAl_2S_4/SnSe_2$ heterostructures as shown in Figure 13 (b). The interaction surfaces of $SnSe_2$ and $MgAl_2S_4$ are negatively and positively charged respectively due to the charge redistribution, creating a built-in electric field from $MgAl_2S_4$ to $SnSe_2$.

Through band decomposition analysis, the band alignment in the $MgAl_2S_4/SnSe_2$ heterostructure is studied, as shown in Figure 17 (b). It is clear that such heterostructure has a staggered band alignment. Upon light irradiation, both $MgAl_2S_4$ and $SnSe_2$ can generate electron-hole pairs. The existence of a built-in electric field favors the recombination between the holes from $MgAl_2S_4$ and the electrons from $SnSe_2$. Meanwhile, the transfer of electrons from $MgAl_2S_4$ to $SnSe_2$ and holes from $SnSe_2$ to $MgAl_2S_4$ is hindered by the electric field. In this way, photoexcited electrons with more positive potential from $MgAl_2S_4$ and holes with more negative potential from $SnSe_2$ are preserved, leading to enhanced oxidation or reduction abilities than individual components. Noticeably, the band edge positions of the heterostructure straddle the water redox potential in all pH conditions from 0 to 7, suggesting its great adaptability to the chemical environment. Besides, the spatially separated electrons and holes can reduce the recombination rate of charge carriers and thus improve photocatalytic efficiency. The light absorption ability of $MgAl_2S_4/SnSe_2$ heterostructure is also studied by BSE calculations. As shown in Figure S (5), the light absorption coefficients of the heterostructures are much higher than the $MgAl_2S_4$ monolayer in the whole visible light region and the light absorption onsets even reach

the near-infrared region of sunlight. Hence, the $MgAl_2S_4/SnSe_2$ heterostructure is expected to have a high photocatalytic water splitting efficiency under a wide range of light conditions.

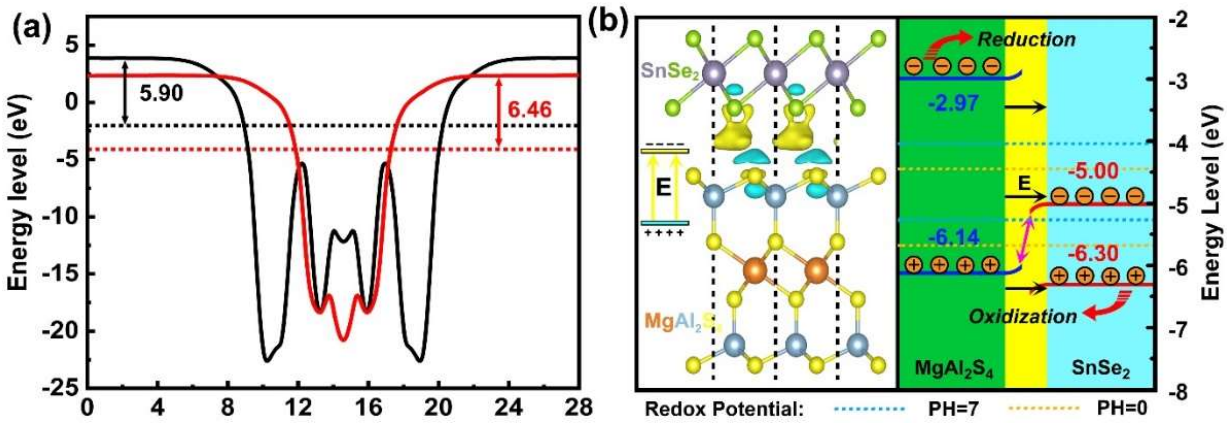

Figure 17 (a) The electrostatic potential of $MgAl_2S_4$ and $SnSe_2$ monolayers. Black and red lines represent $MgAl_2S_4$ and $SnSe_2$ respectively. The dashed line denotes the fermi level. (b) Left panel: The charge density difference for $MgAl_2S_4/SnSe_2$ heterostructures (isosurface values of 0.0001 e/Å^3). Right panel: Direct Z-scheme photocatalytic mechanism for $MgAl_2S_4/SnSe_2$ heterostructures. The band edge levels of $MgAl_2S_4$ and $SnSe_2$ in the heterostructures are shown in blue and red respectively.

4.5 Conclusion

In summary, we theoretically predicated $MgAl_2S_4$ monolayer as a new member of the family of 2D photocatalysts by DFT calculations. The small cleavage and formation energy show the high feasibility to fabricate this monolayer. The dynamical and thermal stabilities are proved by the phonon calculations and AIMD simulations. The band edge positions, and light absorption spectra show the photocatalytic capacity of pristine $MgAl_2S_4$ monolayer upon UV irradiation. A moderate tensile strain can be applied to overcome the poor light absorption in the visible range and improve its oxidation ability. Furthermore, based on 2D $MgAl_2S_4$, we designed direct Z-scheme heterostructures possessing high redox abilities and great visible light absorbance. Our

work not only proposes a potential 2D material for photocatalytic water splitting but also highlights the important role of structural engineering in the design of highly efficient photocatalysts.

Acknowledgments

We acknowledge generous grants of high-performance computing resources provided by NCI National Facility and The Pawsey Supercomputing Centre through the National Computational Merit Allocation Scheme supported by the Australian Government and the Government of Western Australia. A. D. also greatly appreciates the financial support of the Australian Research Council under Discovery Project (DP170103598).

4.6 Support information

Two-dimensional $MgAl_2S_4$ as Potential Photocatalyst for Water Splitting and Strategies to Boost its Performance

Abdulrahman Alhaidar[1,2], Lei Zhang[1,2] and Aijun Du[1,2] *

[1]*Centre for Materials Science, Queensland University of Technology, Brisbane, QLD 4000, Australia*

[2]*School of Chemistry and Physics, Science and Engineering Faculty, Queensland University of Technology, Gardens Point Campus, Brisbane, QLD 4000, Australia*

Table S1 Calculated structural parameters of $MgAl_2S_4$ bulk and monolayer using PBE functional along with corresponding experimental values if available.[203]

	space group	a	B	C
bulk cal. (exp.)	R-3m (R-3m)	3.689 (3.674)	3.689 (3.674)	36.593 (36.100)
monolayer cal.	P3m1	3.687	3.687	N/A

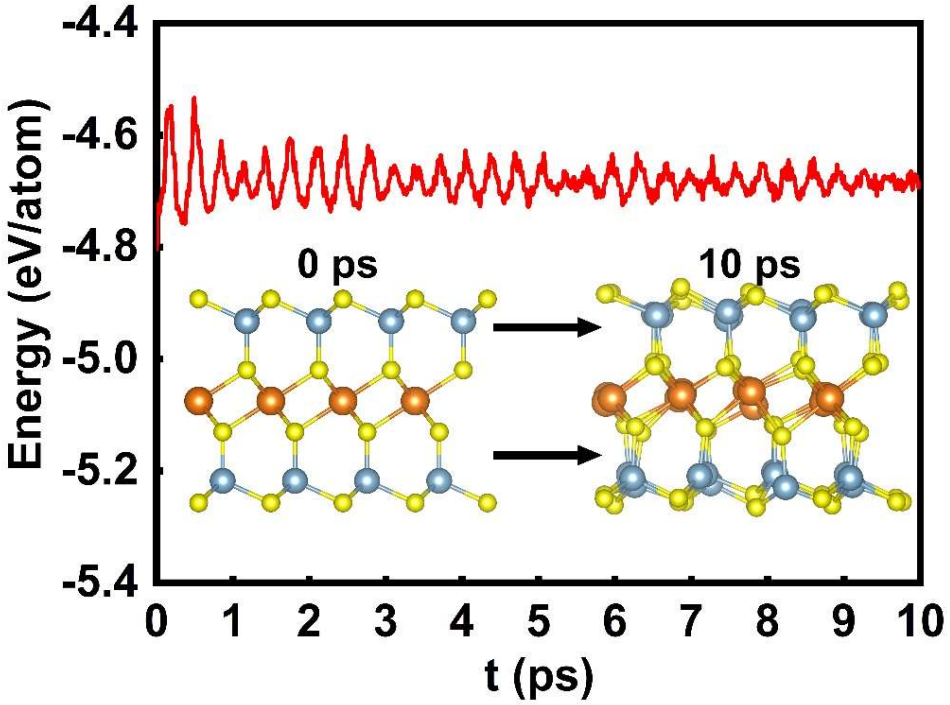

Figure S 1 The evolution of total energy per atom during AIMD simulation at 900 K. The insets are the structures of $MgAl_2S_4$ monolayer at 0 ps and10 ps.

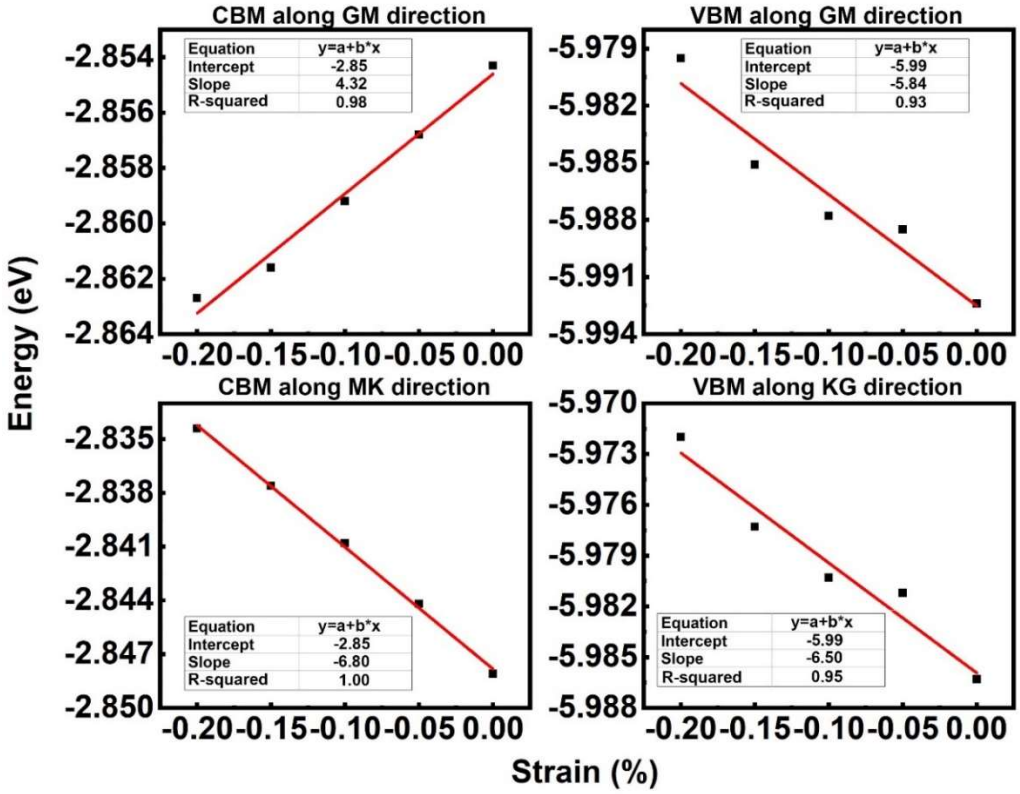

Figure S2. Band edge positions of 2D $MgAl_2S_4$ as a function of lattice deformation. The insets show the fitted equation, intercept, slope, and the R-squared (the coefficient of determination).

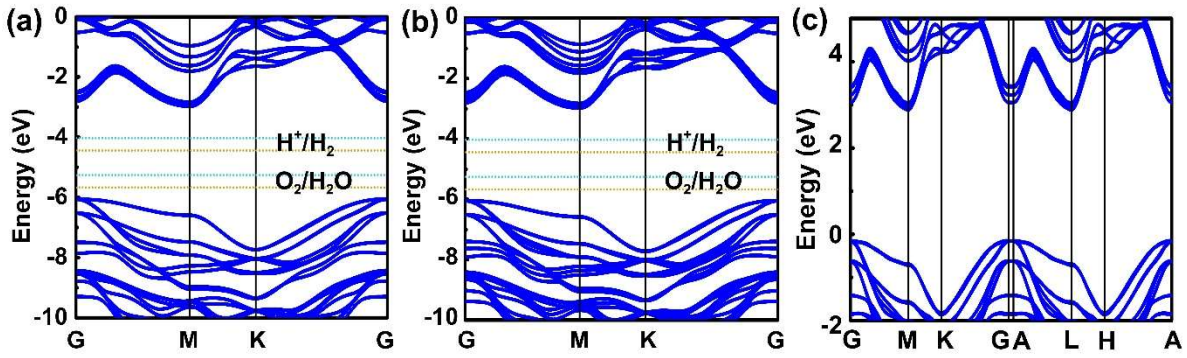

Figure S 3 (a), (b) and (c) The band structures on HSE06 level of the bilayer, trilayer, and bulk $MgAl_2S_4$ respectively. For bilayer and trilayer, the vacuum level is set to zero and the redox potentials at pH = 7 and pH = 0 are shown as blue and brown dotted lines respectively. For bulk phases, the fermi level is set to zero.

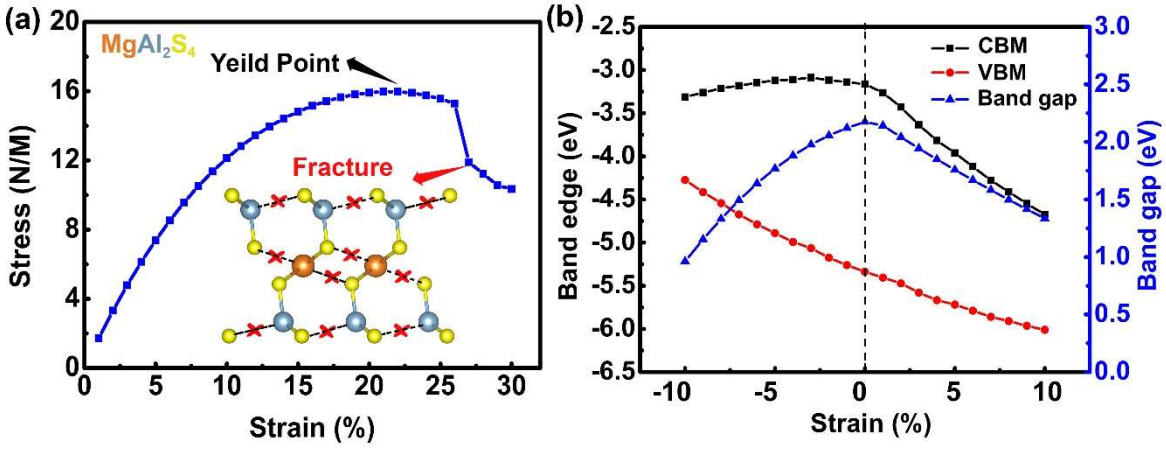

Figure S 4 (a) Stress in the $MgAl_2S_4$ monolayer subjected to biaxial strain. The insets are the ruptured structures after crack points. (b) Band gaps and edges (vs. vacuum level) as a function of biaxial strain for $MgAl_2S_4$ monolayer. Positive and negative strain represents tensile and compressive strain respectively.

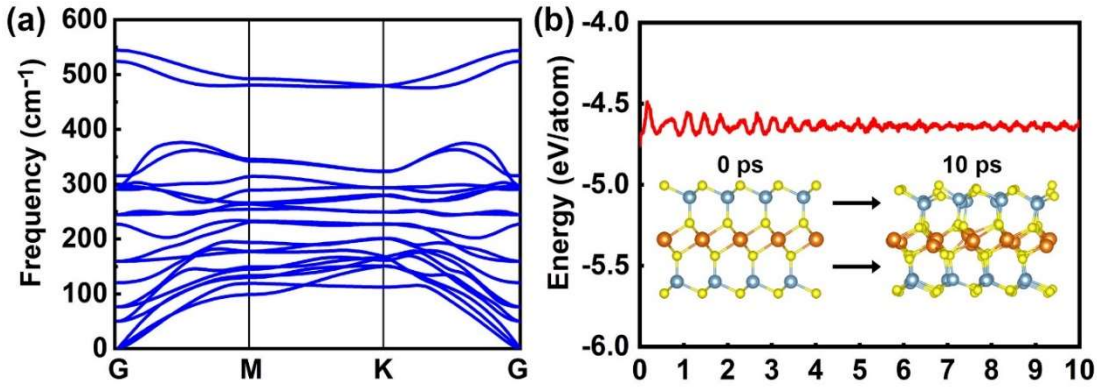

Figure S5. (a) and (b) The phonon spectra and the AIMD simulation results at 900 K for 2D $MgAl_2S_4$ under 6% biaxial tensile strain, respectively. The insets show the structures of $MgAl_2S_4$ at 0 ps and 10 ps. Clearly, no negative frequency can be found in the phonon spectra, which indicates the dynamical stability of 2D $MgAl_2S_4$ under 6% biaxial tensile strain. Moreover, even under a high temperature of 900 K, the atomic structure still survives, and the energy only fluctuates within a small range, suggesting the great thermal stability of 2D $MgAl_2S_4$ under 6% biaxial strain.

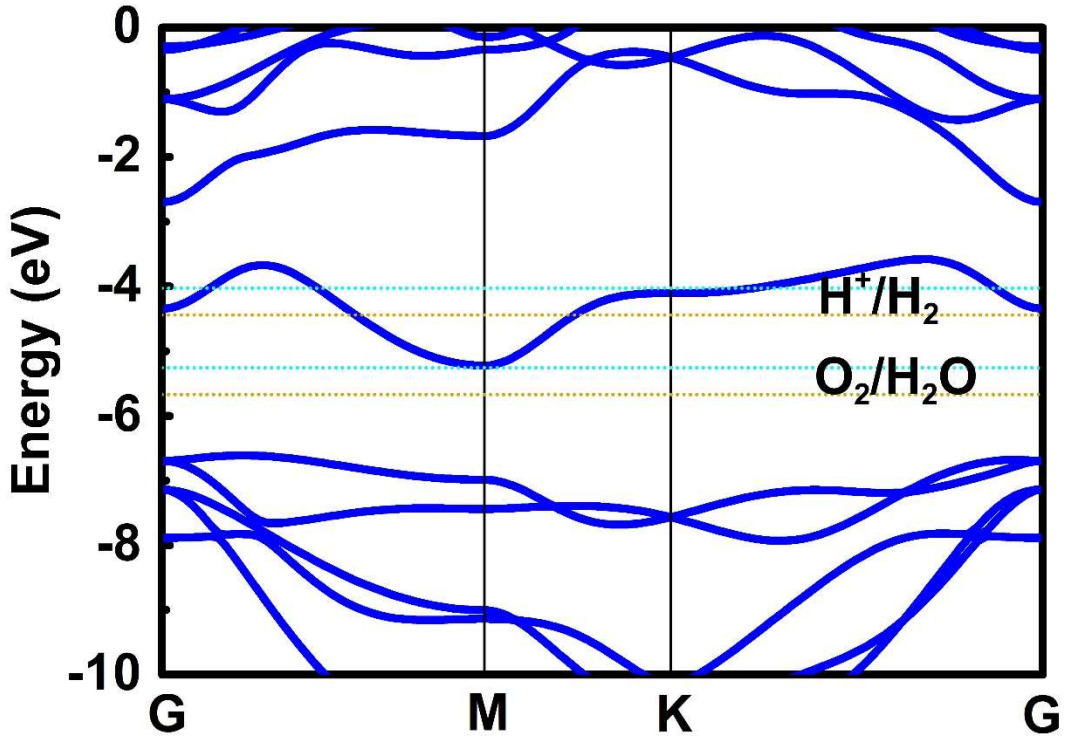

Figure S 6 The band structures on HSE06 level of monolayer $SnSe_2$ The vacuum level is set to zero and the redox potentials at pH = 7 and pH = 0 are shown as blue and brown dotted lines respectively.

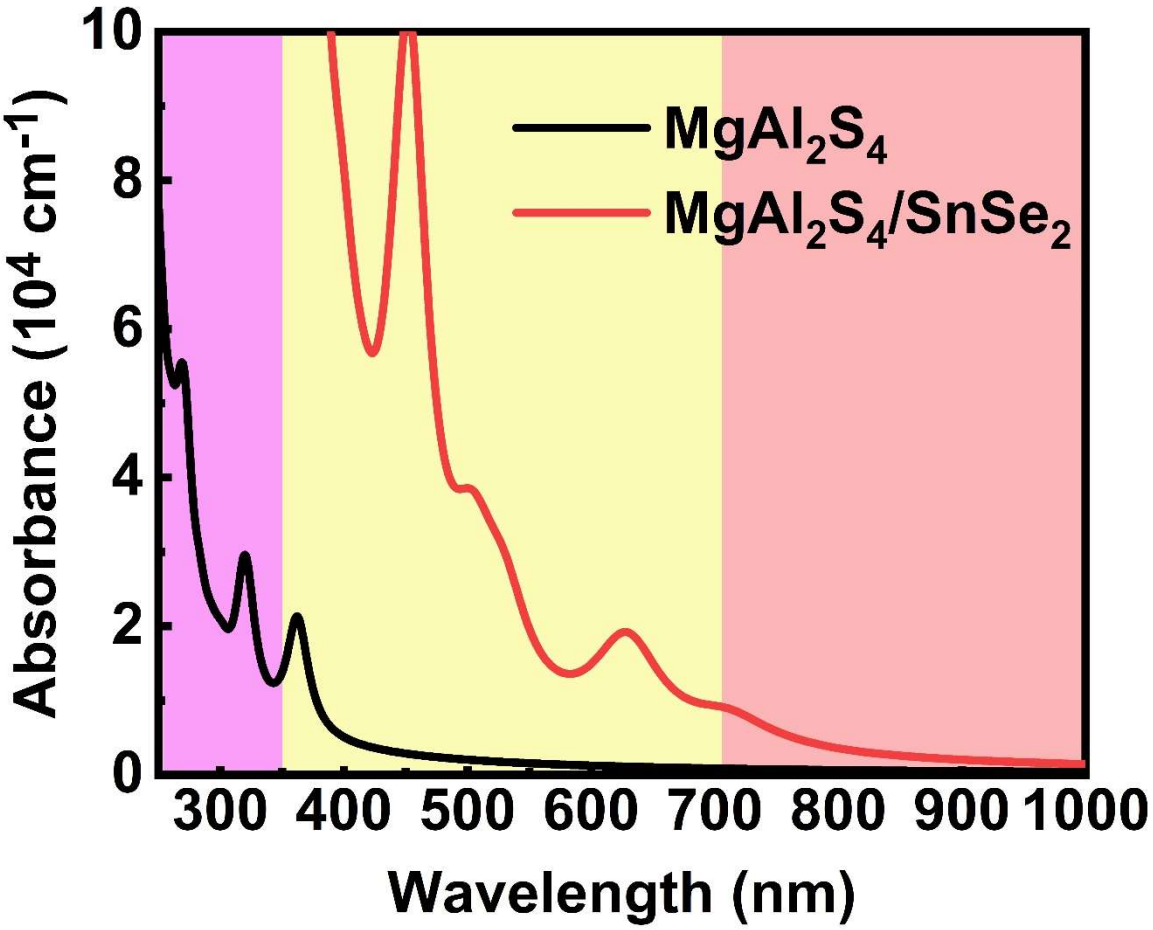

Figure S (7) Light absorption spectra of $MgAl_2S_4$ monolayer and $MgAl_2S_4/SnSe_2$ heterostructure. The purple, yellow, and pink areas represent the ultraviolet, visible, and near-infrared regions of sunlight.

Chapter 5: Strategies to Enhance the Performance of $AgGaP_2Se_6$ as a Two-dimensional Photocatalyst for Water Splitting

5.1 2D material: $AgGaP_2Se_6$

Photocatalytic water splitting is a suggested solution for the rapid increase in energy demand and environmental concerns. There has been an increasing interest in the improvement of efficient photocatalytic two-dimensional materials with excellent light absorption and band alignment for water splitting. In this thesis, we studied an unexplored 2D $AgGaP_2Se_6$ monolayer as a potential photocatalyst for water splitting, based on the first-principal calculations. Two-dimensional $AgGaP_2Se_6$ monolayers can be easily mechanically exfoliated from the bulk phase and are dynamically and thermally stable. The calculated band gaps for $AgGaP_2Se_6$ are 1.83, 1.53, 1.45 eV and 1.309 eV for mono-, bi-, tri-layered and bulk, respectively. In addition, they display excellent sunlight absorption, and the band edge positions for $AgGaP_2Se_6$ monolayers perfectly fit the water oxidation and reduction potentials. Therefore, $AgGaP_2Se_6$ monolayer would be a potential 2D photocatalyst that is suitable for water splitting.

Statement of Contribution of Co-Authors for Thesis.

The authors listed below have certified that:

1. they meet the criteria for authorship in that they have participated in the conception, execution, or interpretation, of at least that part of the publication in their field of expertise;
2. they take public responsibility for their part of the publication, except for the responsible author who accepts overall responsibility for the publication;
3. there are no other authors of the publication according to these criteria;
4. potential conflicts of interest have been disclosed to (a) granting bodies, (b) the editor or publisher of journals or other publications, and (c) the head of the responsible academic unit, and
5. they agree to the use of the publication in the student's thesis and its publication on the QUT's ePrints site consistent with any limitations set by publisher requirements.

Title and Date: Strategies to Enhance the Performance of $AgGaP_2Se_6$ as a Two-dimensional Photocatalyst for Water Splitting**.** This paper is submitted to the Arabian Journal of Chemistry 2023.

Contributor	Statement of contribution*
Abdulrahman Alhaidar	Investigation, Data curation, Writing – original draft.
Aijun Du	Supervision, Funding acquisition.
Lei Zhang	Review & editing, Supervision.

Strategies to Enhance the Performance of $AgGaP_2Se_6$ as a Two-dimensional Photocatalyst for Water Splitting

Abdulrahman Alhaidar[1,2], Lei Zhang[1,2] and Aijun Du[1,2] *
1 Centre for Materials Science, Queensland University of Technology, Brisbane, QLD
4000, Australia

2 School of Chemistry and Physics, Science and Engineering Faculty, Queensland University of Technology, Gardens Point Campus, Brisbane, QLD 4000, Australia

5.2 Introduction

Despite the fact that tremendous efforts have been made to identify materials that possess photocatalytic properties there is still long way to go. In contrast with their 3D equivalents, the 2D monolayers offer a larger surface area for photochemical reactions, while also having minimal carrier migration distances, both of which are extremely desirable for the achievement of highly efficient photocatalysis. The search for water splitting photocatalysts in recent years has therefore focused on 2D materials with a band gap ranging from 1.238 to 3.0 eV[159,194,198,199,201,212,]. Even though a large range of 2D materials has been identified, relatively few of them are capable of photocatalysis due to the need to satisfy the photocatalyst criteria that are mentioned before. Although the band edges of some 2D monolayers perfectly satisfy the redox potentials of water, some of the photogenerated electrons and holes may be insufficient to provide enough driving force for the overall splitting of the water molecules[78,213]. It is still highly desired to explore novel 2D materials with photocatalytic capabilities.

$AgGaP_2Se_6$ was discovered in 1992[214]. The bulk phases possess a layered structures in the space group of $P\bar{3}1c$ and it is possible to exfoliate the bulk to achieve monolayer $AgGaP_2Se_6$[214]. The band gap of the bulk phases is reported to be 1.309 eV, which is relatively small to guaranty to fit the band position of the water oxide and reduction potentials. The 2D $AgGaP_2Se_6$ monolayer has not been synthesised, and no experimental data are available to date. The aim of this work was to theoretically study the potential application of 2D $AgGaP_2Se_6$ as a photocatalyst for water splitting using DFT calculations. Two-dimensional $AgGaP_2Se_6$ monolayers have excellent thermal and dynamical stability, and they are also easy to exfoliate from their bulk phases, once

obtained. It is important to mention that the band edge positions of $AgGaP_2Se_6$ monolayer span the water redox potential.

5.3 Computational details

The DFT calculations have been performed using the Vienna Ab Initio Simulation Package [168,169,215]. As well as exchange-correlation interactions, electron-ion interactions were described by the generalised gradient approximation (GGA) of Perdew-Burke-Ernzerhof (PBE)[173,216] and the projector-augmented-wave (PAW) method[192]. For the first Brillouin zone, the gamma-centred k-point mesh was applied with 5 5 1 a cut-off of 500 eV. The structures were optimised until the maximum residual force acting on each atom and the whole system's energy converged to 0.005 eV/Å and 10^{-6} eV, respectively. A Heyd-Scuseria-Ernzerhof (HSE06) hybrid functional[193] was used to calculate electronic structures and, GW and (G0W0)[195] calculations were used to predict optical absorption spectra including charged electronic excitations. The phonon calculation was performed by PHONOPY code based on the finite-displacement method[217,218], with the convergence criteria for force and energy at 0.001 eV/Å and 10^{-8} eV, respectively. Ab initio molecular dynamics (AIMD) simulations were used to perform the calculation for the thermal stability of $AgGaP_2Se_6$ monolayer with a 3 × 3 × 1 supercell at 300 K for 10 ps with an applied time step of 1 fs. The simulations lasted for 10 ps in NVT ensemble controlled by a Nose−Hoover thermostat.[198]

5.4 Results and discussion

Stratified structures are observed in the bulk phase of $AgGaP_2Se_6$ with a space group of $P\bar{3}1c$[214]. Figure 18 (a) shows the top view, and (b) shows the side view of $AgGaP_2Se_6$ monolayer. The optimised parameters for $AgGaP_2Se_6$ bulk material were

a = 6.40Å, b = 6.40 Å, c = 13.43 Å and β = 120°, at the PBE-D3 level of theory. These values are in good agreement with the experimentally measured values (a = 6.375 Å, b = 6.375 Å, c = 13.320 Å and β = 120°)[214], as shown on Table 3.

Table 3 The $AgGaP_2Se_6$ bulk and monolayer parameters after using PBE functional along with corresponding experimental values where available[214].

	space group	a (Å)	b (Å)	c (Å)
Bulk (cal.)	$P\bar{3}1c$	6.40	6.40	13.43
Bulk (exp.)	$P\bar{3}1c$	6.37	6.37	13.32
Monolayer (cal.)	$P\bar{3}1c$	6.40	6.40	N/A

To provide a more intuitive understanding of the energy required for exfoliating a monolayer of $AgGaP_2Se_6$, the cleavage energy, E_{cl}, was computed by measuring the energy expenditure needed to separate the top layer from the surface of the bulk phase. Figure 18 (c) illustrates that the $AgGaP_2Se_6$ monolayer possesses a low cleavage energy of 18.80 meV/Å^2. The value of cleavage energy of $AgGaP_2Se_6$ is even smaller than the value for graphene (21 meV/Å^2)[206], which has already been synthesised using experimental techniques. Given the low value of cleavage energy, it was anticipated that extracting a monolayer of $AgGaP_2Se_6$ from its bulk forms will incur minimal energy expenses.

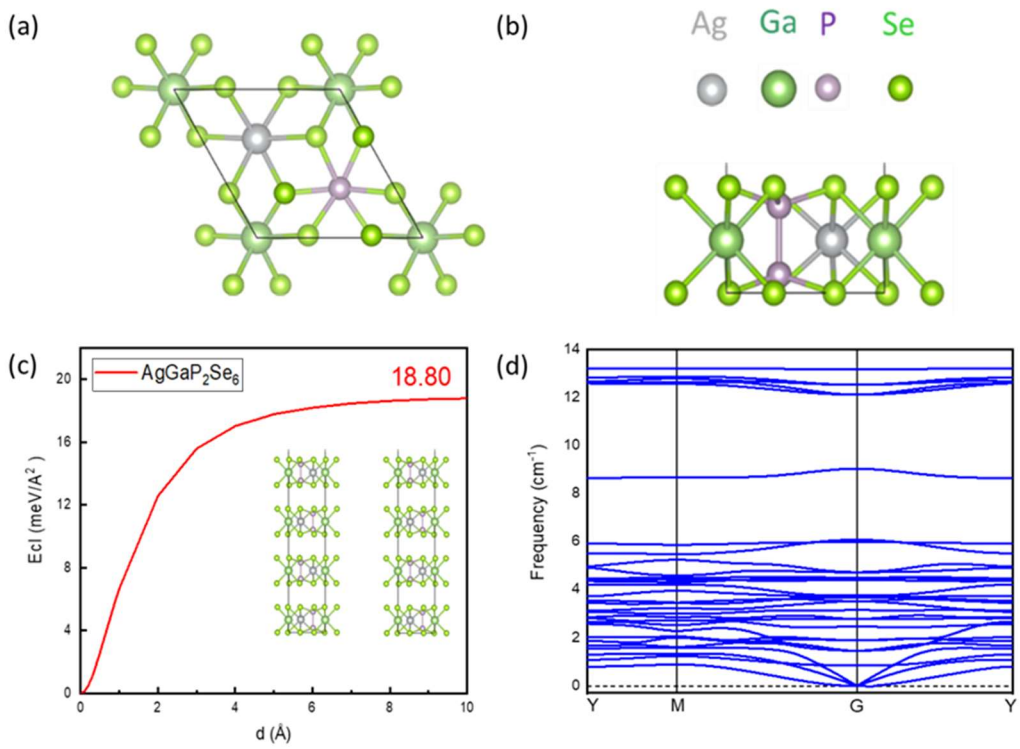

Figure 18 Top view (a) and side view (b) of $AgGaP_2Se_6$ monolayer. The dashed line represents the border of the unit cell. (c) Cleavage energy as a function of separation distance, d. Inset is the model used to calculate E_{cl}. (d) Phonon spectrum.

To investigate the dynamical stability of $AgGaP_2Se_6$ monolayers, their phonon spectra were calculated within the framework of PHONOPY. As can be seen in Figure 18 (d), there was no imaginary frequency in this monolayer, which indicates that this monolayer is dynamically stable. In addition, AIMD calculations confirmed their thermal stability at room temperature. As illustrated in Figure 19, there was no significant structural destruction, and the total energy per atom only fluctuated within a small range (< 0.1 eV) for a period of 10 ps. By approving that this monolayer has high dynamical and thermal stability and low cleavage energy, the material can be experimental feasibility verified as a potential photocatalyst.

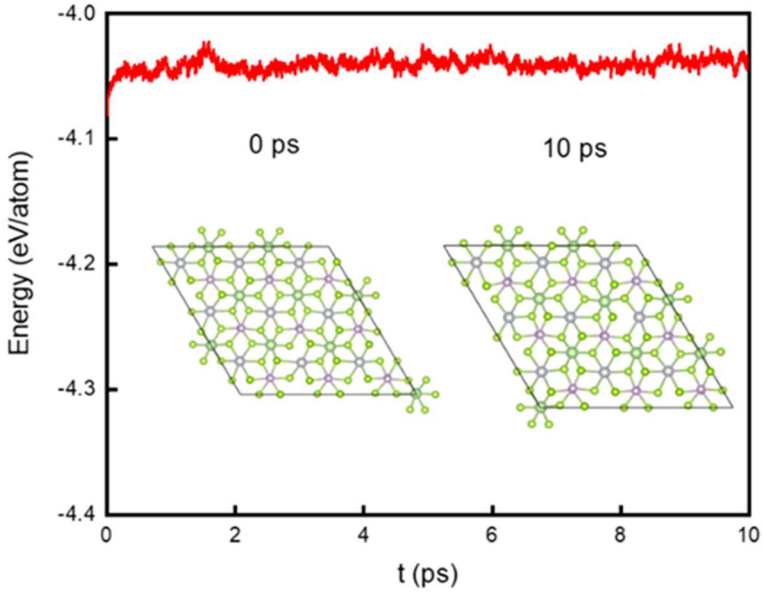

Figure 19 At 300 K, AIMD simulations show how energy per atom changes. The insets are the structures of $AgGaP_2Se_6$ monolayer at 0 ps and10 ps

After checking the stability of $AgGaP_2Se_6$, HSE06 was applied to determine the accurate electronic structure and band gaps of this material[219,220]. Figure 20 (a– d) illustrates the band gaps of $AgGaP_2Se_6$, via HSE06 calculation. The band gaps were 1.83, 1.59, 1.48 and 1.309 eV for monolayer, bilayer, trilayer and bulk, respectively. Moreover, by comparing this band gap with the value for MoS_2 monolayer, which is approximately 1.8 eV, the values can be seen to be similar, and MoS_2 has been identified as an excellent photocatalyst for water splitting.[189,221]

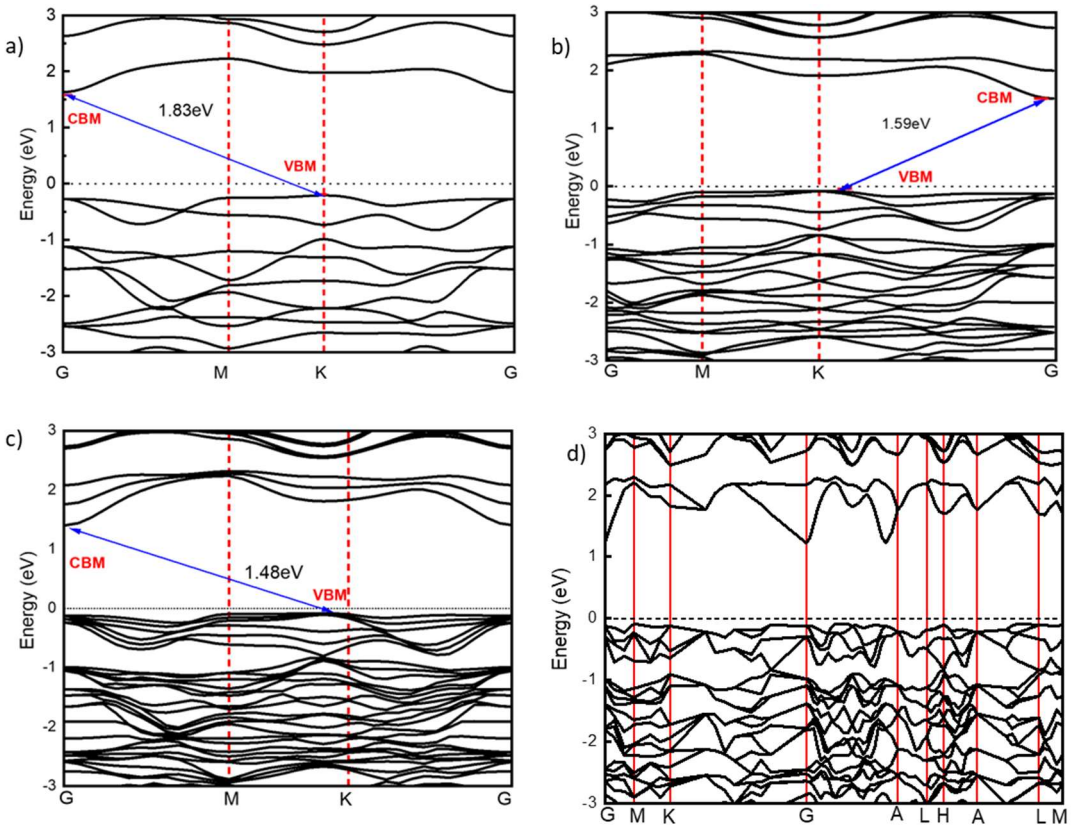

Figure 20 The band structure of $AgGaP_2Se_6$ for monolayer, bilayer, trilayer and bulk (a–d, respectively) calculated using the HSE06 functional.

As outlined in the introduction, 2D materials to be used as efficient photocatalysts must have suitable band edge positions. That is, CBM of the photocatalyst should be above the reduction potential of water, -4.44 eV, and the VBM should be lower than the oxidation potential, -5.67 eV[60,62,101,107,212,213,222–226]. As shown in Figure 21 (a), the CBM of $AgGaP_2Se_6$ monolayer is -4.25 eV, which is greater than the hydrogen reduction potential (-4.44 eV). The VBM of this monolayer is -6.09 eV, which is less than the water oxidation potential (-5.67 eV). In addition, the monolayer has the unique characteristic of having its band edge positioned to cover the water redox potential. On the other hand, bilayer and trilayer forms have favourable positions for the VBM but not for the CBM. However, for bilayer and trilayer forms, the CBM

positions are sufficiently lower than the water reduction potential, indicating a strong driving force for water reduction. [179,207]

One of the crucial features of a photocatalyst is its capacity to absorb light effectively, particularly in the ultraviolet and visible ranges, as photocatalysts must be able to efficiently utilise solar light. In Figure 21 (a), it is clear that the optical gaps of monolayer, bilayer and trilayer fall in the range of 1.48-1.8 eV which are close to the ideal gaps for solar cells (~1.4 eV), indicating their versatile potential for solar harvesting. As shown in Figure 21 (d), the light absorption spectra are anisotropic due to their structural anisotropy. To evaluate the absorbance of monolayer, bilayer, and trilayer forms of $AgGaP_2Se_6$ and to demonstrate their absorbances for wavelengths from 350 to 750 nm, the HSE method was utilised. As shown in Figure 21 (b), the light absorbance region of $AgGaP_2Se_6$ for monolayer, bilayer and trilayer ranges from 500, 570 and 600 nm, respectively. Most encouragingly, we find the light absorption spectra of AgGaP2Se6 monolayer, bilayer and trilayer are extended to near-infrared region (around 900 nm), suggesting their great potential for applications in solar energy conversion such as photocatalytic water splitting or photovoltaic etc.

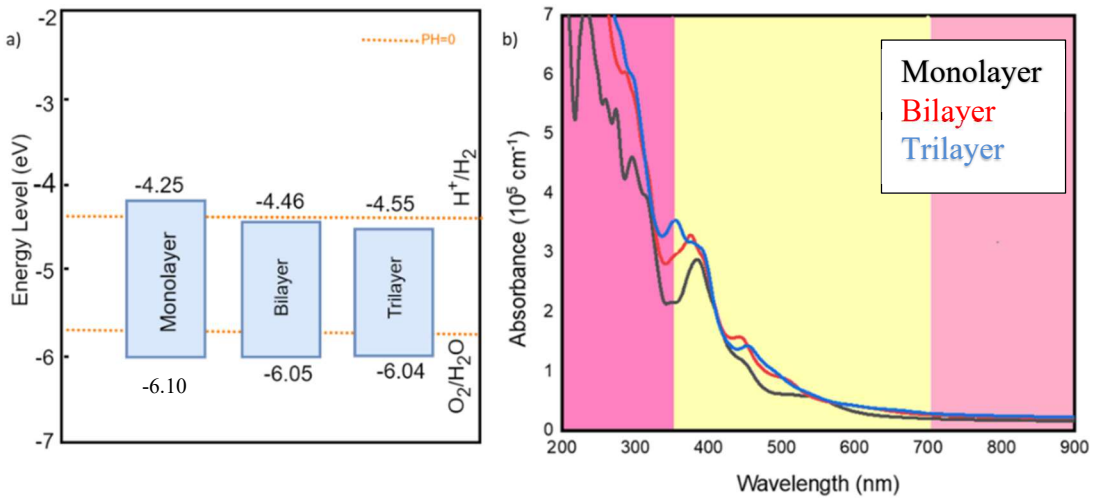

Figure 21 (a) Band edge positions of $AgGaP_2Se_6$ monolayer, bilayer and trilayer. (b) Light absorption spectra of $AgGaP_2Se_6$ monolayer, bilayer and trilayer.

As a result of illustrating the potential applications of 2D $AgGaP_2Se_6$ monolayer, bilayer, and trilayer in photocatalytic water splitting, it has been found that 2D $AgGaP_2Se_6$ can catalyze the redox reaction of water splitting with an excellent visible light absorption. The full potential of 2D semiconductors can be boosted when 2D materials are combined with other semiconductors[189,210]. However, the mismatch between the lattices of the different materials can cause an external strain that subsequently has a significant effect on both the electronic and optical properties of the 2D monolayers. Also, it is possible to deliberately introduce strain in order to alter the electronic structure of a 2D material[209,227]. Therefore, we studied the effect of strain on the electronic properties of $AgGaP_2Se_6$ monolayers. Firstly, we calculated the ideal strength of 2D $AgGaP_2Se_6$ monolayers by the stress–strain relationship, in which the maximum stress corresponds to the instability point. In Error! Reference source not found. (a) it can be seen that as the biaxial strain increases, the stress rises at the beginning but then suddenly drops (corresponding to the fracture of the structure). Clearly, the $AgGaP_2Se_6$ monolayers can sustain 15% strain, providing possibilities for strain engineering.

Secondly, applying strain can affect both the structure and the band gap due to electronic redistribution. We calculated the effect of introducing strains ranging from -10% compressive to +10% tensile, using PBE methods, for $AgGaP_2Se_6$. In Figure 22 (b), the VBM and CBM are considered against the applied strain. The VBM and CBM of the original monolayer were -6.1 and -4.24 eV, respectively. Under tensile strain, both VBM and CBM decreased. In Error! Reference source not found. (c), at strains ranging from -2.5 to 10%, the band gap linearly decreased. Band gap at the -2.5% compressive strain and +10% tensile strain corresponds to 1.1 and 0.3 eV, respectively.

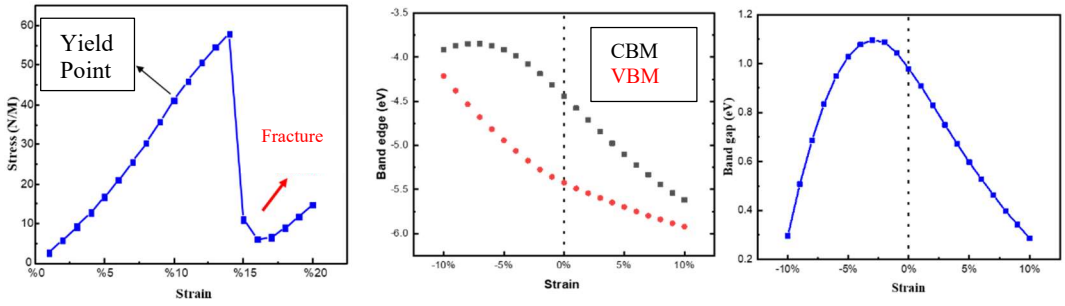

Figure 22 (a) Stress– - strain cuarve of the $AgGaP_2Se_6$ monolayer subjected to biaxial strain. (b) Band edges (CBM vs VBM) as a function of biaxial strain for $AgGaP_2Se_6$ monolayer. Positive and negative strain represents tensile and compressive strain respectively.

5.5 Conclusion

Based on the DFT calculations, we propose the $AgGaP_2Se_6$ monolayer as a novel 2D visible-light-driven water-splitting photocatalyst. Fabrication of this monolayer is highly feasible because of the small cleavage energy. We demonstrated that $AgGaP_2Se_6$ monolayer is a promising photocatalyst with a band gap of 1.83 eV. The CBM and VBM were -4.24 and -6.1 eV, and these values are within the redox potential range of water. Using phonon calculations and AIMD simulations for $AgGaP_2Se_6$ monolayers, we demonstrated their dynamical stability and thermal stability. Under visible region irradiation, $AgGaP_2Se_6$ monolayer displayed good light absorption spectra and band edge positions, indicating its photocatalytic capacity. The exceptional properties of $AgGaP_2Se_6$ monolayer make them ideal materials for photocatalytic water-splitting applications. That is, the excellent light absorption, band alignment and stability of $AgGaP_2Se_6$ **monolayers** make them **promising candidates** for solar energy conversion.

Acknowledgments

We acknowledge generous grants of high-performance computing resources provided by NCI National Facility and The Pawsey Supercomputing Centre through the National Computational Merit Allocation Scheme supported by the Australian Government and the Government of Western Australia. A. D. also greatly appreciates the financial support of the Australian Research Council under Discovery Project (DP170103598).

5.6 Support information

Strategies to Enhance the Performance of $AgGaP_2Se_6$ as a Two-dimensional Photocatalyst for Water Splitting

The $AgGaP_2Se_6$ bulk and monolayer parameters after using PBE functional along with corresponding experimental values where available

	space group	a (Å)	b (Å)	c (Å)
Bulk (cal.)	$P\bar{3}1c$	6.40	6.40	13.43
Bulk (exp.)	$P\bar{3}1c$	6.37	6.37	13.32
Monolayer (cal.)	$P\bar{3}1c$	6.40	6.40	N/A

In order to determine if these materials could be used for water splitting, the PBE functional method was used to calculate their band gap. PBE calculation is not very accurate, but it is faster than HSE to save time. When the band gap exceeded 3.0 eV, the calculation was stopped. The figure below illustrates the band gap colocations for $AgGaP_2Se_6$ via using PBE methods and the band gap are 0.99, 0.97 and 0.68 for monolayer, bilayer trilayer, respectively.

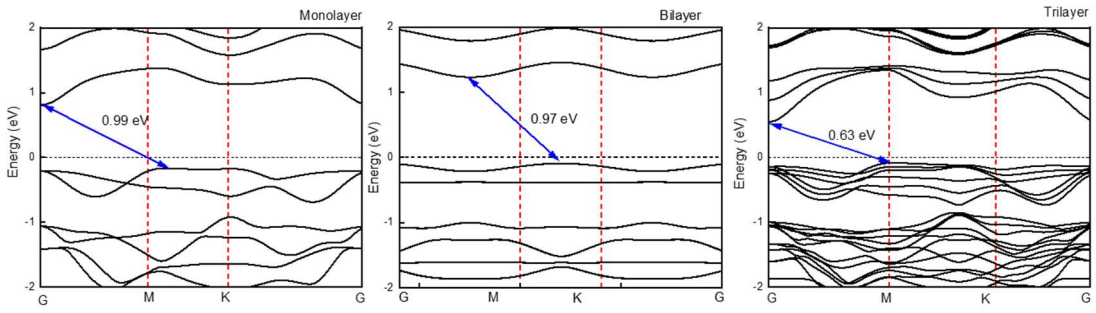

Figure S 1 The band gap calculation via PBE method for $AgGaP_2Se_6$.

In order to determine the accurate electronic structure and band gaps of $AgGaP_2Se_6$, HSE06 was applied after checking the stability of the material. According to HSE06 calculations, Figure S 2 (a-d) illustrates the band gaps of $AgGaP_2Se_6$. A monolayer band gap was 1.83 eV, a bilayer band gap was 1.59 eV, a trilayer band gap was 1.48 eV, and a bulk band gap was 1.309 eV. Furthermore, by comparing this band gap to the value for MoS_2, which is approximately 1.8 eV, we see that the values are very similar, and MoS_2 has been identified as a good photocatalyst for water splitting.

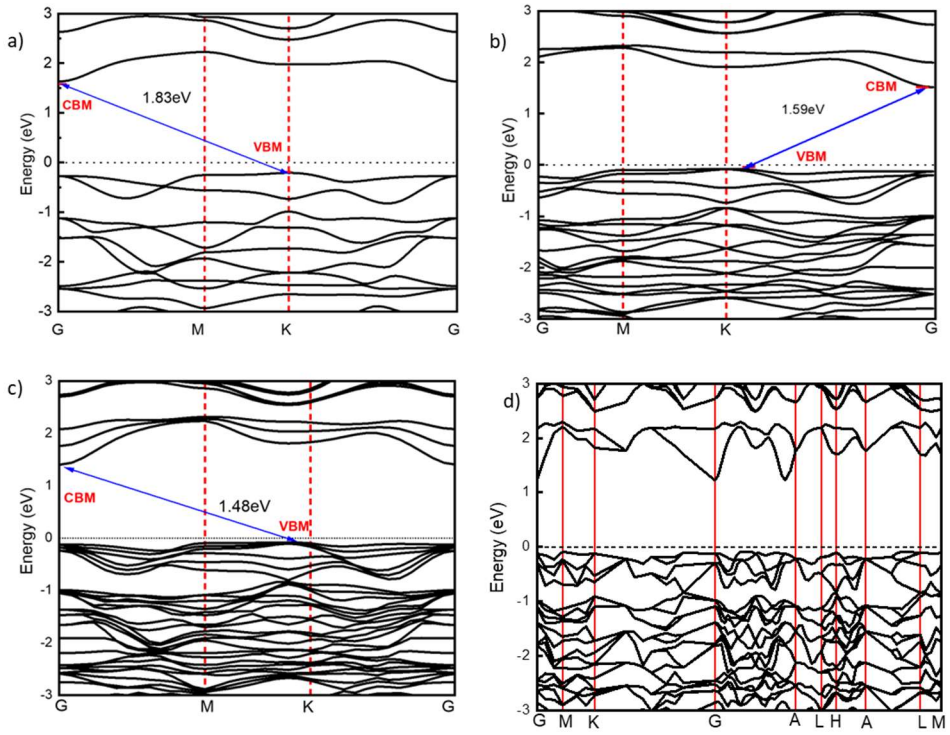

Figure S 2 (a), (d) The band structures on HSE06 level of the bilayer, trilayer, and bulk $AgGaP_2Se_6$ respectively. For monolayer, bilayer and trilayer, the vacuum level is set to zero and the redox potentials pH = 0.

As shown in the finger below the $AgGaP_2Se_6$ monolayer possesses a low cleavage energy of 18.80 meV/Å^2. The value of cleavage energy of $AgGaP_2Se_6$ is even smaller than the value for graphene (21 meV/Å^2)[206], which has already been

synthesised using experimental techniques. Given the low value of cleavage energy, it was anticipated that extracting a monolayer of $AgGaP_2Se_6$ from its bulk forms will incur minimal energy expenses.

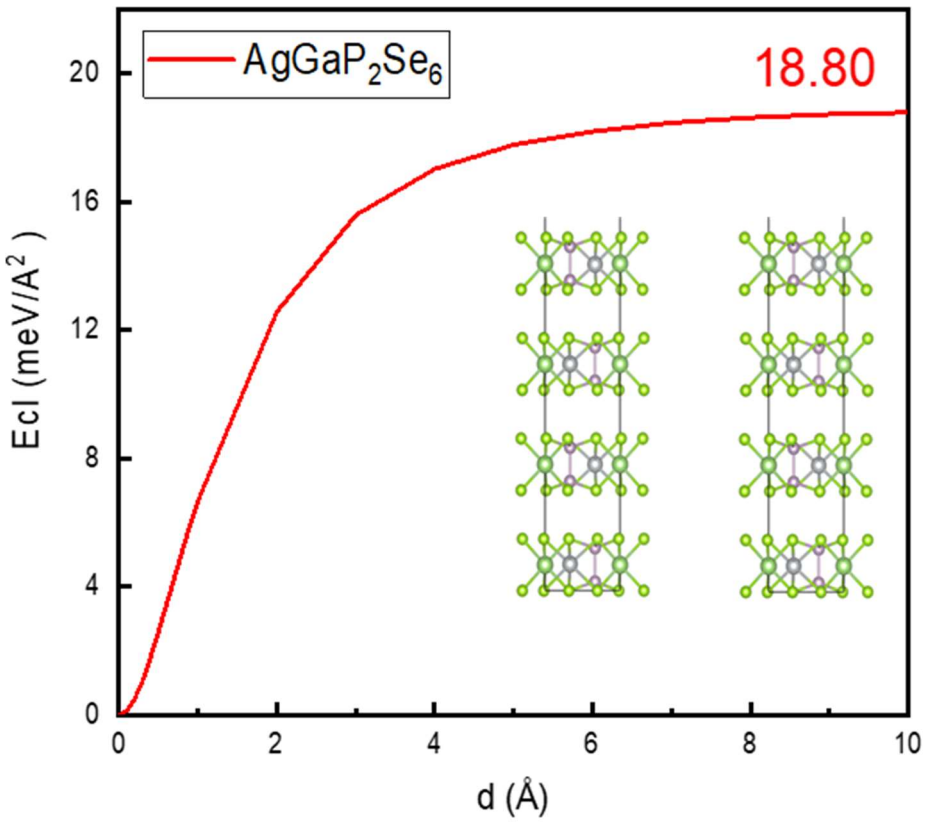

Figure S 3 Cleavage energy as a function of separation distance, d. Inset is the model used to calculate E_{cl}.

PHONOPY was used to calculate the dynamical stability of $AgGaP_2Se_6$ monolayers, as well as their phonon spectra. In figure S 5, it can be seen that this monolayer is dynamically stable since there is no imaginary frequency.

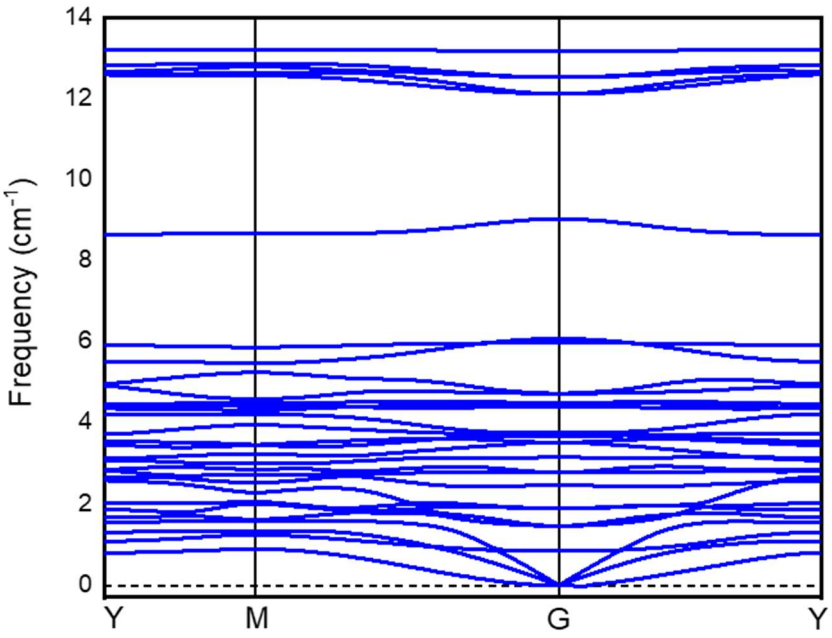

Figure S 4 Phhono spectra of $AgGaP_2Se_6$ monolayers.

Chapter 6: Two-dimensional Materials AlSI, AlSeBr, AlSeI, ScSI, ScSeBr, ScSeCl, ScSeI and InSI for Photocatalytic Water Splitting under Visible Light

6.1 2D materials

This study aims to provide a comprehensive overview of selected materials from the Computational 2D Materials Database (C2DB). Our goal was to investigate several 2D materials that had not yet been synthesized or studied before. We investigated electronic structural, and optical properties of the selected materials. The monolayers that might work as photocatalyst are AlSI, AlSeBr, AlSeI, ScSI, ScSeBr, ScSeCl, ScSeI and InSI monolayers and the space groups of these materials is Pmmn (no.59). Our findings show that of these monolayers possess band gaps of 2.2 to 2.8 eV, and their edge positions of conduction band minimum (CBM) and valence maximum (VBM) fit the water oxidation and reduction potentials in these materials. Therefore, of AlSI, AlSeBr, AlSeI, ScSI, ScSeBr, ScSeCl, ScSeI and InSI monolayers could be a promising photocatalyst for water splitting. This work highlights new and interesting 2D materials with great potential for hydrogen production through water splitting under visible light.

Two-dimensional Materials AlSI, AlSeBr, AlSeI, ScSI, ScSeBr, ScSeCl, ScSeI and InSI for Photocatalytic Water Splitting under Visible Light

Abdulrahman Alhaidar[1,2]

1 Centre for Materials Science, Queensland University of Technology, Brisbane, QLD
4000, Australia

2 School of Chemistry and Physics, Science and Engineering Faculty, Queensland University of Technology, Gardens Point Campus, Brisbane, QLD 4000, Australia

6.2 Introduction

Utilizing sunlight exposure and photocatalysts, water splitting into (H_2) and (O_2) stands out as a viable technique for converting solar energy into chemical energy. The effectiveness of these photocatalysts is intricately linked to the width of the semiconductor bandgap, please refer to previous chapters for more details on the process and requirements of water splitting. Given the inherent advantages of 2D materials, there have been an increasing interest on the potential applications of such materials in the context of photocatalytic water splitting[179,228]. By analysing the light absorption coefficient and energy band of 2D materials, it becomes possible to explore promising candidates for photocatalysts in water splitting.

Despite the wealth of theoretical and computational studies conducted on various photocatalytic materials, along with proposed strategies to enhance hydrogen evolution efficiency, there remains a critical need for researching novel 2D materials in the realm of photocatalytic water splitting for efficient H_2 fuel production. Furthermore, there has been a recent surge in interest surrounding multi-component metal-oxyhalides in many applications such as photocatalysis and electrocatalysis. Although research into 2D metal oxyhalides is still relatively new compared to other 2D materials like graphene or transition metal dichalcogenides. However, their potential for diverse applications, including photocatalysis, is driving significant attention and investigation in the scientific community.

Several 2D MXY (M= metal; X= O, S, Se, Te; Y= Br, Cl, F, and I) have been recently studied for their unique properties. Others proved the efficacy of lithium oxyhalides, and bismuth oxyhalides in electrocatalysis[229], photocatalysis[230]. BiOX monolayers (X= Br, Cl and I) are proved to be a potential photocatalysts for water

splitting[231]. GaOI and InOI have predicted to have suitable band gaps and band edge for photocatalytic water splitting[232].

Our focus on this chapter is to provide a comprehensive study on materials selected from the Computational 2D Materials Database (C2DB). This database is well curated and stands out as an exceptional resource for material researchers seeking to explore and select suitable materials for certain applications. It provides detailed computational and structural information, allowing researchers to efficiently screen and evaluate potential candidates for various applications. C2DB contains a large number of materials that might be suitable for water splitting. Since it might be infeasible and time-consuming to study all these materials, we limited our study to a small subset of photocatalysts by considering some criteria for candidate selection. First, inspired by previous studies on metal-oxyhalides, we selected ABC materials from groups 6 and 7. The band gaps are from 1.6 to 3.0 eV via HSE calculation, and these monolayers should not be magnetic. Then, we conducted a computational study to confirm the reliability of the selected materials for water splitting. Therefore, this study aims to offer an early guideline for further experimental studies on the investigated materials. Our findings show that AlSI, AlSeBr, AlSeI, ScSI, ScSeBr, ScSeCl, ScSeI and InSI monolayers possess band gaps from 2.2 and 2.8 eV. In addition, these monolayers have pronounced absorption in the visible light region of the solar spectrum. Their suitable band edge positions and light absorption make them promising photocatalysts.

6.3 Computational details

All the calculations were based on Density Functional Theory[233–235] as implemented in the Vienna Ab initio Simulation Package[168,169,215]. Generalized Gradient Approximation (GGA) of the Perdew-Burke-Ernzerhof (PBE) functional was utilised to describe the exchange correlation functional[173,216]. Long range van der Waals (vdW) interaction was considered based on Grimme scheme[191]. The gamma-centred k-points grids of 6×8×1 were used for that AlSI, AlSeBr, AlSeI, ScSI, ScSeBr, ScSeCl, ScSeI and InSI, and the plane-wave energy cut-off was set to be 500 eV[236]. Atomic positions and cell shapes were fully relaxed until the maximum force acting on atoms and the energy converged to 0.005 eV/Å and 10^{-6} eV, respectively. A vacuum slab of minimum 18 Å was introduced to avoid interaction between neighbouring images.

PBE functional method was used to calculate the band gap for these materials to determine if they could be used for water splitting. This calculation was very fast, and the band gap could be seen as a result. To save time, the calculation was stopped if the band gap was higher than 3.0 eV. The PBE functional can underestimate the calculation of band gaps of materials[193], so more accurate results were calculated based on the Heyd-Scuseria-Ernzerhof (HSE06) hybrid functional[219,220]. One important condition to assess the photocatalyst properties of 2D semiconductors is sunlight absorption, and for this we used the density functional perturbation (DFPT) method. The spectrum in the visible light region is from 350 to 800 nm. The Phonon calculation was performed by PHONOPY code based on the finite-displacement method[217,218] with the convergence criteria for force and energy at 0.001 eV/Å and 10^{-8} eV, respectively. Moreover, ab inito molecular dynamics simulations were carried out to study the thermal the selected monolayers, performed with a 3×3×1 supercell at 300

K. The simulations lasted for a duration of 10 ps in the NVT ensemble controlled by a Nose−Hoover thermostat[179,198]. The standard oxidation and reduction potentials, namely, $O_2/H_2O = -5.67\ eV$ and $H^+/H_2 = -4.44\ eV$, were employed.

6.4 Results and discussion

Geometry structure. Optimizing the structure of 2D materials is crucial because their properties are highly sensitive to their atomic arrangement. By tuning the arrangement of atoms, we can enhance specific properties like electronic conductivity, mechanical strength, and optical behavior, making them suitable for various applications in electronics, optics, energy storage, and more. After selecting the materials from 2D database and the criteria that we have mentioned in the above section we downloaded the zyx file then we opened it via materials studio for checking and setup the correct lattice parameter and space group. Then we optimized the structure for these monolayers so we can check if the structures have changed during this calculation. The optimised monolayers for AlSI, AlSeBr, AlSeI, ScSI, ScSeBr, ScSeCl, ScSeI and InSI monolayers crystals are shown in Figure 19. They have trigonal symmetry[237] Figure 23 (a) shows the top view and (b and c) shows the sides view of these monolayers.

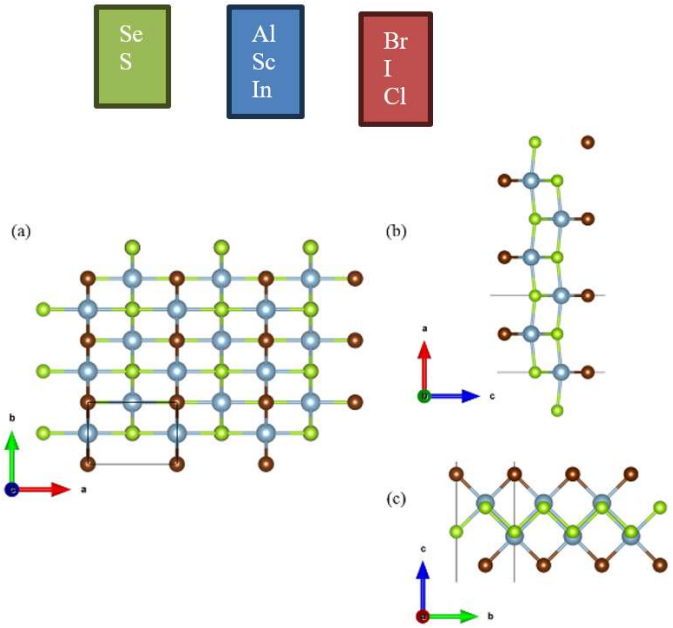

Figure 23 (a) top view and (b and c) sides view of the structure of AlSI, AlSeBr, AlSeI, ScSI, ScSeBr, ScSeCl, ScSeI and InSI monolayers.

We have calculated several ABC materials, and it was found that only eight materials could potentially be used for water splitting. However, some of the materials that are not suitable for water splitting might be useful for other applications, such as solar cells. **Table 4** shows the eight materials used and the calculated lattice parameters. As shown in table 1the the calculated lattice parameters of AlSI, AlSeBr, AlSeI, ScSI, ScSeBr, ScSeCl, ScSeI and InSI monolayers data from previous theoretical studies are well consistent with these findings[238,239]. As indicated by the results in **Table 4**, lattice constants calculated for the x-axis (a-axis) are both larger than for the y-axis (b-axis). It is interesting to note that with increasing atomic mass, the substitution of X atoms has a greater impact on lattice constants and bonds than Y atoms, but the substitution of Y atoms has a greater effect on buckling distances.

Table 4 Calculated structural parameters of AlSI, AlSeBr, AlSeI, ScSI, ScSeBr, ScSeCl, ScSeI and InSI monolayers.

Lattice Parameters	Materials							
	AlSI	AlSeI	AlSeBr	ScSeBr	ScSeCl	InSI	ScSI	ScSeI
a (Å)	4.85	5.31	5.23	5.39	5.38	5.32	5.09	5.37
b (Å)	3.71	3.79	3.61	3.83	3.67	3.99	3.92	3.98

To investigate the thermodynamic stability of AlSI, AlSeBr, AlSeI, ScSI, ScSeBr, ScSeCl, ScSeI and InSI monolayers, we calculated their phonon spectra within the framework of PHONOPY and AIMD. The phonon dispersion spectra of these monolayers were calculated to examine their dynamical stability. Phonon spectra represent the vibrational modes of a crystalline material as a function of wave vector in the Brillouin zone. By examining the generated dispersion plot, we can identify whether the material is dynamically stable based on the absence of imaginary frequencies. As can be seen in Figure 23, in the entire Brillouin zone, there are no imaginary frequencies for the phonon modes this indicates that, these monolayers are dynamically stable. In a primitive cell, there are six atoms, which result in 18 phonon modes, three of which are acoustic and fifteen of which are optical. After the calculations done, we laminated the monolayers that is not stable because of not fit the water splitting equipment as shown in the Table 5.

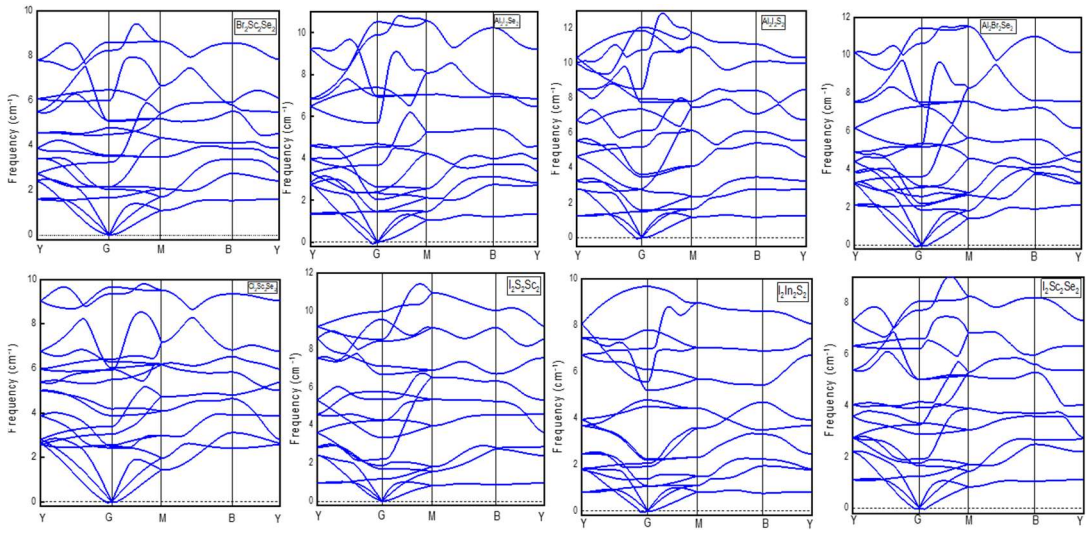

Figure 24 Phonon spectra of AlSI, AlSeBr, AlSeI, ScSI, ScSeBr, ScSeCl, ScSeI and InSI monolayers with no imaginary frequency in any wave vector.

In addition, AIMD simulations prove thermal stability, for the suitable materials out of the materials that have been selected as the mentioned criteria on the introduction section. Thermal stability typically refers to the ability of a material to maintain its structural and energetic integrity at elevated temperatures. AIMD simulations involve modeling the dynamic behavior of atoms and molecules at finite temperature and understanding the thermal stability of the system is crucial for various applications including water splitting. The performed colourations for AIMD are set with a 3×3×1 supercell at 300 K and simulation lasting for 10 ps. The time step of 1 fs and NVT ensemble controlled by Nose-Hoover thermostat[198] were applied in the simulation. As illustrated in Figure 25, for the AlSI, AlSeBr, AlSeI, ScSI, ScSeBr, ScSeCl, ScSeI and InSI monolayers with the energy 300 K and by the time are stable. And the results are -3.85, -4.95, -3.50, -5.68, -3.95, -5.80, -5.35, and -5.35 eV\atom, respectively. Moreover, there were no significant structural destruction, and the total energy per atom only fluctuated within a small range (< 0.1 eV) for a period of 10 ps.

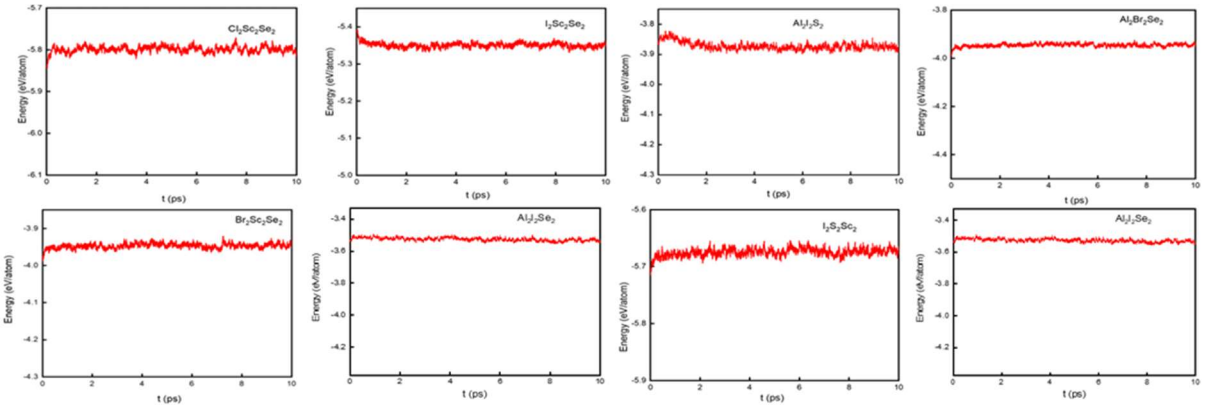

Figure 25 AIMD simulation at 300 K shows the evolution of total energy per atom. The insets are the structures of AlSI, AlSeBr, AlSeI, ScSI, ScSeBr, ScSeCl, ScSeI and InSI monolayers at 0 ps and 10.

Electronic structures. The band gap is another important calculation that is composer for water splitting and there are two methods that we can get the band gap BPE and HSE06. For accurate results, HSE06 was applied to determine the accurate electronic structure and band gaps of these materials[219,220]. Figure 26 shows the HSE06 functional calculation obtained from indirect band gaps of AlSI, AlSeBr, AlSeI, ScSI, ScSeBr, ScSeCl, ScSeI and InSI monolayers are 2.56, 2.27, 2.22, 2.8, 2.4, 2.29, 2.38 and 2.49 eV, respectively. By comparing these values with the band gap of Ag_2S and $NaTAO_3$ monolayer, which is approximately 2.83 and 2.25 eV, most of the values are quite close to Ag_2S and $NaTAO_3$ which have been identified as photocatalysts for water splitting[240,241]. We also investigate other materials (see Table 5), however some of these materials that highlighted red colour cannot be used as photocatalytic water splitters due to large band gaps (over 3 eV).

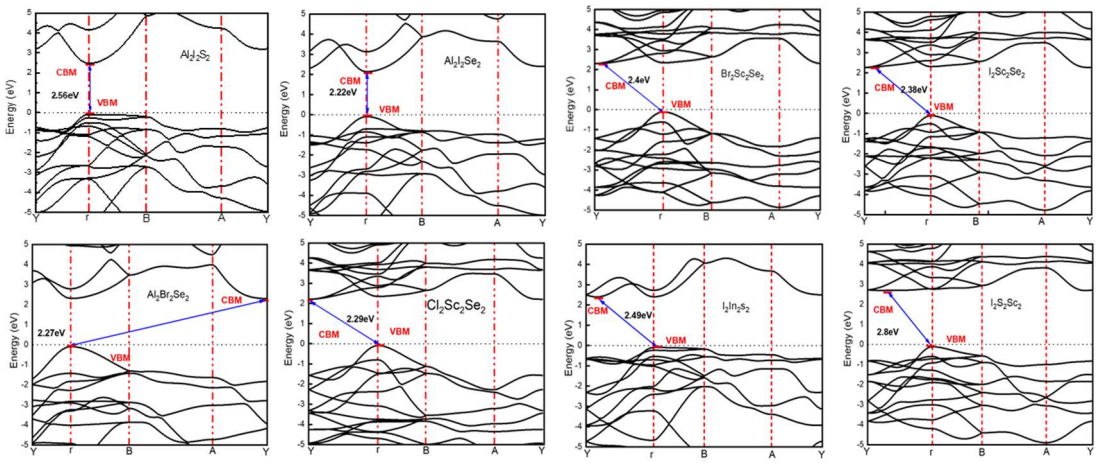

Figure 26 The band structures on HSE06 level of the AlSI, AlSeBr, AlSeI, ScSI, ScSeBr, ScSeCl, ScSeI and InSI monolayers and the rang are between 2.2 to 2.8 eV.

Photocatalytic properties. As described in Chapter 2, for 2D materials to be used as efficient photocatalysts, they must have suitable band edge positions. That is, the CBM of the photocatalyst should be above the reduction potential of water, -4.44 eV, and the VBM should be lower than the oxidation potential of water, -5.67 eV[60,62,63]. The VBMs are calculated from the difference between the vacuum potential and Fermi level. As shown in Figure 27, the CBMs of the monolayers were above -4.44 eV, which is greater than the hydrogen reduction potential. The VBMs of these monolayers were not below the water oxidation potential, -5.67 eV. The band edge positions are connected to the water redox potentials, which means that these monolayers could work as photocatalysts without an external bias voltage[59,179,207]. The calculated positions of VBM and CBM are shown in a schematic diagram in Figure 27 the red line indicated the CBM level, and the blue line indicated the VBM level. The VBM band edges of these monolayers were located at approximately -7.1 eV, which is significantly lower than the oxidation potential of water, whereas the CBM of the monolayers was slightly higher than the reduction potential of water. Therefore, we are approved that AlSI, AlSeBr, AlSeI, ScSI, ScSeBr, ScSeCl, ScSeI and InSI monolayers are suitable for water splitting. There are some monolayers that are

laminated after checking the band position because the CBM or VBM does not fit with the requirement mentioned and shown in Table 5 highlighted with red colour.

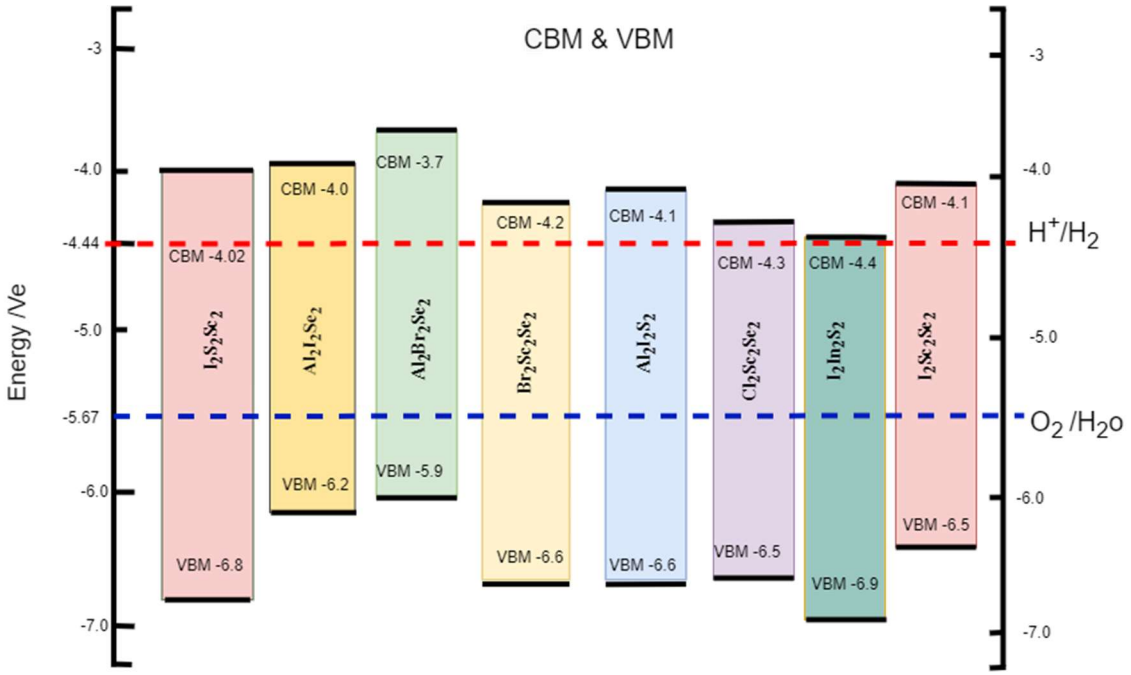

Figure 27 Shows band positions of AlSI, AlSeBr, AlSeI, ScSI, ScSeBr, ScSeCl, ScSeI and InSI monolayers compared to the redox potential of water splitting.

Table 5 The selected materials from 2D database (D2CB) and the highlighted with red colour are not fit with requirements of water splitting.

Materials	HSE band gap	eV	CBM	VBM
BrInS	2.80	3.46	-4.44	-7.24
AsClTe	1.57	3.09	-4.53	-6.10
BrGaS	2.34	3.25	-4.67	-7.02
BrSSc	3.24	3.16	-4.14	-7.39
ClGaS	2.31	3.27	-4.64	-6.96
ClHfN	3.32	3.29	-3.53	-6.86
ClInO	4.11	3.78	-4.56	-8.67
ClInS	2.79	3.53	-4.48	-7.28
ClSSc	3.12	3.15	-4.20	-7.33
ClScSe	2.29	2.96	-4.25	-6.55
AsClSe	2.26	3.32	-4.93	-7.19
BrSbSe	1.81	3.82	-5.13	-6.94
AlBrS	3.17	3.46	-3.57	-6.74
AlClS	3.24	3.50	-3.2	-6.45
AlClSe	2.10	3.23	-3.53	-5.64
AlIS	2.56	4.05	-4.08	-6.64

Materials	HSE band gap	eV	CBM	VBM
AlISe	2.22	3.73	-3.96	-6.19
BrGaO	4.04	3.47	-3.50	-7.55
BrHfN	3.27	3.32	-3.57	-6.85
BrInO	3.60	3.76	-4.38	-7.99
BrNZr	3.70	4.32	-3.02	-6.72
AlBrSe	2.27	3.20	-3.68	-5.95
AsClTe	1.57	3.09	-4.53	-6.10
HfIN	2.71	4.03	-3.63	-6.16
IInS	2.49	3.93	-4.41	-6.90
ISSc	2.80	3.70	-4.02	-6.82
IScSe	2.38	3.52	-4.10	-6.48
AsClSe	2.26	3.32	-4.93	-7.20
BrSbSe	1.81	3.82	-5.13	-6.94

Optical absorption. Another important property to assess for a photocatalyst is its ability to absorb sunlight. High response to a broad range of solar light is highly desirable to generating more electron-hole pairs for the full utilization of the solar energy**.** Using the dielectric function with the HSE06 hybrid functional, the absorption coefficient was calculated from the complex dielectric constants and Energy conversion can be more efficient when there is high response to solar light. A spectrum of visible light (approximately 350 - 800 nm). Figure 28 shows that light absorption occurs predominantly in the ultraviolet (UV) range, with a small contribution from the visible range. These monolayers have significant absorption peaks in the ultraviolet range, as well as in the x- and y-directions. Usually, solar blind deep-UV detectors operate under severe conditions, which allows these monolayers to be used in UV optoelectronic devices in solar blinds. Moreover, the light absorption of AlSI, AlSeBr, AlSeI, ScSI, ScSeBr, ScSeCl, ScSeI and InSI monolayers were 500, 420, 430, 550, 420, 510, 510, and 440 nm, as shown in Figure 28. These materials exhibit a highly

favorable phonon spectra that is closely resembles those of synthesized and experimentally investigated materials such as the CdS nanorod/ZnS nanoparticle composite[242].

It is worth mentioning that there are some of some of the materials having large band gap (over than 3 eV) which indicate that large band gap can have poor light absorption, as can be seen in Table 5.

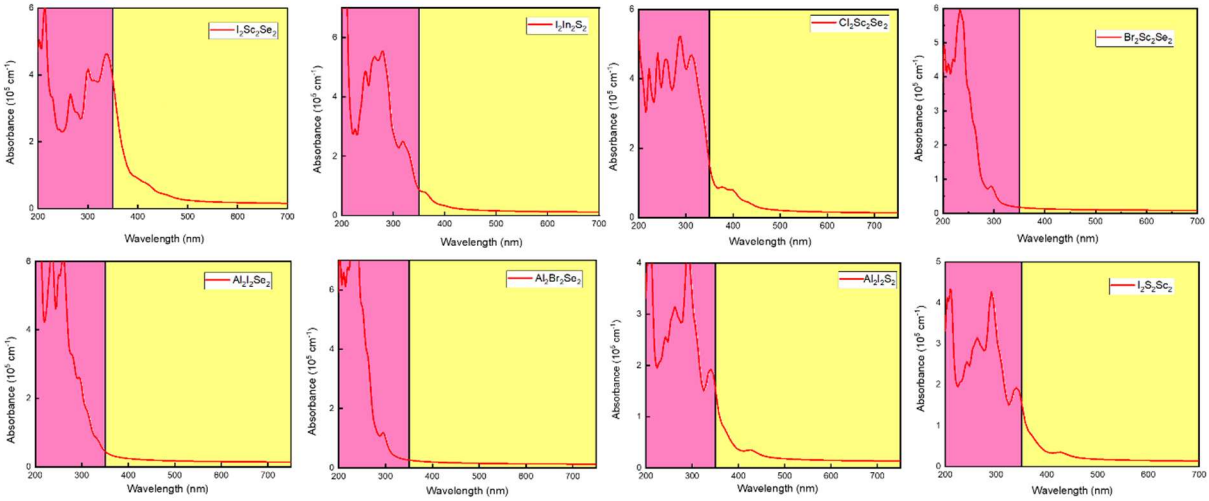

Figure 28 Calculated light absorption of these monolayers in direction. Ppurple and yellow areas represent the ultraviolet and visible regions of sunlight.

6.5 Conclusion

In this research, we calculated electronic structure, band edge positions, phonon spectra, and light absorption for wide range of not synthesized materials. After calculating their phonon spectra, we found that there is no imaginary frequency in AlSI, AlSeBr, AlSeI, ScSI, ScSeBr, ScSeCl, ScSeI and InSI monolayers. This finding indicates some of these monolayers are dynamically stable while, for the remainder of these monolayers that have small imaginary frequency, we might solve this by increasing the supercell. In addition, we calculated the light absorption, and we found

that these monolayers have good light absorption with proximately 420 and 680 nm. Moreover, the band gaps of AlSI, AlSeBr, AlSeI, ScSI, ScSeBr, ScSeCl, ScSeI and InSI monolayers are between 2.2 and 2.8 eV which is an excellent position for water splitting. The CBMs and the VBMs have exceptional fit for water oxidation and reduction potentials. Based on our findings, these materials have excellent band gap position, and some of these monolayers are dynamically stable and have good light absorption. These 2D materials are suitable photocatalysts for photoelectrochemical water splitting. Therefore, they could be promising photocatalysts for water splitting. Our work not only enriches the family of 2D materials but also highlights new candidates for the development of high efficiency photocatalysts in the near future.

Acknowledgments

We acknowledge generous grants of high-performance computing resources provided by NCI National Facility and The Pawsey Supercomputing Centre through the National Computational Merit Allocation Scheme supported by the Australian Government and the Government of Western Australia. A. D. also greatly appreciates the financial support of the Australian Research Council under Discovery Project (DP170103598).

Chapter 7: Conclusions and Future work

7.1 Conclusion

In conclusion, the production of hydrogen through photocatalytic water splitting shows great promise in addressing the environmental and energy challenges of the twenty-first century. The use of two-dimensional materials with excellent visible light absorption and suitable band alignment is crucial for efficient photostatic water splitting. Through computational studies using DFT, this thesis has contributed to the exploration of previously unexplored 2D materials and provides insights into their structural, electronic and optical properties, as well as the edge positions of the CBM and VBM. Further research in this field is essential to realise the full potential of water splitting for sustainable energy production.

We have theoretically demonstrated, by DFT calculations, that $MgAl_2S_4$ monolayer should be included as a new member of the family of 2D photocatalysts. The small cleavage and formation energies show high feasibility for fabrication of this monolayer. The dynamical and thermal stabilities are demonstrated by the phonon calculations and AIMD simulations. The band edge positions, and light absorption spectra show the photocatalytic capacity of pristine $MgAl_2S_4$ monolayer upon UV irradiation. A moderate tensile strain could be applied to overcome the poor light absorption in the visible range and improve its oxidation ability. Furthermore, based on 2D $MgAl_2S_4$, we designed direct Z-scheme heterostructures possessing high redox abilities and high visible light absorbance. This work not only proposes a potential 2D material for photocatalytic water splitting but also highlights the important role of structural engineering in the design of highly efficient photocatalysts.

The $AgGaP_2Se_6$ monolayer was also proposed as a novel 2D photocatalyst. Fabrication of this monolayer is highly feasible because of the small cleavage and formation energies. Using phonon calculations and AIMD simulations, we demonstrated the dynamical and thermal stabilities. Under UV irradiation, pristine $AgGaP_2Se_6$ monolayers displayed good light absorption spectra and band edge positions, indicating their photocatalytic capacity. To improve its oxidation ability and visible light absorption, a moderate tensile strain could be applied. A direct Z-scheme heterostructure based on 2D $AgGaP_2Se_6$ was designed, exhibiting high redox ability and high light absorption. This work illustrates the importance of structural engineering in the design of high efficiency photocatalysts and presents a potential 2D material for photocatalytic water splitting.

A comprehensive overview of selected materials from the Computational 2D Materials Database (C2DB) is presented in this study. We investigated several 2D materials that had not been synthesized or studied before. The selected materials were analyzed for their electronic and structural properties, as well as their optical properties. Among the studied materials, AlSI, AlSeBr, AlSeI, ScSI, ScSeBr, ScSeCl, ScSeI and InSI appeared to be new candidates for efficient water splitting. After calculating their phonon spectra, we found that there was negligible or no imaginary frequency in these monolayers, which indicates these monolayers are dynamically stable. In addition, these monolayers showed good light absorption, at approximately 420 and 580 nm. Moreover, the band gaps of the monolayers were between 2.2 to 2.8 eV, representing excellent compatibility with the requirements for water splitting. The CBMs and VBMs showed exceptional fit for the water oxidation and reduction potentials. Based on these findings, these 2D materials are suitable photocatalysts for

water splitting. This work adds to the family of 2D materials and highlights new promising and efficient photocatalysts for development in the near future.

7.2 Future work

In order to achieve sustainable energy production and to preserve the environment, photocatalytic water splitting must be studied. We are striving to combat climate change and the depletion of finite energy resources by finding efficient and renewable ways to produce hydrogen, a clean and versatile fuel. Hydrogen fuel can be generated without harming the environment, through photocatalytic water splitting, which harnesses the power of sunlight to split water into hydrogen and oxygen. It is possible to unlock the potential of clean energy solutions by delving into this field, as well as reduce our dependence on fossil fuels and pave the way for a greener, more sustainable future. This section provides specific limitations and future directions for the work presented in this thesis.

In Chapter 4, it was identified that the $MgAl_2S_4$ monolayer has the potential to be used as a photocatalytic water-splitting agent. There is also the possibility for this monolayer to be used in other applications. In addition, it may be possible to find other materials for designing heterostructures, which can be investigated and compared to previous studies.

Chapter 5 of this thesis showed that $AgGaP_2Se_6$ monolayer is an excellent material for the splitting of water, as can be seen from the results. In spite of this, future work is planned to investigate two further aspects of this approach. The first of these plans to use a bilayer and insert hydrogen or semiconductor elements between the two layers in an attempt to improve the CBM to further satisfy the conditions for water

splitting. It is also possible to investigate this material for other applications, such as hydrogen cells or solar cells.

Chapter 6 examined over large number of materials for the purpose of discovering new 2D materials that have not yet been synthesised. As can be seen in the following Table 6, there are 16 materials that cannot be used as photocatalytic water-splitting materials due to failing to meet one of the conditions necessary for photocatalytic water splitting. As can be seen for these materials, they have an excellent band gap, which makes them very suitable for other applications. As a result, the further research to expand the scope of Chapter 6 is intended to determine whether these materials can be used as solar cells.

Moreover, it can be very beneficial to collaborate with experimental researchers in QUT or other universities to transform our theoretical predictions into tangible outcomes. Some of the materials investigated in this thesis have good potential of producing efficient photocatalysts, therefore, there is a reasonably suitable scope for future experimental work in the area of photocatalytic water splitting.

Table 6 List of some materials investigated in Chapter 6 that can be used for other applications in future.

M	Materials	Space Group	Band Gap HSE06
1	AgBrS	P1	2.27
2	CuBrS		1.85
3	CuISe		1.66
4	AgClSe		2.07
5	BrInS	Pmmn	2.80
6	BrGaS		2.34

7	ClGaS	P3m1	2.31
8	ClInS		2.79
9	AsClTe		1.57
10	AsClSe		2.26
11	BrSbSe		1.81
12	BiIO	bilayer	
14	BiFO		
15	BiBrO		
16	BiClO		

Bibliography

(1) Krewitt, W.; Heck, T.; Trukenmüller, A.; Friedrich, R. Environmental Damage Costs from Fossil Electricity Generation in Germany and Europe. *Energy Policy* **1999**, *27* (3), 173–183. https://doi.org/10.1016/S0301-4215(99)00008-7.

(2) Plantinga, A.; Scholtens, B. The Financial Impact of Fossil Fuel Divestment. *Climate Policy* **2021**, *21* (1), 107–119. https://doi.org/10.1080/14693062.2020.1806020.

(3) *Climate Change 2014: Mitigation of Climate Change: Working Group III Contribution to the Fifth Assessment Report of the Intergovernmental Panel on Climate Change*; Intergovernmental Panel on Climate Change, Edenhofer, O., Eds.; Cambridge University Press: New York, NY, 2014.

(4) Bach, W. Fossil Fuel Resources and Their Impacts on Environment and Climate. *International Journal of Hydrogen Energy* **1981**, *6* (2), 185–201. https://doi.org/10.1016/0360-3199(81)90007-0.

(5) Barbir, F.; Veziroğlu, T. N.; Plass, H. J. Environmental Damage Due to Fossil Fuels Use. *International Journal of Hydrogen Energy* **1990**, *15* (10), 739–749. https://doi.org/10.1016/0360-3199(90)90005-J.

(6) Andres, R. J.; Fielding, D. J.; Marland, G.; Boden, T. A.; Kumar, N.; Kearney, A. T. Carbon Dioxide Emissions from Fossil-Fuel Use, 1751–1950. *Tellus B: Chemical and Physical Meteorology* **1999**, *51* (4), 759–765. https://doi.org/10.3402/tellusb.v51i4.16483.

(7) Wuebbles, D. J.; Jain, A. K. Concerns about Climate Change and the Role of Fossil Fuel Use. *Fuel Processing Technology* **2001**, *71* (1–3), 99–119. https://doi.org/10.1016/S0378-3820(01)00139-4.

(8) OECD. *Climate and Electricity Annual 2011: Data and Analyses*; Organisation for Economic Co-operation and Development: Paris, 2011.

(9) Mikhaylov, A.; Moiseev, N.; Aleshin, K.; Burkhardt, T. Global Climate Change and Greenhouse Effect. *Entrepreneurship and Sustainability Issues* **2020**, *7* (4), 2897–2913. https://doi.org/10.9770/jesi.2020.7.4(21).

(10) Woodward, A.; Smith, K. R.; Campbell-Lendrum, D.; Chadee, D. D.; Honda, Y.; Liu, Q.; Olwoch, J.; Revich, B.; Sauerborn, R.; Chafe, Z.; Confalonieri, U.; Haines, A. Climate Change and Health: On the Latest IPCC Report. *Lancet* **2014**, *383* (9924), 1185–1189. https://doi.org/10.1016/S0140-6736(14)60576-6.

(11) *Renewable energy explained - U.S. Energy Information Administration (EIA)*. https://www.eia.gov/energyexplained/renewable-sources/ (accessed 2023-03-01).

(12) Roberts, S.; Weightman, F. Cleaning up the World with Renewable Energy: From Possibilities to Practicalities. *Renewable Energy* **1994**, *5* (5), 1314–1321. https://doi.org/10.1016/0960-1481(94)90167-8.

(13) *World energy consumption by energy source 2050*. Statista. https://www.statista.com/statistics/222066/projected-global-energy-consumption-by-source/ (accessed 2024-01-29).

(14) Chen, K.; Winter, R. C.; Bergman, M. K. Carbon Dioxide from Fossil Fuels: Adapting to Uncertainty. *Energy Policy* **1980**, *8* (4), 318–330. https://doi.org/10.1016/0301-4215(80)90108-1.

(15) Owen, A. D. Evaluating the Costs and Benefits of Renewable Energy Technologies. *Australian Economic Review* **2006**, *39* (2), 207–215. https://doi.org/10.1111/j.1467-8462.2006.00413.x.
(16) *Renewable Energy Statistics 2021*. https://www.irena.org/publications/2021/Aug/Renewable-energy-statistics-2021 (accessed 2023-03-01).
(17) Sawin, J. L.; Martinot, E.; Sonntag-O'Brien, V.; McCrone, A.; Roussell, J.; Barnes, D.; Flavin, C.; Mastny, L.; Kraft, D.; Wang, S.; Ellenbeck, S.; Ilieva, L.; Griebenow, C.; Adib, R.; Lempp, P.; Welker, B. *Renewables 2010 - Global Status Report*; France, 2010; p 164.
(18) Painuly, J. P. Barriers to Renewable Energy Penetration; a Framework for Analysis. *Renewable Energy* **2001**, *24* (1), 73–89. https://doi.org/10.1016/S0960-1481(00)00186-5.
(19) Panwar, N. L.; Kaushik, S. C.; Kothari, S. Role of Renewable Energy Sources in Environmental Protection: A Review. *Renewable and Sustainable Energy Reviews* **2011**, *15* (3), 1513–1524. https://doi.org/10.1016/j.rser.2010.11.037.
(20) Chen, X.; Shen, S.; Guo, L.; Mao, S. S. Semiconductor-Based Photocatalytic Hydrogen Generation. *Chem Rev* **2010**, *110* (11), 6503–6570. https://doi.org/10.1021/cr1001645.
(21) Kärkäs, M. D.; Verho, O.; Johnston, E. V.; Åkermark, B. Artificial Photosynthesis: Molecular Systems for Catalytic Water Oxidation. *Chem. Rev.* **2014**, *114* (24), 11863–12001. https://doi.org/10.1021/cr400572f.
(22) *Semiconductor heterojunction photocatalysts: design, construction, and photocatalytic performances - Chemical Society Reviews (RSC Publishing)*. https://pubs.rsc.org/en/content/articlelanding/2014/cs/c4cs00126e (accessed 2023-03-02).
(23) Bockris, J. O. The Origin of Ideas on a Hydrogen Economy and Its Solution to the Decay of the Environment. *International Journal of Hydrogen Energy* **2002**, *27* (7), 731–740. https://doi.org/10.1016/S0360-3199(01)00154-9.
(24) Kim, T. Hydrogen Generation from Sodium Borohydride Using Microreactor for Micro Fuel Cells. *International Journal of Hydrogen Energy* **2011**, *36* (2), 1404–1410. https://doi.org/10.1016/j.ijhydene.2010.10.079.
(25) McDowall, W.; Eames, M. Forecasts, Scenarios, Visions, Backcasts and Roadmaps to the Hydrogen Economy: A Review of the Hydrogen Futures Literature. *Energy Policy* **2006**, *34* (11), 1236–1250. https://doi.org/10.1016/j.enpol.2005.12.006.
(26) Wang, F.; Li, C.; Chen, H.; Jiang, R.; Sun, L.-D.; Li, Q.; Wang, J.; Yu, J. C.; Yan, C.-H. Plasmonic Harvesting of Light Energy for Suzuki Coupling Reactions. *J. Am. Chem. Soc.* **2013**, *135* (15), 5588–5601. https://doi.org/10.1021/ja310501y.
(27) Kudo, A.; Miseki, Y. Heterogeneous Photocatalyst Materials for Water Splitting. *Chemical Society Reviews* **2009**, *38* (1), 253–278. https://doi.org/10.1039/B800489G.
(28) Walter, M. G.; Warren, E. L.; McKone, J. R.; Boettcher, S. W.; Mi, Q.; Santori, E. A.; Lewis, N. S. Solar Water Splitting Cells. *Chem. Rev.* **2010**, *110* (11), 6446–6473. https://doi.org/10.1021/cr1002326.
(29) Osterloh, F. E. Inorganic Nanostructures for Photoelectrochemical and Photocatalytic Water Splitting. *Chem. Soc. Rev.* **2013**, *42* (6), 2294–2320. https://doi.org/10.1039/C2CS35266D.

(30) Bard, A. J. Photoelectrochemistry. *Science* **1980**, *207* (4427), 139–144. https://doi.org/10.1126/science.207.4427.139.
(31) Yang, W. S.; Park, B.-W.; Jung, E. H.; Jeon, N. J.; Kim, Y. C.; Lee, D. U.; Shin, S. S.; Seo, J.; Kim, E. K.; Noh, J. H.; Seok, S. I. Iodide Management in Formamidinium-Lead-Halide–Based Perovskite Layers for Efficient Solar Cells. *Science* **2017**, *356* (6345), 1376–1379. https://doi.org/10.1126/science.aan2301.
(32) Ismael, M. A Review and Recent Advances in Solar-to-Hydrogen Energy Conversion Based on Photocatalytic Water Splitting over Doped-TiO2 Nanoparticles. *Solar Energy* **2020**, *211*, 522–546. https://doi.org/10.1016/j.solener.2020.09.073.
(33) De Luna, M. D. G.; Lu, M.-C. Titanium Dioxide for Visible-Light Photocatalytic Purification of Gaseous Indoor Air Pollutants. *Chemical Physics Research Journal* **2014**, *7* (1), 113–132.
(34) Pham, T.-D.; Lee, B.-K. Cu Doped TiO2/GF for Photocatalytic Disinfection of Escherichia Coli in Bioaerosols under Visible Light Irradiation: Application and Mechanism. *Applied Surface Science* **2014**, *296*, 15–23. https://doi.org/10.1016/j.apsusc.2014.01.006.
(35) Linsebigler, A. L.; Lu, G.; Yates, J. T. Jr. Photocatalysis on TiO2 Surfaces: Principles, Mechanisms, and Selected Results. *Chem. Rev.* **1995**, *95* (3), 735–758. https://doi.org/10.1021/cr00035a013.
(36) Balasubramanian, G.; Dionysiou, D. D.; Suidan, M. T.; Baudin, I.; Laîné, J.-M. Evaluating the Activities of Immobilized TiO2 Powder Films for the Photocatalytic Degradation of Organic Contaminants in Water. *Applied Catalysis B: Environmental* **2004**, *47* (2), 73–84. https://doi.org/10.1016/j.apcatb.2003.04.002.
(37) Mukherjee, P. S.; Ray, A. K. Major Challenges in the Design of a Large-Scale Photocatalytic Reactor for Water Treatment. *Chemical Engineering & Technology* **1999**, *22* (3), 253–260. https://doi.org/10.1002/(SICI)1521-4125(199903)22:3<253::AID-CEAT253>3.0.CO;2-X.
(38) Gusain, R.; Gupta, K.; Joshi, P.; Khatri, O. P. Adsorptive Removal and Photocatalytic Degradation of Organic Pollutants Using Metal Oxides and Their Composites: A Comprehensive Review. *Advances in Colloid and Interface Science* **2019**, *272*, 102009. https://doi.org/10.1016/j.cis.2019.102009.
(39) Ager, J. W.; Shaner, M. R.; Walczak, K. A.; Sharp, I. D.; Ardo, S. Experimental Demonstrations of Spontaneous, Solar-Driven Photoelectrochemical Water Splitting. *Energy Environ. Sci.* **2015**, *8* (10), 2811–2824. https://doi.org/10.1039/C5EE00457H.
(40) Naber, J. D.; Siebers, D. L. Hydrogen Combustion under Diesel Engine Conditions. *International Journal of Hydrogen Energy* **1998**, *23* (5), 363–371. https://doi.org/10.1016/S0360-3199(97)00083-9.
(41) Cheng, X.; Shi, Z.; Glass, N.; Zhang, L.; Zhang, J.; Song, D.; Liu, Z.-S.; Wang, H.; Shen, J. A Review of PEM Hydrogen Fuel Cell Contamination: Impacts, Mechanisms, and Mitigation. *Journal of Power Sources* **2007**, *165*, 739–756. https://doi.org/10.1016/j.jpowsour.2006.12.012.
(42) Ohashi, K.; Mccann, J.; Bockris, J. O. Stable Photoelectrochemical Cells for the Splitting of Water. *Nature* **1977**, *266* (5603), 610–611. https://doi.org/10.1038/266610a0.

(43) Grätzel, M. Photoelectrochemical Cells. *Nature* **2001**, *414* (6861), 338–344. https://doi.org/10.1038/35104607.
(44) Miao, F.; Wijeratne, S.; Zhang, Y.; Coskun, U. C.; Bao, W.; Lau, C. N. Phase-Coherent Transport in Graphene Quantum Billiards. *Science* **2007**, *317* (5844), 1530–1533. https://doi.org/10.1126/science.1144359.
(45) Novoselov, K. S.; Geim, A. K.; Morozov, S. V.; Jiang, D.; Katsnelson, M. I.; Grigorieva, I. V.; Dubonos, S. V.; Firsov, A. A. Two-Dimensional Gas of Massless Dirac Fermions in Graphene. *Nature* **2005**, *438* (7065), 197–200. https://doi.org/10.1038/nature04233.
(46) Kane, C. L.; Mele, E. J. Quantum Spin Hall Effect in Graphene. *Phys. Rev. Lett.* **2005**, *95* (22), 226801. https://doi.org/10.1103/PhysRevLett.95.226801.
(47) Novoselov, K. S.; Geim, A. K.; Morozov, S. V.; Jiang, D.; Zhang, Y.; Dubonos, S. V.; Grigorieva, I. V.; Firsov, A. A. Electric Field Effect in Atomically Thin Carbon Films. *Science* **2004**, *306* (5696), 666–669. https://doi.org/10.1126/science.1102896.
(48) Morozov, S. V.; Novoselov, K. S.; Katsnelson, M. I.; Schedin, F.; Ponomarenko, L. A.; Jiang, D.; Geim, A. K. *Strong suppression of weak (anti)localization in graphene*. arXiv.org. https://doi.org/10.1103/PhysRevLett.97.016801.
(49) Peres, N. M. R.; Castro Neto, A. H.; Guinea, F. Conductance Quantization in Mesoscopic Graphene. *Phys. Rev. B* **2006**, *73* (19), 195411. https://doi.org/10.1103/PhysRevB.73.195411.
(50) Abanin, D. A.; Lee, P. A.; Levitov, L. S. Randomness-Induced XY Ordering in a Graphene Quantum Hall Ferromagnet. *Phys Rev Lett* **2007**, *98* (15), 156801. https://doi.org/10.1103/PhysRevLett.98.156801.
(51) Zhao, S.; Li, Z.; Yang, J. Obtaining Two-Dimensional Electron Gas in Free Space without Resorting to Electron Doping: An Electride Based Design. *J. Am. Chem. Soc.* **2014**, *136* (38), 13313–13318. https://doi.org/10.1021/ja5065125.
(52) Xu, B.; Tian, H.; Bi, D.; Gabrielsson, E.; Johansson, E. M. J.; Boschloo, G.; Hagfeldt, A.; Sun, L. Efficient Solid State Dye-Sensitized Solar Cells Based on an Oligomer Hole Transport Material and an Organic Dye. *J. Mater. Chem. A* **2013**, *1* (46), 14467–14470. https://doi.org/10.1039/C3TA13646A.
(53) Miró, P.; Audiffred, M.; Heine, T. An Atlas of Two-Dimensional Materials. *Chem. Soc. Rev.* **2014**, *43* (18), 6537–6554. https://doi.org/10.1039/C4CS00102H.
(54) Fujishima, A.; Honda, K. Electrochemical Photolysis of Water at a Semiconductor Electrode. *Nature* **1972**, *238* (5358), 37–38. https://doi.org/10.1038/238037a0.
(55) Li, Y.; Li, Y.-L.; Sa, B.; Ahuja, R. Review of Two-Dimensional Materials for Photocatalytic Water Splitting from a Theoretical Perspective. *Catal. Sci. Technol.* **2017**, *7* (3), 545–559. https://doi.org/10.1039/C6CY02178F.
(56) Tang, C.; Zhang, C.; Matta, S. K.; Jiao, Y.; Ostrikov, K.; Liao, T.; Kou, L.; Du, A. Predicting New Two-Dimensional Pd3(PS4)2 as an Efficient Photocatalyst for Water Splitting. *J. Phys. Chem. C* **2018**, *122* (38), 21927–21932. https://doi.org/10.1021/acs.jpcc.8b06622.
(57) Schultz, M. G.; Diehl, T.; Brasseur, G. P.; Zittel, W. Air Pollution and Climate-Forcing Impacts of a Global Hydrogen Economy. *Science* **2003**, *302* (5645), 624–627. https://doi.org/10.1126/science.1089527.

(58) Acar, C.; Dincer, I.; Naterer, G. F. Review of Photocatalytic Water-Splitting Methods for Sustainable Hydrogen Production. *International Journal of Energy Research* **2016**, *40* (11), 1449–1473. https://doi.org/10.1002/er.3549.
(59) Matta, S. K.; Zhang, C.; Jiao, Y.; O'Mullane, A.; Du, A. Versatile Two-Dimensional Silicon Diphosphide (SiP2) for Photocatalytic Water Splitting. *Nanoscale* **2018**, *10* (14), 6369–6374. https://doi.org/10.1039/C7NR07994J.
(60) Ni, M.; Leung, M. K. H.; Leung, D. Y. C.; Sumathy, K. A Review and Recent Developments in Photocatalytic Water-Splitting Using TiO2 for Hydrogen Production. *Renewable and Sustainable Energy Reviews* **2007**, *11* (3), 401–425. https://doi.org/10.1016/j.rser.2005.01.009.
(61) Navarro Yerga, R. M.; Álvarez Galván, M. C.; del Valle, F.; Villoria de la Mano, J. A.; Fierro, J. L. G. Water Splitting on Semiconductor Catalysts under Visible-Light Irradiation. *ChemSusChem* **2009**, *2* (6), 471–485. https://doi.org/10.1002/cssc.200900018.
(62) Khaselev, O.; Turner, J. A. A Monolithic Photovoltaic-Photoelectrochemical Device for Hydrogen Production via Water Splitting. *Science* **1998**, *280* (5362), 425–427. https://doi.org/10.1126/science.280.5362.425.
(63) Bai, Y.; Zhang, Q.; Luo, G.; Bu, Y.; Zhu, L.; Fan, L.; Wang, B. GaS0.5Te0.5 Monolayer as an Efficient Water Splitting Photocatalyst. *Phys. Chem. Chem. Phys.* **2017**, *19* (23), 15394–15402. https://doi.org/10.1039/C7CP01627A.
(64) Maeda, K.; Domen, K. New Non-Oxide Photocatalysts Designed for Overall Water Splitting under Visible Light. *J. Phys. Chem. C* **2007**, *111* (22), 7851–7861. https://doi.org/10.1021/jp070911w.
(65) Liao, J.; Sa, B.; Zhou, J.; Ahuja, R.; Sun, Z. Design of High-Efficiency Visible-Light Photocatalysts for Water Splitting: MoS2/AlN(GaN) Heterostructures. *J. Phys. Chem. C* **2014**, *118* (31), 17594–17599. https://doi.org/10.1021/jp5038014.
(66) Wang, G.; Dang, S.; Zhang, P.; Xiao, S.; Wang, C.; Zhong, M. Hybrid Density Functional Study on the Photocatalytic Properties of AlN/MoSe2, AlN/WS2, and AlN/WSe2 Heterostructures. *J. Phys. D: Appl. Phys.* **2017**, *51* (2), 025109. https://doi.org/10.1088/1361-6463/aa9df9.
(67) Faraji, M.; Yousefi, M.; Yousefzadeh, S.; Zirak, M.; Naseri, N.; Jeon, T. H.; Choi, W.; Moshfegh, A. Z. Two-Dimensional Materials in Semiconductor Photoelectrocatalytic Systems for Water Splitting. *Energy Environ. Sci.* **2019**, *12* (1), 59–95. https://doi.org/10.1039/C8EE00886H.
(68) Asahi, R.; Morikawa, T.; Ohwaki, T.; Aoki, K.; Taga, Y. Visible-Light Photocatalysis in Nitrogen-Doped Titanium Oxides. *Science* **2001**, *293* (5528), 269–271. https://doi.org/10.1126/science.1061051.
(69) Khan, S. U. M.; Al-Shahry, M.; Ingler, W. B. Efficient Photochemical Water Splitting by a Chemically Modified N-TiO2. *Science* **2002**, *297* (5590), 2243–2245. https://doi.org/10.1126/science.1075035.
(70) Liu, M.; Inde, R.; Nishikawa, M.; Qiu, X.; Atarashi, D.; Sakai, E.; Nosaka, Y.; Hashimoto, K.; Miyauchi, M. Enhanced Photoactivity with Nanocluster-Grafted Titanium Dioxide Photocatalysts. *ACS Nano* **2014**, *8* (7), 7229–7238. https://doi.org/10.1021/nn502247x.
(71) Roy, P.; Berger, S.; Schmuki, P. TiO2 Nanotubes: Synthesis and Applications. *Angewandte Chemie International Edition* **2011**, *50* (13), 2904–2939. https://doi.org/10.1002/anie.201001374.
(72) Schneider, J.; Matsuoka, M.; Takeuchi, M.; Zhang, J.; Horiuchi, Y.; Anpo, M.; Bahnemann, D. W. Understanding TiO2 Photocatalysis: Mechanisms and

Materials. *Chem. Rev.* **2014**, *114* (19), 9919–9986. https://doi.org/10.1021/cr5001892.
(73) Yang, H. G.; Sun, C. H.; Qiao, S. Z.; Zou, J.; Liu, G.; Smith, S. C.; Cheng, H. M.; Lu, G. Q. Anatase TiO2 Single Crystals with a Large Percentage of Reactive Facets. *Nature* **2008**, *453* (7195), 638–641. https://doi.org/10.1038/nature06964.
(74) Zhang, H.; Lv, X.; Li, Y.; Wang, Y.; Li, J. P25-Graphene Composite as a High Performance Photocatalyst. *ACS Nano* **2010**, *4* (1), 380–386. https://doi.org/10.1021/nn901221k.
(75) Zuo, F.; Bozhilov, K.; Dillon, R. J.; Wang, L.; Smith, P.; Zhao, X.; Bardeen, C.; Feng, P. Active Facets on Titanium(III)-Doped TiO2: An Effective Strategy to Improve the Visible-Light Photocatalytic Activity. *Angewandte Chemie International Edition* **2012**, *51* (25), 6223–6226. https://doi.org/10.1002/anie.201202191.
(76) Yu, J. C.; Zhang, L.; Zheng, Z.; Zhao, J. Synthesis and Characterization of Phosphated Mesoporous Titanium Dioxide with High Photocatalytic Activity. *Chem. Mater.* **2003**, *15* (11), 2280–2286. https://doi.org/10.1021/cm0340781.
(77) Kochuveedu, S. T. *Photocatalytic and Photoelectrochemical Water Splitting on TiO2 via Photosensitization*. Journal of Nanomaterials. https://doi.org/10.1155/2016/4073142.
(78) Zhang, L.; Mao, X.; Matta, S. K.; Gu, Y.; Du, A. Two-Dimensional CuTe2X (X = Cl, Br, and I): Potential Photocatalysts for Water Splitting under the Visible/Infrared Light. *J. Phys. Chem. C* **2019**, *123* (42), 25543–25548. https://doi.org/10.1021/acs.jpcc.9b06116.
(79) Wq, C.; L, L.; Ss, M.; Yh, L.; Zs, Z. CdS-sensitized K2La2Ti3O10 composite: A new photocatalyst for hydrogen evolution under visible light irradiation. *Catal. Today* **2013**, *207*, 44–49.
(80) Hantanasirisakul, K.; Gogotsi, Y. Electronic and Optical Properties of 2D Transition Metal Carbides and Nitrides (MXenes). *Advanced Materials* **2018**, *30* (52), 1804779. https://doi.org/10.1002/adma.201804779.
(81) Ang, Y. S.; Sultan, S.; Zhang, C. Nonlinear Optical Spectrum of Bilayer Graphene in the Terahertz Regime. *Appl. Phys. Lett.* **2010**, *97* (24), 243110. https://doi.org/10.1063/1.3527934.
(82) Zhao, J.; Wu, W.; Zhu, J.; Lu, Y.; Xiang, B.; Yang, S. A. Highly Anisotropic Two-Dimensional Metal in Monolayer ${\mathrm{MoOCl}}_{2}$. *Phys. Rev. B* **2020**, *102* (24), 245419. https://doi.org/10.1103/PhysRevB.102.245419.
(83) Malekpour, H.; Chang, K.-H.; Chen, J.-C.; Lu, C.-Y.; Nika, D. L.; Novoselov, K. S.; Balandin, A. A. Thermal Conductivity of Graphene Laminate. *Nano Lett.* **2014**, *14* (9), 5155–5161. https://doi.org/10.1021/nl501996v.
(84) Zhou, W.-X.; Cheng, Y.; Chen, K.-Q.; Xie, G.; Wang, T.; Zhang, G. Thermal Conductivity of Amorphous Materials. *Advanced Functional Materials* **2020**, *30* (8), 1903829. https://doi.org/10.1002/adfm.201903829.
(85) Esposito, M.; Harbola, U.; Mukamel, S. Nonequilibrium Fluctuations, Fluctuation Theorems, and Counting Statistics in Quantum Systems. *Rev. Mod. Phys.* **2009**, *81* (4), 1665–1702. https://doi.org/10.1103/RevModPhys.81.1665.
(86) Ang, Y. S.; Yang, S. A.; Zhang, C.; Ma, Z.; Ang, L. K. Valleytronics in Merging Dirac Cones: All-Electric-Controlled Valley Filter, Valve, and

Universal Reversible Logic Gate. *Phys. Rev. B* **2017**, *96* (24), 245410. https://doi.org/10.1103/PhysRevB.96.245410.
(87) Ang, Y. S.; Yang, H. Y.; Ang, L. K. Universal Scaling Laws in Schottky Heterostructures Based on Two-Dimensional Materials. *Phys. Rev. Lett.* **2018**, *121* (5), 056802. https://doi.org/10.1103/PhysRevLett.121.056802.
(88) Yu, Z.; Ong, Z.-Y.; Li, S.; Xu, J.-B.; Zhang, G.; Zhang, Y.-W.; Shi, Y.; Wang, X. Analyzing the Carrier Mobility in Transition-Metal Dichalcogenide MoS2 Field-Effect Transistors. *Advanced Functional Materials* **2017**, *27* (19), 1604093. https://doi.org/10.1002/adfm.201604093.
(89) Ni, X.; Guo, X.; Li, J.; Huang, Y.; Zhang, Y.; Rogers, J. A. 2D Mechanical Metamaterials with Widely Tunable Unusual Modes of Thermal Expansion. *Advanced Materials* **2019**, *31* (48), 1905405. https://doi.org/10.1002/adma.201905405.
(90) López-Polín, G.; Gómez-Herrero, J.; Gómez-Navarro, C. Confining Crack Propagation in Defective Graphene. *Nano Lett.* **2015**, *15* (3), 2050–2054. https://doi.org/10.1021/nl504936q.
(91) Hu, J.; Wu, R. Giant Magnetic Anisotropy of Transition-Metal Dimers on Defected Graphene. *Nano Lett.* **2014**, *14* (4), 1853–1858. https://doi.org/10.1021/nl404627h.
(92) Lherbier, A.; Blase, X.; Niquet, Y.-M.; Triozon, F.; Roche, S. Charge Transport in Chemically Doped 2D Graphene. *Phys. Rev. Lett.* **2008**, *101* (3), 036808. https://doi.org/10.1103/PhysRevLett.101.036808.
(93) Bostwick, A.; Speck, F.; Seyller, T.; Horn, K.; Polini, M.; Asgari, R.; MacDonald, A. H.; Rotenberg, E. Observation of Plasmarons in Quasi-Freestanding Doped Graphene. *Science* **2010**, *328* (5981), 999–1002. https://doi.org/10.1126/science.1186489.
(94) Balog, R.; Jørgensen, B.; Nilsson, L.; Andersen, M.; Rienks, E.; Bianchi, M.; Fanetti, M.; Lægsgaard, E.; Baraldi, A.; Lizzit, S.; Sljivancanin, Z.; Besenbacher, F.; Hammer, B.; Pedersen, T. G.; Hofmann, P.; Hornekær, L. Bandgap Opening in Graphene Induced by Patterned Hydrogen Adsorption. *Nature Mater* **2010**, *9* (4), 315–319. https://doi.org/10.1038/nmat2710.
(95) Kunitski, M.; Eicke, N.; Huber, P.; Köhler, J.; Zeller, S.; Voigtsberger, J.; Schlott, N.; Henrichs, K.; Sann, H.; Trinter, F.; Schmidt, L. P. H.; Kalinin, A.; Schöffler, M. S.; Jahnke, T.; Lein, M.; Dörner, R. Double-Slit Photoelectron Interference in Strong-Field Ionization of the Neon Dimer. *Nat Commun* **2019**, *10* (1), 1. https://doi.org/10.1038/s41467-018-07882-8.
(96) Dai, Z.; Liu, L.; Zhang, Z. Strain Engineering of 2D Materials: Issues and Opportunities at the Interface. *Advanced Materials* **2019**, *31* (45), 1805417. https://doi.org/10.1002/adma.201805417.
(97) Wang, G.; Zhi, Y.; Xia, L.; Chang, J.; Yuan, B.; Guo, X.; Li, Y.; Xiao, S.; Yuan, H. 2D CdO-Based Heterostructure as a Promising Visible Light Water-Splitting Photocatalyst. *physica status solidi (a)* **2020**, *217* (8), 1900859. https://doi.org/10.1002/pssa.201900859.
(98) Li, L. J.; O'Farrell, E. C. T.; Loh, K. P.; Eda, G.; Özyilmaz, B.; Castro Neto, A. H. Controlling Many-Body States by the Electric-Field Effect in a Two-Dimensional Material. *Nature* **2016**, *529* (7585), 185–189. https://doi.org/10.1038/nature16175.
(99) Liu, F.; Zhou, J.; Zhu, C.; Liu, Z. Electric Field Effect in Two-Dimensional Transition Metal Dichalcogenides. *Advanced Functional Materials* **2017**, *27* (19), 1602404. https://doi.org/10.1002/adfm.201602404.

(100) Guo, B.; Tian, L.; Xie, W.; Batool, A.; Xie, G.; Xiang, Q.; Jan, S. U.; Boddula, R.; Gong, J. R. Vertically Aligned Porous Organic Semiconductor Nanorod Array Photoanodes for Efficient Charge Utilization. *Nano Lett.* **2018**, *18* (9), 5954–5960. https://doi.org/10.1021/acs.nanolett.8b02740.
(101) Rahman, M. Z.; Kwong, C. W.; Davey, K.; Qiao, S. Z. 2D Phosphorene as a Water Splitting Photocatalyst: Fundamentals to Applications. *Energy Environ. Sci.* **2016**, *9* (3), 709–728. https://doi.org/10.1039/C5EE03732H.
(102) Wu, D.; Zhang, X.; Jing, Y.; Zhao, X.; Zhou, Z. Towards Visible-Light Water Splitting Photocatalysts: Band Engineering of Two-Dimensional A5B4O15 Perovskites. *Nano Energy* **2016**, *28*, 390–396. https://doi.org/10.1016/j.nanoen.2016.08.064.
(103) Ong, W.-J.; Tan, L.-L.; Ng, Y. H.; Yong, S.-T.; Chai, S.-P. Graphitic Carbon Nitride (g-C3N4)-Based Photocatalysts for Artificial Photosynthesis and Environmental Remediation: Are We a Step Closer To Achieving Sustainability? *Chem. Rev.* **2016**, *116* (12), 7159–7329. https://doi.org/10.1021/acs.chemrev.6b00075.
(104) Wu, Z.; Neaton, J. B.; Grossman, J. C. Charge Separation via Strain in Silicon Nanowires. *Nano Lett.* **2009**, *9* (6), 2418–2422. https://doi.org/10.1021/nl9010854.
(105) Kamat, P. V. Graphene-Based Nanoassemblies for Energy Conversion. *J. Phys. Chem. Lett.* **2011**, *2* (3), 242–251. https://doi.org/10.1021/jz101639v.
(106) Bhardwaj, A.; Kaur, J.; Wuest, M.; Wuest, F. In Situ Click Chemistry Generation of Cyclooxygenase-2 Inhibitors. *Nat Commun* **2017**, *8* (1), 1. https://doi.org/10.1038/s41467-016-0009-6.
(107) Su, J.; Guo, L.; Bao, N.; Grimes, C. A. Nanostructured WO3/BiVO4 Heterojunction Films for Efficient Photoelectrochemical Water Splitting. *Nano Lett.* **2011**, *11* (5), 1928–1933. https://doi.org/10.1021/nl2000743.
(108) Wang, J.; Liu, C. Preparation of 2D WO3 Nanomaterials with Enhanced Catalytic Activities: Current Status and Perspective. *ChemBioEng Reviews* **2015**, *2* (5), 335–350. https://doi.org/10.1002/cben.201500014.
(109) Zhang, Q.; Li, Z.; Wang, S.; Li, R.; Zhang, X.; Liang, Z.; Han, H.; Liao, S.; Li, C. Effect of Redox Cocatalysts Location on Photocatalytic Overall Water Splitting over Cubic NaTaO3 Semiconductor Crystals Exposed with Equivalent Facets. *ACS Catal.* **2016**, *6* (4), 2182–2191. https://doi.org/10.1021/acscatal.5b02503.
(110) Maeda, K.; Domen, K. Photocatalytic Water Splitting: Recent Progress and Future Challenges. *J. Phys. Chem. Lett.* **2010**, *1* (18), 2655–2661. https://doi.org/10.1021/jz1007966.
(111) Qi, K.; Xing, X.; Zada, A.; Li, M.; Wang, Q.; Liu, S.; Lin, H.; Wang, G. Transition Metal Doped ZnO Nanoparticles with Enhanced Photocatalytic and Antibacterial Performances: Experimental and DFT Studies. *Ceramics International* **2020**, *46* (2), 1494–1502. https://doi.org/10.1016/j.ceramint.2019.09.116.
(112) Iwashina, K.; Kudo, A. Rh-Doped SrTiO3 Photocatalyst Electrode Showing Cathodic Photocurrent for Water Splitting under Visible-Light Irradiation. *J. Am. Chem. Soc.* **2011**, *133* (34), 13272–13275. https://doi.org/10.1021/ja2050315.
(113) Kato, H.; Asakura, K.; Kudo, A. Highly Efficient Water Splitting into H2 and O2 over Lanthanum-Doped NaTaO3 Photocatalysts with High Crystallinity

and Surface Nanostructure. *J. Am. Chem. Soc.* **2003**, *125* (10), 3082–3089. https://doi.org/10.1021/ja027751g.
(114) Katsumata, K.; Cordonier, C. E. J.; Shichi, T.; Fujishima, A. Photocatalytic Activity of NaNbO3 Thin Films. *J. Am. Chem. Soc.* **2009**, *131* (11), 3856–3857. https://doi.org/10.1021/ja900394x.
(115) Li, L.; Yan, J.; Wang, T.; Zhao, Z.-J.; Zhang, J.; Gong, J.; Guan, N. Sub-10 Nm Rutile Titanium Dioxide Nanoparticles for Efficient Visible-Light-Driven Photocatalytic Hydrogen Production. *Nature Communications* **2015**, *6* (1), 5881. https://doi.org/10.1038/ncomms6881.
(116) *A Novel Aqueous Process for Preparation of Crystal Form-Controlled and Highly Crystalline BiVO4 Powder from Layered Vanadates at Room Temperature and Its Photocatalytic and Photophysical Properties | Journal of the American Chemical Society*. https://pubs.acs.org/doi/10.1021/ja992541y (accessed 2023-04-04).
(117) *Photocatalytic O2 evolution under visible light irradiation on BiVO4 in aqueous AgNO3 solution | SpringerLink*. https://link.springer.com/article/10.1023/A:1019034728816 (accessed 2023-04-04).
(118) Jeong, H. W.; Jeon, T. H.; Jang, J. S.; Choi, W.; Park, H. Strategic Modification of BiVO4 for Improving Photoelectrochemical Water Oxidation Performance. *J. Phys. Chem. C* **2013**, *117* (18), 9104–9112. https://doi.org/10.1021/jp400415m.
(119) Aiga, N.; Jia, Q.; Watanabe, K.; Kudo, A.; Sugimoto, T.; Matsumoto, Y. Electron–Phonon Coupling Dynamics at Oxygen Evolution Sites of Visible-Light-Driven Photocatalyst: Bismuth Vanadate. *J. Phys. Chem. C* **2013**, *117* (19), 9881–9886. https://doi.org/10.1021/jp4013027.
(120) Park, Y.; McDonald, K. J.; Choi, K.-S. Progress in Bismuth Vanadate Photoanodes for Use in Solar Water Oxidation. *Chem. Soc. Rev.* **2013**, *42* (6), 2321–2337. https://doi.org/10.1039/C2CS35260E.
(121) Luo, W.; Wang, Z.; Wan, L.; Li, Z.; Yu, T.; Zou, Z. Synthesis, Growth Mechanism and Photoelectrochemical Properties of BiVO4 Microcrystal Electrodes. *J. Phys. D: Appl. Phys.* **2010**, *43* (40), 405402. https://doi.org/10.1088/0022-3727/43/40/405402.
(122) Xi, G.; Ye, J. Synthesis of Bismuth Vanadate Nanoplates with Exposed {001} Facets and Enhanced Visible-Light Photocatalytic Properties. *Chem. Commun.* **2010**, *46* (11), 1893–1895. https://doi.org/10.1039/B923435G.
(123) Zhong, D. K.; Choi, S.; Gamelin, D. R. Near-Complete Suppression of Surface Recombination in Solar Photoelectrolysis by "Co-Pi" Catalyst-Modified W:BiVO4. *J. Am. Chem. Soc.* **2011**, *133* (45), 18370–18377. https://doi.org/10.1021/ja207348x.
(124) Jeon, T. H.; Choi, W.; Park, H. Cobalt–Phosphate Complexes Catalyze the Photoelectrochemical Water Oxidation of BiVO4 Electrodes. *Phys. Chem. Chem. Phys.* **2011**, *13* (48), 21392–21401. https://doi.org/10.1039/C1CP23135A.
(125) Zhang, H.; Cai, J.; Wang, Y.; Wu, M.; Meng, M.; Tian, Y.; Li, X.; Zhang, J.; Zheng, L.; Jiang, Z.; Gong, J. Insights into the Effects of Surface/Bulk Defects on Photocatalytic Hydrogen Evolution over TiO2 with Exposed {001} Facets. *Applied Catalysis B: Environmental* **2018**, *220*, 126–136. https://doi.org/10.1016/j.apcatb.2017.08.046.

(126) Puthirath Balan, A.; Radhakrishnan, S.; Woellner, C. F.; Sinha, S. K.; Deng, L.; Reyes, C. de L.; Rao, B. M.; Paulose, M.; Neupane, R.; Apte, A.; Kochat, V.; Vajtai, R.; Harutyunyan, A. R.; Chu, C.-W.; Costin, G.; Galvao, D. S.; Martí, A. A.; van Aken, P. A.; Varghese, O. K.; Tiwary, C. S.; Malie Madom Ramaswamy Iyer, A.; Ajayan, P. M. Exfoliation of a Non-van Der Waals Material from Iron Ore Hematite. *Nat Nanotechnol* **2018**, *13* (7), 602–609. https://doi.org/10.1038/s41565-018-0134-y.
(127) Li, H.; Wu, J.; Yin, Z.; Zhang, H. Preparation and Applications of Mechanically Exfoliated Single-Layer and Multilayer MoS2 and WSe2 Nanosheets. *Acc. Chem. Res.* **2014**, *47* (4), 1067–1075. https://doi.org/10.1021/ar4002312.
(128) Yu, J.; Xu, C.-Y.; Ma, F.-X.; Hu, S.-P.; Zhang, Y.-W.; Zhen, L. Monodisperse SnS2 Nanosheets for High-Performance Photocatalytic Hydrogen Generation. *ACS Appl. Mater. Interfaces* **2014**, *6* (24), 22370–22377. https://doi.org/10.1021/am506396z.
(129) Mak, K. F.; Lee, C.; Hone, J.; Shan, J.; Heinz, T. F. Atomically Thin MoS_2: A New Direct-Gap Semiconductor. *Phys Rev Lett* **2010**, *105* (13), 136805. https://doi.org/10.1103/PhysRevLett.105.136805.
(130) Bonaccorso, F.; Bartolotta, A.; Coleman, J. N.; Backes, C. 2D-Crystal-Based Functional Inks. *Advanced Materials* **2016**, *28* (29), 6136–6166. https://doi.org/10.1002/adma.201506410.
(131) Singh, N.; Jabbour, G.; Schwingenschlögl, U. Optical and Photocatalytic Properties of Two-Dimensional MoS2. *Eur. Phys. J. B* **2012**, *85* (11), 392. https://doi.org/10.1140/epjb/e2012-30449-7.
(132) Lin, C.; Zhu, X.; Feng, J.; Wu, C.; Hu, S.; Peng, J.; Guo, Y.; Peng, L.; Zhao, J.; Huang, J.; Yang, J.; Xie, Y. Hydrogen-Incorporated TiS2 Ultrathin Nanosheets with Ultrahigh Conductivity for Stamp-Transferrable Electrodes. *J. Am. Chem. Soc.* **2013**, *135* (13), 5144–5151. https://doi.org/10.1021/ja400041f.
(133) Sang, Y.; Zhao, Z.; Zhao, M.; Hao, P.; Leng, Y.; Liu, H. From UV to Near-Infrared, WS2 Nanosheet: A Novel Photocatalyst for Full Solar Light Spectrum Photodegradation. *Advanced Materials* **2015**, *27* (2), 363–369. https://doi.org/10.1002/adma.201403264.
(134) Jang, J.; Jeong, S.; Seo, J.; Kim, M.-C.; Sim, E.; Oh, Y.; Nam, S.; Park, B.; Cheon, J. Ultrathin Zirconium Disulfide Nanodiscs. *J. Am. Chem. Soc.* **2011**, *133* (20), 7636–7639. https://doi.org/10.1021/ja200400n.
(135) Wu, Y.; Xu, M.; Chen, X.; Yang, S.; Wu, H.; Pan, J.; Xiong, X. CTAB-Assisted Synthesis of Novel Ultrathin MoSe2 Nanosheets Perpendicular to Graphene for the Adsorption and Photodegradation of Organic Dyes under Visible Light. *Nanoscale* **2015**, *8* (1), 440–450. https://doi.org/10.1039/C5NR05748E.
(136) Li, S.-L.; Tsukagoshi, K.; Orgiu, E.; Samorì, P. Charge Transport and Mobility Engineering in Two-Dimensional Transition Metal Chalcogenide Semiconductors. *Chem. Soc. Rev.* **2015**, *45* (1), 118–151. https://doi.org/10.1039/C5CS00517E.
(137) Allen, M. J.; Tung, V. C.; Kaner, R. B. Honeycomb Carbon: A Review of Graphene. *Chem. Rev.* **2010**, *110* (1), 132–145. https://doi.org/10.1021/cr900070d.
(138) Yasaei, P.; Kumar, B.; Foroozan, T.; Wang, C.; Asadi, M.; Tuschel, D.; Indacochea, J. E.; Klie, R. F.; Salehi-Khojin, A. High-Quality Black

Phosphorus Atomic Layers by Liquid-Phase Exfoliation. *Advanced Materials* **2015**, *27* (11), 1887–1892. https://doi.org/10.1002/adma.201405150.
(139) Niu, P.; Zhang, L.; Liu, G.; Cheng, H.-M. Graphene-Like Carbon Nitride Nanosheets for Improved Photocatalytic Activities. *Advanced Functional Materials* **2012**, *22* (22), 4763–4770. https://doi.org/10.1002/adfm.201200922.
(140) Nag, A.; Raidongia, K.; Hembram, K. P. S. S.; Datta, R.; Waghmare, U. V.; Rao, C. N. R. Graphene Analogues of BN: Novel Synthesis and Properties. *ACS Nano* **2010**, *4* (3), 1539–1544. https://doi.org/10.1021/nn9018762.
(141) Xia, F.; Wang, H.; Xiao, D.; Dubey, M.; Ramasubramaniam, A. Two-Dimensional Material Nanophotonics. *Nature Photonics* **2014**, *8* (12), 899–907. https://doi.org/10.1038/nphoton.2014.271.
(142) Zheng, Y.; Jiao, Y.; Chen, J.; Liu, J.; Liang, J.; Du, A.; Zhang, W.; Zhu, Z.; Smith, S. C.; Jaroniec, M.; Lu, G. Q. (Max); Qiao, S. Z. Nanoporous Graphitic-C_3N_4@Carbon Metal-Free Electrocatalysts for Highly Efficient Oxygen Reduction. *J. Am. Chem. Soc.* **2011**, *133* (50), 20116–20119. https://doi.org/10.1021/ja209206c.
(143) Yeh, T.-F.; Syu, J.-M.; Cheng, C.; Chang, T.-H.; Teng, H. Graphite Oxide as a Photocatalyst for Hydrogen Production from Water. *Advanced Functional Materials* **2010**, *20* (14), 2255–2262. https://doi.org/10.1002/adfm.201000274.
(144) Algara-Siller, G.; Severin, N.; Chong, S. Y.; Björkman, T.; Palgrave, R. G.; Laybourn, A.; Antonietti, M.; Khimyak, Y. Z.; Krasheninnikov, A. V.; Rabe, J. P.; Kaiser, U.; Cooper, A. I.; Thomas, A.; Bojdys, M. J. Triazine-Based Graphitic Carbon Nitride: A Two-Dimensional Semiconductor. *Angew Chem Int Ed Engl* **2014**, *53* (29), 7450–7455. https://doi.org/10.1002/anie.201402191.
(145) Lin, Z.; Wang, X. Nanostructure Engineering and Doping of Conjugated Carbon Nitride Semiconductors for Hydrogen Photosynthesis. *Angewandte Chemie International Edition* **2013**, *52* (6), 1735–1738. https://doi.org/10.1002/anie.201209017.
(146) Liu, J.; Liu, Y.; Liu, N.; Han, Y.; Zhang, X.; Huang, H.; Lifshitz, Y.; Lee, S.-T.; Zhong, J.; Kang, Z. Water Splitting. Metal-Free Efficient Photocatalyst for Stable Visible Water Splitting via a Two-Electron Pathway. *Science* **2015**, *347* (6225), 970–974. https://doi.org/10.1126/science.aaa3145.
(147) Wang, X.; Maeda, K.; Thomas, A.; Takanabe, K.; Xin, G.; Carlsson, J. M.; Domen, K.; Antonietti, M. A Metal-Free Polymeric Photocatalyst for Hydrogen Production from Water under Visible Light. *Nature Mater* **2009**, *8* (1), 76–80. https://doi.org/10.1038/nmat2317.
(148) Wang, X.; Maeda, K.; Chen, X.; Takanabe, K.; Domen, K.; Hou, Y.; Fu, X.; Antonietti, M. Polymer Semiconductors for Artificial Photosynthesis: Hydrogen Evolution by Mesoporous Graphitic Carbon Nitride with Visible Light. *J. Am. Chem. Soc.* **2009**, *131* (5), 1680–1681. https://doi.org/10.1021/ja809307s.
(149) Zhang, J.; Chen, X.; Takanabe, K.; Maeda, K.; Domen, K.; Epping, J. D.; Fu, X.; Antonietti, M.; Wang, X. Synthesis of a Carbon Nitride Structure for Visible-Light Catalysis by Copolymerization. *Angew Chem Int Ed Engl* **2010**, *49* (2), 441–444. https://doi.org/10.1002/anie.200903886.
(150) Zheng, D.; Pang, C.; Liu, Y.; Wang, X. Shell-Engineering of Hollow g-C3N4 Nanospheres via Copolymerization for Photocatalytic Hydrogen Evolution. *Chem. Commun.* **2015**, *51* (47), 9706–9709. https://doi.org/10.1039/C5CC03143E.

(151) Chu, S.; Wang, Y.; Guo, Y.; Feng, J.; Wang, C.; Luo, W.; Fan, X.; Zou, Z. Band Structure Engineering of Carbon Nitride: In Search of a Polymer Photocatalyst with High Photooxidation Property. *ACS Catal.* **2013**, *3* (5), 912–919. https://doi.org/10.1021/cs4000624.
(152) Liu, G.; Niu, P.; Sun, C.; Smith, S. C.; Chen, Z.; Lu, G. Q. (Max); Cheng, H.-M. Unique Electronic Structure Induced High Photoreactivity of Sulfur-Doped Graphitic C3N4. *J. Am. Chem. Soc.* **2010**, *132* (33), 11642–11648. https://doi.org/10.1021/ja103798k.
(153) Zhang, J.; Sun, J.; Maeda, K.; Domen, K.; Liu, P.; Antonietti, M.; Fu, X.; Wang, X. Sulfur-Mediated Synthesis of Carbon Nitride: Band-Gap Engineering and Improved Functions for Photocatalysis. *Energy Environ. Sci.* **2011**, *4* (3), 675–678. https://doi.org/10.1039/C0EE00418A.
(154) Zhu, B.; Zhang, L.; Cheng, B.; Yu, J. First-Principle Calculation Study of Tri-s-Triazine-Based g-C3N4: A Review. *Applied Catalysis B: Environmental* **2018**, *224*, 983–999. https://doi.org/10.1016/j.apcatb.2017.11.025.
(155) Yeh, T.-F.; Teng, C.-Y.; Chen, S.-J.; Teng, H. Nitrogen-Doped Graphene Oxide Quantum Dots as Photocatalysts for Overall Water-Splitting under Visible Light Illumination. *Advanced Materials* **2014**, *26* (20), 3297–3303. https://doi.org/10.1002/adma.201305299.
(156) Hu, S.; Ma, L.; You, J.; Li, F.; Fan, Z.; Lu, G.; Liu, D.; Gui, J. Enhanced Visible Light Photocatalytic Performance of G-C3N4 Photocatalysts Co-Doped with Iron and Phosphorus. *Applied Surface Science* **2014**, *311*, 164–171. https://doi.org/10.1016/j.apsusc.2014.05.036.
(157) Okamoto, Y.; Ida, S.; Hyodo, J.; Hagiwara, H.; Ishihara, T. Synthesis and Photocatalytic Activity of Rhodium-Doped Calcium Niobate Nanosheets for Hydrogen Production from a Water/Methanol System without Cocatalyst Loading. *J. Am. Chem. Soc.* **2011**, *133* (45), 18034–18037. https://doi.org/10.1021/ja207103j.
(158) Ida, S.; Koga, S.; Daio, T.; Hagiwara, H.; Ishihara, T. Direct Imaging of Light Emission Centers in Two-Dimensional Crystals and Their Luminescence and Photocatalytic Properties. *Angewandte Chemie International Edition* **2014**, *53* (48), 13078–13082. https://doi.org/10.1002/anie.201406638.
(159) Ataca, C.; Ciraci, S. Dissociation of H$\{\}_\{2\}$O at the Vacancies of Single-Layer MoS$\{\}_\{2\}$. *Phys. Rev. B* **2012**, *85* (19), 195410. https://doi.org/10.1103/PhysRevB.85.195410.
(160) Tay, Q.; Kanhere, P.; Ng, C. F.; Chen, S.; Chakraborty, S.; Huan, A. C. H.; Sum, T. C.; Ahuja, R.; Chen, Z. Defect Engineered G-C3N4 for Efficient Visible Light Photocatalytic Hydrogen Production. *Chem. Mater.* **2015**, *27* (14), 4930–4933. https://doi.org/10.1021/acs.chemmater.5b02344.
(161) Sa, B.; Li, Y.-L.; Qi, J.; Ahuja, R.; Sun, Z. Strain Engineering for Phosphorene: The Potential Application as a Photocatalyst. *J. Phys. Chem. C* **2014**, *118* (46), 26560–26568. https://doi.org/10.1021/jp508618t.
(162) Bard, A. J.; Fox, M. A. Artificial Photosynthesis: Solar Splitting of Water to Hydrogen and Oxygen. *Acc. Chem. Res.* **1995**, *28* (3), 141–145. https://doi.org/10.1021/ar00051a007.
(163) Abe, R. Recent Progress on Photocatalytic and Photoelectrochemical Water Splitting under Visible Light Irradiation. *Journal of Photochemistry and Photobiology C: Photochemistry Reviews* **2010**, *11* (4), 179–209. https://doi.org/10.1016/j.jphotochemrev.2011.02.003.

(164) Repins, I.; Contreras, M. A.; Egaas, B.; DeHart, C.; Scharf, J.; Perkins, C. L.; To, B.; Noufi, R. 19.9%-Efficient ZnO/CdS/CuInGaSe2 Solar Cell with 81.2% Fill Factor. *Progress in Photovoltaics: Research and Applications* **2008**, *16* (3, May 2008). https://doi.org/10.1002/pip.822.
(165) Carlson, D. E.; Wronski, C. R. Amorphous Silicon Solar Cell. *Appl. Phys. Lett.* **1976**, *28* (11), 671–673. https://doi.org/10.1063/1.88617.
(166) Wang, P.; Zakeeruddin, S. M.; Moser, J. E.; Nazeeruddin, M. K.; Sekiguchi, T.; Grätzel, M. A Stable Quasi-Solid-State Dye-Sensitized Solar Cell with an Amphiphilic Ruthenium Sensitizer and Polymer Gel Electrolyte. *Nat Mater* **2003**, *2* (6), 402–407. https://doi.org/10.1038/nmat904.
(167) Joshi, A. S.; Dincer, I.; Reddy, B. V. Solar Hydrogen Production: A Comparative Performance Assessment. *International Journal of Hydrogen Energy* **2011**, *36* (17), 11246–11257. https://doi.org/10.1016/j.ijhydene.2010.11.122.
(168) Kresse, G.; Furthmüller, J. Efficient Iterative Schemes for Ab Initio Total-Energy Calculations Using a Plane-Wave Basis Set. *Phys. Rev. B* **1996**, *54* (16), 11169–11186. https://doi.org/10.1103/PhysRevB.54.11169.
(169) Kresse, G.; Furthmüller, J. Efficiency of Ab-Initio Total Energy Calculations for Metals and Semiconductors Using a Plane-Wave Basis Set. *Computational Materials Science* **1996**, *6* (1), 15–50. https://doi.org/10.1016/0927-0256(96)00008-0.
(170) Perdew, J. P.; Zunger, A. Self-Interaction Correction to Density-Functional Approximations for Many-Electron Systems. *Phys. Rev. B* **1981**, *23* (10), 5048–5079. https://doi.org/10.1103/PhysRevB.23.5048.
(171) Cole, L. A.; Perdew, J. P. Calculated Electron Affinities of the Elements. *Phys. Rev. A* **1982**, *25* (3), 1265–1271. https://doi.org/10.1103/PhysRevA.25.1265.
(172) Perdew, J. P.; Wang, Y. Accurate and Simple Analytic Representation of the Electron-Gas Correlation Energy. *Phys. Rev. B* **1992**, *45* (23), 13244–13249. https://doi.org/10.1103/PhysRevB.45.13244.
(173) Perdew, J. P.; Burke, K.; Ernzerhof, M. Generalized Gradient Approximation Made Simple. *Phys. Rev. Lett.* **1996**, *77* (18), 3865–3868. https://doi.org/10.1103/PhysRevLett.77.3865.
(174) Becke, A. D. Density-Functional Exchange-Energy Approximation with Correct Asymptotic Behavior. *Phys. Rev. A* **1988**, *38* (6), 3098–3100. https://doi.org/10.1103/PhysRevA.38.3098.
(175) Akatsuka, K.; Takanashi, G.; Ebina, Y.; Haga, M.; Sasaki, T. Electronic Band Structure of Exfoliated Titanium- and/or Niobium-Based Oxide Nanosheets Probed by Electrochemical and Photoelectrochemical Measurements. *J. Phys. Chem. C* **2012**, *116* (23), 12426–12433. https://doi.org/10.1021/jp302417a.
(176) Shibata, T.; Takanashi, G.; Nakamura, T.; Fukuda, K.; Ebina, Y.; Sasaki, T. Titanoniobate and Niobate Nanosheet Photocatalysts: Superior Photoinduced Hydrophilicity and Enhanced Thermal Stability of Unilamellar Nb3O8 Nanosheet. *Energy Environ. Sci.* **2011**, *4* (2), 535–542. https://doi.org/10.1039/C0EE00437E.
(177) McCrory, C. C. L.; Jung, S.; Ferrer, I. M.; Chatman, S. M.; Peters, J. C.; Jaramillo, T. F. Benchmarking Hydrogen Evolving Reaction and Oxygen Evolving Reaction Electrocatalysts for Solar Water Splitting Devices. *J. Am. Chem. Soc.* **2015**, *137* (13), 4347–4357. https://doi.org/10.1021/ja510442p.

(178) Takanabe, K. Photocatalytic Water Splitting: Quantitative Approaches toward Photocatalyst by Design. *ACS Catal.* **2017**, *7* (11), 8006–8022. https://doi.org/10.1021/acscatal.7b02662.
(179) Qiao, M.; Liu, J.; Wang, Y.; Li, Y.; Chen, Z. PdSeO3 Monolayer: Promising Inorganic 2D Photocatalyst for Direct Overall Water Splitting Without Using Sacrificial Reagents and Cocatalysts. *J. Am. Chem. Soc.* **2018**, *140* (38), 12256–12262. https://doi.org/10.1021/jacs.8b07855.
(180) Zhang, X.; Zhao, X.; Wu, D.; Jing, Y.; Zhou, Z. MnPSe3 Monolayer: A Promising 2D Visible-Light Photohydrolytic Catalyst with High Carrier Mobility. *Advanced Science* **2016**, *3* (10), 1600062. https://doi.org/10.1002/advs.201600062.
(181) Zhao, P.; Ma, Y.; Lv, X.; Li, M.; Huang, B.; Dai, Y. Two-Dimensional III2-VI3 Materials: Promising Photocatalysts for Overall Water Splitting under Infrared Light Spectrum. *Nano Energy* **2018**, *51*, 533–538. https://doi.org/10.1016/j.nanoen.2018.07.010.
(182) Fu, C.-F.; Sun, J.; Luo, Q.; Li, X.; Hu, W.; Yang, J. Intrinsic Electric Fields in Two-Dimensional Materials Boost the Solar-to-Hydrogen Efficiency for Photocatalytic Water Splitting. *Nano Letters* **2018**, *18*. https://doi.org/10.1021/acs.nanolett.8b02561.
(183) Peng, R.; Ma, Y.; Huang, B.; Dai, Y. Two-Dimensional Janus PtSSe for Photocatalytic Water Splitting under the Visible or Infrared Light. *J. Mater. Chem. A* **2019**, *7* (2), 603–610. https://doi.org/10.1039/C8TA09177C.
(184) Yu, Z.; Ong, Z.-Y.; Pan, Y.; Cui, Y.; Xin, R.; Shi, Y.; Wang, B.; Wu, Y.; Chen, T.; Zhang, Y.-W.; Zhang, G.; Wang, X. Realization of Room-Temperature Phonon-Limited Carrier Transport in Monolayer MoS2 by Dielectric and Carrier Screening. *Advanced Materials* **2016**, *28* (3), 547–552. https://doi.org/10.1002/adma.201503033.
(185) Ong, W.-J.; Tan, L.-L.; Chai, S.-P.; Yong, S.-T.; Mohamed, A. R. Surface Charge Modification via Protonation of Graphitic Carbon Nitride (g-C3N4) for Electrostatic Self-Assembly Construction of 2D/2D Reduced Graphene Oxide (rGO)/g-C3N4 Nanostructures toward Enhanced Photocatalytic Reduction of Carbon Dioxide to Methane. *Nano Energy* **2015**, *13*, 757–770. https://doi.org/10.1016/j.nanoen.2015.03.014.
(186) Feng, H.; Xu, Z.; Wang, L.; Yu, Y.; Mitchell, D.; Cui, D.; Xu, X.; Shi, J.; Sannomiya, T.; Du, Y.; Hao, W.; Dou, S. Modulation of Photocatalytic Properties by Strain in 2d BiOBr Nanosheets. *Australian Institute for Innovative Materials - Papers* **2015**, 27592–27596. https://doi.org/10.1021/acsami.5b08904.
(187) Jiao, Y.; Zhou, L.; Ma, F.; Gao, G.; Kou, L.; Bell, J.; Sanvito, S.; Du, A. Predicting Single-Layer Technetium Dichalcogenides (TcX2, X = S, Se) with Promising Applications in Photovoltaics and Photocatalysis. *ACS Appl. Mater. Interfaces* **2016**, *8* (8), 5385–5392. https://doi.org/10.1021/acsami.5b12606.
(188) Jiao, Y.; Ma, F.; Gao, G.; Bell, J.; Frauenheim, T.; Du, A. Versatile Single-Layer Sodium Phosphidostannate(II): Strain-Tunable Electronic Structure, Excellent Mechanical Flexibility, and an Ideal Gap for Photovoltaics. *J. Phys. Chem. Lett.* **2015**, *6* (14), 2682–2687. https://doi.org/10.1021/acs.jpclett.5b01136.
(189) Deng, D.; Novoselov, K. S.; Fu, Q.; Zheng, N.; Tian, Z.; Bao, X. Catalysis with Two-Dimensional Materials and Their Heterostructures. *Nature Nanotech* **2016**, *11* (3), 218–230. https://doi.org/10.1038/nnano.2015.340.

(190) Cheon, G.; Duerloo, K.-A. N.; Sendek, A. D.; Porter, C.; Chen, Y.; Reed, E. J. Data Mining for New Two- and One-Dimensional Weakly Bonded Solids and Lattice-Commensurate Heterostructures. *Nano Lett.* **2017**, *17* (3), 1915–1923. https://doi.org/10.1021/acs.nanolett.6b05229.
(191) Perdew, J. P.; Ernzerhof, M.; Burke, K. Rationale for Mixing Exact Exchange with Density Functional Approximations. *J. Chem. Phys.* **1996**, *105* (22), 9982–9985. https://doi.org/10.1063/1.472933.
(192) Kresse, G.; Joubert, D. From Ultrasoft Pseudopotentials to the Projector Augmented-Wave Method. *Phys. Rev. B* **1999**, *59* (3), 1758–1775. https://doi.org/10.1103/PhysRevB.59.1758.
(193) Krukau, A. V.; Vydrov, O. A.; Izmaylov, A. F.; Scuseria, G. E. Influence of the Exchange Screening Parameter on the Performance of Screened Hybrid Functionals. *J. Chem. Phys.* **2006**, *125* (22), 224106. https://doi.org/10.1063/1.2404663.
(194) Rohlfing, M.; Louie, S. G. Electron-Hole Excitations in Semiconductors and Insulators. *Phys. Rev. Lett.* **1998**, *81* (11), 2312–2315. https://doi.org/10.1103/PhysRevLett.81.2312.
(195) Shishkin, M.; Marsman, M.; Kresse, G. Accurate Quasiparticle Spectra from Self-Consistent GW Calculations with Vertex Corrections. *Phys. Rev. Lett.* **2007**, *99* (24), 246403. https://doi.org/10.1103/PhysRevLett.99.246403.
(196) Giannozzi, P.; Andreussi, O.; Brumme, T.; Bunau, O.; Nardelli, M. B.; Calandra, M.; Car, R.; Cavazzoni, C.; Ceresoli, D.; Cococcioni, M.; Colonna, N.; Carnimeo, I.; Corso, A. D.; de Gironcoli, S.; Delugas, P.; DiStasio Jr., R. A.; Ferretti, A.; Floris, A.; Fratesi, G.; Fugallo, G.; Gebauer, R.; Gerstmann, U.; Giustino, F.; Gorni, T.; Jia, J.; Kawamura, M.; Ko, H.-Y.; Kokalj, A.; Küçükbenli, E.; Lazzeri, M.; Marsili, M.; Marzari, N.; Mauri, F.; Nguyen, N. L.; Nguyen, H.-V.; Otero-de-la-Roza, A.; Paulatto, L.; Poncé, S.; Rocca, D.; Sabatini, R.; Santra, B.; Schlipf, M.; Seitsonen, A. P.; Smogunov, A.; Timrov, I.; Thonhauser, T.; Umari, P.; Vast, N.; Wu, X.; Baroni, S. Advanced Capabilities for Materials Modelling with Quantum ESPRESSO. **2017**. https://doi.org/10.1088/1361-648X/aa8f79.
(197) Giannozzi, P.; Baroni, S.; Bonini, N.; Calandra, M.; Car, R.; Cavazzoni, C.; Ceresoli, D.; Chiarotti, G. L.; Cococcioni, M.; Dabo, I.; Dal Corso, A.; de Gironcoli, S.; Fabris, S.; Fratesi, G.; Gebauer, R.; Gerstmann, U.; Gougoussis, C.; Kokalj, A.; Lazzeri, M.; Martin-Samos, L.; Marzari, N.; Mauri, F.; Mazzarello, R.; Paolini, S.; Pasquarello, A.; Paulatto, L.; Sbraccia, C.; Scandolo, S.; Sclauzero, G.; Seitsonen, A. P.; Smogunov, A.; Umari, P.; Wentzcovitch, R. M. QUANTUM ESPRESSO: A Modular and Open-Source Software Project for Quantum Simulations of Materials. *J Phys Condens Matter* **2009**, *21* (39), 395502. https://doi.org/10.1088/0953-8984/21/39/395502.
(198) Martyna, G. J.; Klein, M. L.; Tuckerman, M. Nosé–Hoover Chains: The Canonical Ensemble via Continuous Dynamics. *J. Chem. Phys.* **1992**, *97* (4), 2635–2643. https://doi.org/10.1063/1.463940.
(199) Long, M.-Q.; Tang, L.; Wang, D.; Wang, L.; Shuai, Z. Theoretical Predictions of Size-Dependent Carrier Mobility and Polarity in Graphene. *J. Am. Chem. Soc.* **2009**, *131* (49), 17728–17729. https://doi.org/10.1021/ja907528a.
(200) Bruzzone, S.; Fiori, G. Ab-Initio Simulations of Deformation Potentials and Electron Mobility in Chemically Modified Graphene and Two-Dimensional

Hexagonal Boron-Nitride. *Appl. Phys. Lett.* **2011**, *99* (22), 222108. https://doi.org/10.1063/1.3665183.
(201) Xie, J.; Zhang, Z. Y.; Yang, D. Z.; Xue, D. S.; Si, M. S. Theoretical Prediction of Carrier Mobility in Few-Layer BC2N. *J. Phys. Chem. Lett.* **2014**, *5* (23), 4073–4077. https://doi.org/10.1021/jz502006z.
(202) Qiao, J.; Kong, X.; Hu, Z.-X.; Yang, F.; Ji, W. High-Mobility Transport Anisotropy and Linear Dichroism in Few-Layer Black Phosphorus. *Nat Commun* **2014**, *5* (1), 4475. https://doi.org/10.1038/ncomms5475.
(203) Haeuseler, H.; Srivastava, S. K. Phase Equilibria and Layered Phases in the Systems A2X3-M2X3-M'X (A = Ga, In; M = Trivalent Metal; M' = Divalent Metal; X = S, Se). *Zeitschrift für Kristallographie - Crystalline Materials* **2000**, *215* (4), 205–221. https://doi.org/10.1524/zkri.2000.215.4.205.
(204) Range, K.-J. The Space Group of MgAl2Se4 and MgIn2Se4. *Zeitschrift für Naturforschung B* **2014**, *51*. https://doi.org/10.1515/znb-1996-0925.
(205) Zhuang, H. L.; Hennig, R. G. Computational Search for Single-Layer Transition-Metal Dichalcogenide Photocatalysts. *J. Phys. Chem. C* **2013**, *117* (40), 20440–20445. https://doi.org/10.1021/jp405808a.
(206) Jung, J. H.; Park, C.-H.; Ihm, J. A Rigorous Method of Calculating Exfoliation Energies from First Principles. *Nano Lett.* **2018**, *18* (5), 2759–2765. https://doi.org/10.1021/acs.nanolett.7b04201.
(207) Ashwin Kishore, M. R.; Ravindran, P. Tailoring the Electronic Band Gap and Band Edge Positions in the C2N Monolayer by P and As Substitution for Photocatalytic Water Splitting. *J. Phys. Chem. C* **2017**, *121* (40), 22216–22224. https://doi.org/10.1021/acs.jpcc.7b07776.
(208) Yan, H.; Yang, H. TiO2–g-C3N4 Composite Materials for Photocatalytic H2 Evolution under Visible Light Irradiation. *Journal of Alloys and Compounds* **2011**, *509* (4), L26–L29. https://doi.org/10.1016/j.jallcom.2010.09.201.
(209) Si, C.; Sun, Z.; Liu, F. Strain Engineering of Graphene: A Review. *Nanoscale* **2016**, *8* (6), 3207–3217. https://doi.org/10.1039/C5NR07755A.
(210) Low, J.; Jiang, C.; Cheng, B.; Wageh, S.; Al-Ghamdi, A. A.; Yu, J. A Review of Direct Z-Scheme Photocatalysts. *Small Methods* **2017**, *1* (5), 1700080. https://doi.org/10.1002/smtd.201700080.
(211) Mukhokosi, E. P.; Krupanidhi, S. B.; Nanda, K. K. Band Gap Engineering of Hexagonal SnSe2 Nanostructured Thin Films for Infra-Red Photodetection. *Sci Rep* **2017**, *7* (1), 15215. https://doi.org/10.1038/s41598-017-15519-x.
(212) Lin, Y.; Yuan, G.; Liu, R.; Zhou, S.; Sheehan, S.; Wang, D. Semiconductor Nanostructure-Based Photoelectrochemical Water Splitting: A Brief Review. *Chemical Physics Letters - CHEM PHYS LETT* **2011**, *507*, 209–215. https://doi.org/10.1016/j.cplett.2011.03.074.
(213) Luo, B.; Liu, G.; Wang, L. Recent Advances in 2D Materials for Photocatalysis. *Nanoscale* **2016**, *8* (13), 6904–6920. https://doi.org/10.1039/C6NR00546B.
(214) Pfeiff, R.; Kniep, R. Quaternary Selenodiphosphates(IV): MIMIII[P2Se6], (MI =Cu, Ag; MIII = Cr, Al, Ga, In). *Journal of Alloys and Compounds* **1992**, *186* (1), 111–133. https://doi.org/10.1016/0925-8388(92)90626-K.
(215) Kresse, G.; Hafner, J. Ab Initio Molecular-Dynamics Simulation of the Liquid-Metal--Amorphous-Semiconductor Transition in Germanium. *Phys. Rev. B* **1994**, *49* (20), 14251–14269. https://doi.org/10.1103/PhysRevB.49.14251.

(216) Grimme, S. Semiempirical GGA-type density functional constructed with a long-range dispersion correction. *Journal of Computational Chemistry* **2006**, *27* (15), 1787–1799. https://doi.org/10.1002/jcc.20495.
(217) Togo, A.; Tanaka, I. First Principles Phonon Calculations in Materials Science. *Scripta Materialia* **2015**, *108*, 1–5. https://doi.org/10.1016/j.scriptamat.2015.07.021.
(218) Baroni, S.; de Gironcoli, S.; Dal Corso, A.; Giannozzi, P. Phonons and Related Crystal Properties from Density-Functional Perturbation Theory. *Rev. Mod. Phys.* **2001**, *73* (2), 515–562. https://doi.org/10.1103/RevModPhys.73.515.
(219) Heyd, J.; Scuseria, G. E.; Ernzerhof, M. Hybrid Functionals Based on a Screened Coulomb Potential. *J. Chem. Phys.* **2003**, *118* (18), 8207–8215. https://doi.org/10.1063/1.1564060.
(220) Heyd, J.; Peralta, J. E.; Scuseria, G. E.; Martin, R. L. Energy Band Gaps and Lattice Parameters Evaluated with the Heyd-Scuseria-Ernzerhof Screened Hybrid Functional. *J. Chem. Phys.* **2005**, *123* (17), 174101. https://doi.org/10.1063/1.2085170.
(221) Yang, L. *Optical Properties of Metal-Molybdenum Disulfide Hybrid Nanosheets and Their Application for Enhanced Photocatalytic Hydrogen Evolution*.
(222) Singh, A. K.; Mathew, K.; Zhuang, H. L.; Hennig, R. G. Computational Screening of 2D Materials for Photocatalysis. *J. Phys. Chem. Lett.* **2015**, *6* (6), 1087–1098. https://doi.org/10.1021/jz502646d.
(223) Zhuang, H. L.; Hennig, R. G. Single-Layer Group-III Monochalcogenide Photocatalysts for Water Splitting. *Chem. Mater.* **2013**, *25* (15), 3232–3238. https://doi.org/10.1021/cm401661x.
(224) Hisatomi, T.; Kubota, J.; Domen, K. Recent Advances in Semiconductors for Photocatalytic and Photoelectrochemical Water Splitting. *Chem. Soc. Rev.* **2014**, *43* (22), 7520–7535. https://doi.org/10.1039/C3CS60378D.
(225) Cook, T. R.; Dogutan, D. K.; Reece, S. Y.; Surendranath, Y.; Teets, T. S.; Nocera, D. G. Solar Energy Supply and Storage for the Legacy and Nonlegacy Worlds. *Chem Rev* **2010**, *110* (11), 6474–6502. https://doi.org/10.1021/cr100246c.
(226) Yang, L.; Li, X.; Zhang, G.; Cui, P.; Wang, X.; Jiang, X.; Zhao, J.; Luo, Y.; Jiang, J. Combining Photocatalytic Hydrogen Generation and Capsule Storage in Graphene Based Sandwich Structures. *Nat Commun* **2017**, *8* (1), 16049. https://doi.org/10.1038/ncomms16049.
(227) Fei, R.; Yang, L. Strain-Engineering the Anisotropic Electrical Conductance of Few-Layer Black Phosphorus. *Nano Lett* **2014**, *14* (5), 2884–2889. https://doi.org/10.1021/nl500935z.
(228) Yao, S.; Zhang, X.; Zhang, Z.; Chen, A.; Zhou, Z. 2D Triphosphides: SbP3 and GaP3 Monolayer as Promising Photocatalysts for Water Splitting. *International Journal of Hydrogen Energy* **2019**, *44*. https://doi.org/10.1016/j.ijhydene.2019.01.106.
(229) García de Arquer, F. P.; Bushuyev, O. S.; De Luna, P.; Dinh, C.-T.; Seifitokaldani, A.; Saidaminov, M. I.; Tan, C.-S.; Quan, L. N.; Proppe, A.; Kibria, M. G.; Kelley, S. O.; Sinton, D.; Sargent, E. H. 2D Metal Oxyhalide-Derived Catalysts for Efficient CO2 Electroreduction. *Advanced Materials* **2018**, *30* (38). https://doi.org/10.1002/adma.201802858.

(230) Di, J.; Xia, J.; Li, H.; Guo, S.; Dai, S. Bismuth Oxyhalide Layered Materials for Energy and Environmental Applications. *Nano Energy* **2017**, *41*, 172–192. https://doi.org/10.1016/j.nanoen.2017.09.008.
(231) Cheng, H.; Huang, B.; Dai, Y. Engineering BiOX (X = Cl, Br, I) Nanostructures for Highly Efficient Photocatalytic Applications. *Nanoscale* **2014**, *6* (4), 2009–2026. https://doi.org/10.1039/C3NR05529A.
(232) He, J.; Lyu, P.; Nachtigall, P. Two-Dimensional Tetragonal GaOI and InOI Sheets: In-Plane Anisotropic Optical Properties and Application to Photocatalytic Water Splitting. *Catalysis Today* **2020**, *340*, 178–182. https://doi.org/10.1016/j.cattod.2018.10.012.
(233) Sham, L. J.; Schlüter, M. Density-Functional Theory of the Energy Gap. *Phys. Rev. Lett.* **1983**, *51* (20), 1888–1891. https://doi.org/10.1103/PhysRevLett.51.1888.
(234) Gross, E. K. U.; Kohn, W. Local Density-Functional Theory of Frequency-Dependent Linear Response. *Phys. Rev. Lett.* **1985**, *55* (26), 2850–2852. https://doi.org/10.1103/PhysRevLett.55.2850.
(235) Kresse, G.; Furthmüller, J.; Hafner, J. Ab Initio Force Constant Approach to Phonon Dispersion Relations of Diamond and Graphite. **1995**. https://doi.org/10.1209/0295-5075/32/9/005.
(236) Monkhorst, H. J.; Pack, J. D. Special Points for Brillouin-Zone Integrations. *Phys. Rev. B* **1976**, *13* (12), 5188–5192. https://doi.org/10.1103/PhysRevB.13.5188.
(237) Ma, F.; Zhou, M.; Jiao, Y.; Gao, G.; Gu, Y.; Bilic, A.; Chen, Z.; Du, A. Single Layer Bismuth Iodide: Computational Exploration of Structural, Electrical, Mechanical and Optical Properties. *Sci Rep* **2015**, *5* (1), 17558. https://doi.org/10.1038/srep17558.
(238) Qi, H.; Sun, Z.; Wang, N.; Qin, G.; Zhang, H.; Shen, C. Two-Dimensional Al2I2Se2: A Promising Anisotropic Thermoelectric Material. *Journal of Alloys and Compounds* **2021**, *876*, 160191. https://doi.org/10.1016/j.jallcom.2021.160191.
(239) Haastrup, S.; Strange, M.; Pandey, M.; Deilmann, T.; Schmidt, P. S.; Hinsche, N. F.; Gjerding, M. N.; Torelli, D.; Larsen, P. M.; Riis-Jensen, A. C.; Gath, J.; Jacobsen, K. W.; Mortensen, J. J.; Olsen, T.; Thygesen, K. S. The Computational 2D Materials Database: High-Throughput Modeling and Discovery of Atomically Thin Crystals. *2D Mater.* **2018**, *5* (4), 042002. https://doi.org/10.1088/2053-1583/aacfc1.
(240) Peng, R.; Ma, Y.; He, Z.; Huang, B.; Kou, L.; Dai, Y. Single-Layer Ag2S: A Two-Dimensional Bidirectional Auxetic Semiconductor. *Nano Lett.* **2019**, *19* (2), 1227–1233. https://doi.org/10.1021/acs.nanolett.8b04761.
(241) Liu, Y.-L.; Yang, C.-L.; Wang, M.-S.; Ma, X.-G.; Yi, Y.-G. Te-Doped Perovskite NaTaO3 as a Promising Photocatalytic Material for Hydrogen Production from Water Splitting Driven by Visible Light. *Materials Research Bulletin* **2018**, *107*, 125–131. https://doi.org/10.1016/j.materresbull.2018.06.040.
(242) Jiang, D.; Sun, Z.; Jia, H.; Lu, D.; Du, P. A Cocatalyst-Free CdS Nanorod/ZnS Nanoparticle Composite for High-Performance Visible-Light-Driven Hydrogen Production from Water. *J. Mater. Chem. A* **2015**, *4* (2), 675–683. https://doi.org/10.1039/C5TA07420G.